EFFECTS OF DISCONTINUITIES ON THE BEHAVIOR OF TUNNELS IN JOINTED ROCK MASS

Ph.D. Thesis

NISHANT ROY
ID NO. 2014RCE9544

DEPARTMENT OF CIVIL ENGINEERING
MALAVIYA NATIONAL INSTITUTE OF TECHNOLOGY JAIPUR, INDIA

July 2018

EFFECTS OF DISCONTINUITIES ON THE BEHAVIOR OF TUNNELS IN JOINTED ROCK MASS

Submitted in

fulfillment of the requirements for the degree of

Doctor of Philosophy

by

Nishant Roy
ID: 2014RCE9544

Under the Supervision of
Prof. S.D. Bharti

DEPARTMENT OF CIVIL ENGINEERING
MALAVIYA NATIONAL INSTITUTE OF TECHNOLOGY JAIPUR, INDIA

July 2018

DECLARATION

I, **Nishant Roy**, declare that this thesis titled,"**Effects of Discontinuities on the Behavior of Tunnels in Jointed Rock Mass**" and the work presented in it, are my own. I confirm that:

- This work was done wholly or mainly while in candidature for a research degree at this university.
- Where any part of this thesis has previously been submitted for a degree or any other qualification at this university or any other institution, this has been clearly stated.
- Where I have consulted the published work of others, this is always clearly attributed.
- Where I have quoted from the work of others, the source is always given. With the exception of such quotations, this thesis is entirely my own work.
- I have acknowledged all main sources of help.
- Where the thesis is based on work done by myself, jointly with others, I have made clear exactly what was done by others and what I have contributed myself.

Date:

Nishant Roy
(2014RCE9544)

CERTIFICATE

This is to certify that the thesis entitled **"EFFECTS OF DISCONTINUITIES ON THE BEHAVIOR OF TUNNELS IN JOINTED ROCK MASS"** being submitted by **Nishant Roy (2014RCE9544)**is a bonafide research work carried outunder my supervision and guidance in fulfillment of the requirement for the award of the degree of **Doctor of Philosophy** in the Department of Civil Engineering, Malaviya National Institute of Technology,Jaipur, India. Thematter embodied in this thesis is original and has not been submitted to any other University or Institute for the award of any other degree.

Place: Jaipur
Date:

Dr. S.D. Bharti
Professor
Dept of Civil Engineering

Acknowledgement

The present work would not have been possible without the constant support and encouragement of a number of individuals. First and foremost,I would like to express my gratitude to Dr. S.D. Bharti, who has provided constant support, encouragement, and guidance since the inception of this work. His willingness to share his knowledge and discuss questions at any time has been instrumental in this journey. More than a supervisor, he has played the role of a friend and mentor who was always ready to provide help on both professional and personal matters. I feel lucky and fortunate to have got the opportunity to be associated with him.

I would like to thank Dr. Rajib Sarkar for providing all the necessary help, support and his words of encouragement are gratefully acknowledged.

The support and encouragement of colleagues and seniors served me well during this phase of my journey. In this regard, the role of seniors such as Vishisht Sir, Shashi Sir, Arnav Sir and Pankaj Sir is gratefully acknowledged. Also, the constant encouragement provided by my close friends Kabeer, Vaibhav and Ravi since the start of this journey requires special mention.

Last but not the least, the support and care of my parents, brother, and sister-in-law,has played a pivotal role in the completion of this work.

ABSTRACT

The expansion of railway and highway networks in mountainous regions has led to the construction of tunnels through geologically complex and seismically active regions. However, the hazard associated with these complex conditions pose significant challenges to the engineering community. Numerous cases of instabilities during the excavation of tunnels have led to loss of lives, damage to construction equipment, delay in completion of projects and cost over-runs. In addition, recent cases of damage of tunnels under seismic events has challenged the long held view of underground structures possessing adequate earthquake resistant features.

The present work provides a discussion on the critical issues dealing with the stability of tunnel excavations in the jointed rock mass. It is understood that the deformation response is structurally-controlled *viz.* large-scale movement of discrete rock blocks along the discontinuities with the possibility of their subsequent detachment governs the overall stability. In this regard, the limitations of the current state of numerical analysis adopted for the assessment of stability of tunnel excavations are highlighted. Mostly, the current state of practise relies heavily on the idealization of the discontinuities in the rock mass with parallel joint sets which do not hold good for all the cases leading to errornoeus results. The need for an alternative method of idealization of the joints and their implications on the stability assessment are investigated. It is found that the manner of joint idealization has a significant influence on the mode of rock block movement. Also, the relative contribution of various joint parameters on the deformation response is found to significantly depend on the pattern of joint idealization.

For the dynamic behavior of tunnels, a rigorous review of cases of seismically induced damage has been made. It is found that in the majority of the cases, the damaged sections pass through highly weathered and fractured rock mass conditions. In addition, large movement and detachment of rock blocks have also been noted, suggesting the interaction of waves with the joints to govern the dynamic response. However, a clear understanding of the effect of the discontinuities on the dynamic behavior of tunnels is lacking. Most of the

investigations reported in the literature have been performed by idealizing the geological medium as being continuous, thereby neglecting the interaction between the waves and joints. Such an approximation fails to accurately capture the mechanical and kinematic response of discontinuous rock mass, such as the structurally controlled movement of rock blocks, dissipation of energy along the joints, multiple reflection and refraction of seismic waves and the frequency filtering effect. Thus, an assessment of the dynamic behavior of tunnels using discrete method is required.

Given the ensuing discussion, the dynamic response of a circular lined tunnel in the blocky rock mass has been numerically investigated using the distinct element method. Specifically, an assessment of the influence of wave frequency, type of wave action (P and S waves), overburden depth and the in-situ stress ratio on the demand imposed on the tunnel liner is presented. The results of the numerical simulations have been utilized to corroborate the damage patterns reported in the literature. Finally, the concept of seismic isolation of buried structures have been extended for tunnels in the blocky rock mass. The promising capability offered by Expanded Polystyrene (EPS) Geofoam as a potential seismic buffer for lined tunnels has been assessed.

Keywords: *Tunnel; Voronoi; Blocky Rock Mass; Distinct Element Method; Dynamic; Expanded Polystyrene (EPS) Geofoam*

LIST OF CONTENTS

LIST OF FIGURES

LIST OF TABLES

LIST OF NOTATIONS

a,b,c	Random parameters in factorial design
A,B,C	Main effect of parameter a, b and c using statistical approach
AB	Interaction effect between parameters a and b
C_{jc}	Cohesion of continuous joints
C_{jb}	Cohesion of joints for blocky rock mass
C_p	Compressional wave velocity
C_s	Shear wave velocity
d	Depth of tunnel from ground surface
D	Diameter of the tunnel
E	Young's modulus of the rock
ε_0	Critical strain
k_n	Joint normal stiffness
k_s	Joint shear stiffness
K_{nb}	Normal stiffness of joints for blocky rock mass
K_{nc}	Normal stiffness of continuous joints,
K_{sb}	Shear stiffness of joints for blocky rock mass
K_{sc}	Shear stiffness of continuous joints,
K_0	In-situ stress ratio
n	Number of parameters in factorial design
P_1	In-situ stress in vertical direction
P_2	In-situ stress in horizontal direction
SS	Sum of squares
T_l	Transmission coefficient for wave propagation
Δu_n	Incremental normal displacement at the joint
Δu_s	Incremental shear displacement along the joint
V_p	Particle velocity in normal direction
V_s	Particle velocity in shear direction
ρ	Mass density of the geological medium
σ_c	Unconfined compressive strength
μ_{xi}	Mean of random parameter

σ_{xi}	Standard deviation of random parameter
$\Delta\sigma_n$	Incremental normal stress
$\Delta\sigma_s$	Incremental shear stress
ϕ_{jb}	Friction angle of joints for blocky rock mass
ϕ_{jc}	Friction angle of continuous joints
ω	Angular frequency of the harmonic wave
Z_p	P-wave impedance

Chapter 1

INTRODUCTION

1.1 Overview

The construction of tunnels in mountainous regions pose a significant challenge to the engineering community. Instabilities during the excavation of tunnels in complex and difficult ground conditions, leading to delays, accidents and damage to construction equipment have been common. Majority of these instabilities arise due to large movement of rock blocks along pre-existing geological discontinuities. In adverse geological settings, complete detachment of rock blocks and collapse of excavation opening is also observed. Figure. 1.1 (a) and (b) shows some cases of instabilities encountered during the excavation of underground openings in the jointed rock mass.

Another major issue is the risk posed to the integrity of the lined tunnels due to the seismicity of the mountainous regions. Severe damages have been observed following some recent seismic events - Kobe (1995), ChiChi (1999), Mid-Niigata (2004) and Wenchuan (2008) earthquakes. Most of the damaged sections have been identified to be located in highly weathered and fractured rock mass. This suggests the interaction of the seismic waves with the fractured geological medium to significantly influence the dynamic behavior of mountain tunnels.

Fig. 1.1. Cases of instabilities during excavation (a) detachment of rock blocks and (b) collapse of the opening (*Zhu et al.* 2017)

1.2 Jointed Rock Mass

The expansion of railway and highway networks in mountainous regions has led to the construction of tunnels in some highly variable rock mass conditions. The term rock mass refers to the geological medium which comprises of two components – i. *Intact rock*, which is the unfractured and relatively strong entity and ii. *Discontinuities,* which are geological features and includes faults, joints, fractures, foliations and bedding planes. A typical outcrop of a rock mass is shown in Fig. 1.2. The discontinuities in the rock mass serve as weak links which bring down the strength of the geological volume.

The presence of the discontinuities has a significant influence on the overall behavior of the rock mass and hence on the integrity of the structure built in or on them. In fact, for a particular type of rock mass subjected to a given set of loading/unloading conditions, relatively different behaviors are possible depending on the distribution and condition of the discontinuities. This fact is reflected in most of the rock mass classification systems available in the rock mechanics literature, where the strength is suggested to depend on the discontinuity distribution. Hence, attempts to evaluate the anticipated behavior of the rock mass due to any construction activity must explicitly account for the discontinuous nature of the medium.

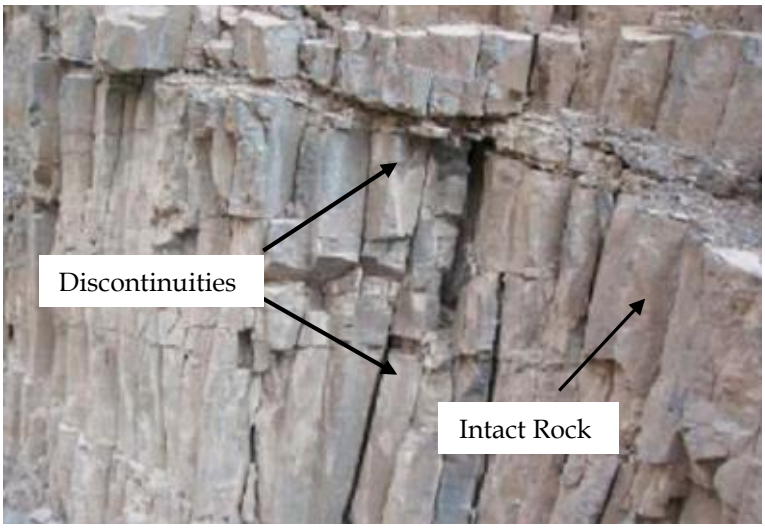

Fig. 1.2. An outcrop of jointed rock mass (Xu *et al.* 2015)

1.2.1 Tunnels in Jointed Rock Mass

The excavation of tunnels in jointed rock mass offers a unique challenge to engineers, where one has to disrupt the initial equilibrium and proceed to a new state of stability. The *action* of excavating a cavity in the ground disrupts the pre-existing equilibrium and modifies the original state of stress. It leads to a redistribution of stress in the surrounding material which *reacts* by converging inwards.

Since the intact rock material possesses sufficiently high strength, the convergence of the opening majorly occurs due to movement of discrete rock blocks along the discontinuities. In some cases, the movement along the discontinuities becomes very high, resulting in the detachment of well-defined rock blocks. A schematic representation of the deformation response of circular tunnel excavation in the jointed rock mass is shown in Fig. 1.3 (a) and (b). Excessive movements and block detachments pose difficulty in support installations and lining placements, thereby having an adverse impact on the progress of underground projects.

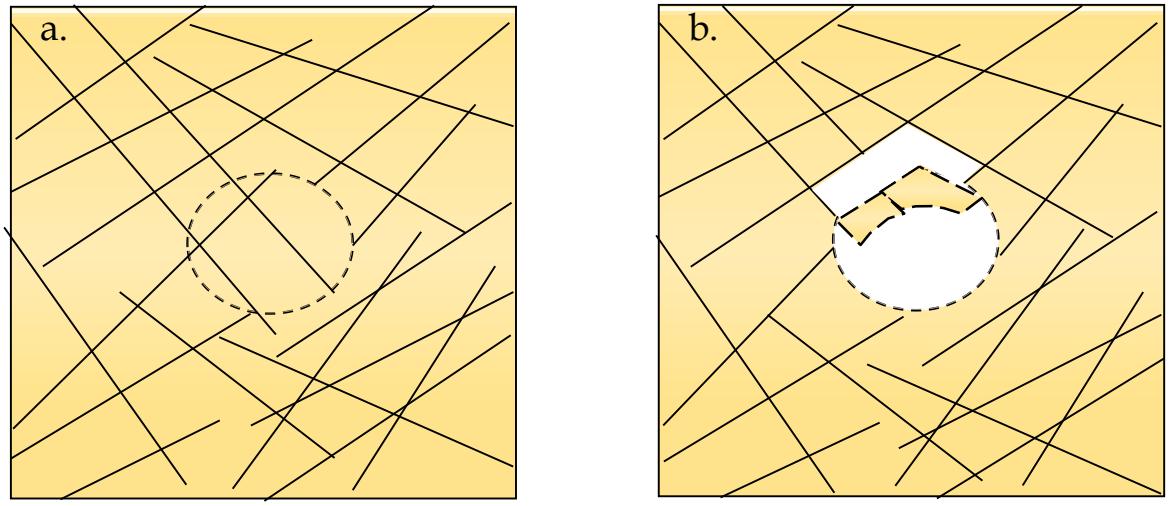

Fig. 1.3. Response of tunnel excavation in the jointed rock mass (a) ground is in equilibrium before the excavation (b) redistribution of stresses in surrounding medium leads to detachment of rock blocks

The discontinuities also have a significant impact on the propagation of waves in the rock mass. Interaction of the wave with a discontinuity leads to reflection, transmission, and dissipation of the energy. Depending on the wave frequency, spacing, orientation and stiffness of the discontinuities and the relative angle of

incidence of the wave, the amplitudes of the reflected and transmitted energy vary. There is also a possibility of formation of loose rock blocks under the influence of the wave action. For tunnels in the jointed rock mass, these phenomena may increase the seismic vulnerability. Interestingly, field survey undertaken to assess the damages sustained by tunnels following earthquakes reveal most of the vulnerable sections to pass through highly weathered and fractured zones. Detachment of well-defined rock blocks is also noted. Although attempts have been made to understand the dynamic behavior of tunnels, extensive investigations with due consideration of the interaction of the wave with the discontinuities are lacking and require further examination.

1.2.2 Numerical Modeling of Jointed Rock Mass

The numerical methods available to assess and predict the behavior of structures built in or on the jointed rock mass is broadly classified into two categories: i. *Continuum method* and ii. *Discrete method*.

The continuum method is one of the most widely used simulation approaches for rock mechanics applications. In this approach, the rock mass is treated as a continuous material, in which equivalent continuum properties of the rock mass are utilized. To account for the effect of the discontinuities, the parameters characterizing the strength and deformation of the equivalent rock mass is lowered. This method is most suitable for relatively massive rock with few discontinuities, where large movement and detachment of rock blocks is not anticipated. To advance the applicability of the method for a more broader application in rock mechanics, joint elements have also been developed. However, the assumptions of the continuum approach do not permit these elements to replicate block detachment and rotations.

The discrete method provides an alternative for modeling the discontinuous nature of the rock mass. This approach treats the entire problem domain as an assembly of discrete blocks, which may be either rigid or deformable, with interfaces between them. The interfaces represent the discontinuities to which stiffness and strength properties are specified. Large-scale sliding and rotation of rock blocks along the

discontinuities, with the possibility of complete detachment can be simulated. Also, the method is capable of capturing the interaction between the discontinuities and the waves, thereby providing a robust alternative for investigating problems in rock dynamics.

1.3 Numerical Analysis of Tunnels in the Jointed Rock Mass: Current State and Its Limitations

Majority of the research investigations of tunnel excavations in the jointed rock mass have considered the joints (discontinuities) in a simplified manner through the adoption of the equivalent continuum method. Although popular and extensively used, the method does not account for the structurally-controlled deformation response *viz.* large-scale movement of discrete rock blocks along the discontinuities with the possibility of detachment. Having realized the limitations of the approach, some studies adopted the discrete methods to further advance the understanding of the role of the discontinuities in the deformation response. However, barring a few cases, most investigations have idealized the discontinuities as being parallel with exaggerated continuity. As highlighted by Barton(2002), such generalized idealization of the discontinuities in the rock mass may not hold good for all the cases. Also, it may be possible that the relative contribution of factors affecting the response of tunnel excavations may vary, based on a more realistic idealization of the discontinuities and requires further investigation.

For the dynamic case, the idealization of the geological medium as being continuous, fail to accurately capture the mechanical and kinematic response of rock mass, such as the opening and detachment of rock blocks, dissipation of energy along the joints, multiple reflection and refraction of seismic waves and the frequency filtering phenomena. These effects will have a dominant role in governing the behavior of tunnels in the jointed rock mass and must be considered. Hence, there is a need to investigate the dynamic behavior of tunnels using discrete methods.

1.4 Organization of the Thesis

The structure of the thesis is as follows:

Chapter 1 highlights some major issues related to mountain tunnels constructed in the jointed rock mass.

Chapter 2 provides a review of the literature pertaining to the deformation behavior of tunnel excavations in the jointed rock mass. A compilation of case histories of major tunnel damages sustained during past earthquakes is provided. Some major issues with the present approach of numerical analysis of tunnels in the jointed rock mass are discussed based on which the gap areas are identified. The major objectives and scope of the present study are presented.

Chapter 3 discusses the major features of the Universal Distinct Element Code (UDEC) software used in the present study. The configuration of the numerical model for the static and dynamic analyses have been explained. The statistical framework to evaluate the influence of parameters on the deformation response of tunnel excavation is presented.

Chapter 4 describes the verification studies carried out in the distinct element based software Universal Distinct Element Code (UDEC).

Chapter 5 highlights the significant influence which joint idealization has on the deformation response of tunnels in the jointed rock mass. The probable mode of rock block movement and the influence of various parameters is discussed. Some suggestions to enhance the current practice dealing with the assessment of tunnel deformation is presented.

Chapter 6 provides a detailed discussion on the influence of frequency of input motion, PGA, type of wave action, tunnel depth and in-situ stress ratio on the dynamic behavior of tunnels in the blocky rock mass. The numerical results are utilized to corroborate the patterns of damage reported in the literature.

Chapter 7 presents the results of the numerical simulations which highlight the promising potential of Expanded Polystyrene (EPS) Geofoam as an effective seismic buffer material for reducing the seismic demand imposed on the tunnel liner.

Chapter 8 summarizes the major conclusions from this work. The implications of the findings of the present work are highlighted. Suggestions on the future scope of work are also made.

…

Chapter 2

REVIEW OF LITERATURE

2.1 Introduction

Over the past three decades, there has been a tremendous expansion of highway and railway networks in mountainous regions. As tunnels constitute an integral component of this network, tunneling activities have advanced through difficult and complex geological and seismic settings. However, the complex conditions have brought some challenging issues at the forefront. While some have been solved, there are still others which require further investigations.

This chapter provides a discussion on some critical issues reported in the literature for tunnels in the jointed rock mass. A brief review of the dominating influence of the discontinuities on the behavior of tunnel excavations is presented. This is followed by a detailed account of the observations of the seismic performance of tunnels following some recent earthquakes. Based on the review, the gap areas are identified and listed. At the end of the chapter, the objectives and scope of the present study are presented.

2.2 Influence of Geological Discontinuities on the Behavior of Tunnel Excavations

The construction of mountain tunnels is a risky affair and has posed complex challenges for engineers. The presence of multiple joint sets, which break the geological medium into rock blocks of various shapes and sizes, induce anisotropy and inhomogeneity in the rock mass, significantly influencing the mechanical response (Jaegar and Cook, 1979, Bidgoli and Jing 2014, Lu et al. 2017, Xu et al. 2017). This has a major implication on the stability of tunnel excavations in the jointed rock mass.

The deformation following an excavation is primarily a reaction to the disturbance created in the ground. The action of excavating the ground disturbs the initial equilibrium and is associated with the release of pre-existing stresses. The redistribution of stress leads to stress development in both the intact rock and the

joints (discontinuities). Since the strength of the intact rock is sufficiently large, in the majority of the cases, they do not undergo large deformations. However, the strength of the joints being low is exceeded, leading to comparatively large movement and detachment of well-defined rock blocks. Thus, the deformation response of tunnel excavations in the jointed rock mass is dominated by the presence of the geological joints.

2.3 Past Investigations of Tunnel Excavation in Jointed Rock Mass

Various researchers have attempted to study the response and stability of tunnel excavation in jointed rock mass. The relative orientation and density of the joints, which breaks the geological medium into rock blocks of various shapes and sizes, have been extensively reported to influence the deformation around an underground opening (Goodman *et al.* 1968, Cundall *et al.* 1975, Manfredini *et al.* 1975, Bandis *et al.* 1983). Also, the shear strength of the joints is reported to influence the stability (Hao and Azzam 2005, Yeung and Leong 1997, Satici and Unver 2015, Panthee *et al.* 2016). The findings of some critical literature dealing with the subject matter follow.

Shen and Barton (1997) used the discrete method to examine the disturbed zone around a circular opening. Two sets of parallel joints with variable spacing and orientation were considered in the study. The deformation response was found to be governed by the formation of loosened blocks of rock, highlighting the significance of the spatial characteristics of the discontinuities. The findings reported by Bhasin and Hoeg (1997a, b; 1998) concurred with the influencing role of spatial characteristics of the discontinuities on tunnel deformations. For two sets of parallel and persistent joints, a combination of translational shear along the discontinuities followed by rock block rotation was suggested as the probable mechanism governing the deformation response. Solak (2009) also evaluated the behavior of ground surrounding a circular opening with two sets of parallel joints, in which the spacing of one of the joint sets was varied to simulate blocky rock mass conditions of various shape and size. Specific emphasis on the role of in-situ stress ratio and strength characteristic of the joints, *i.e.*, the residual friction angle, was

examined. Block detachment with sliding along the joints was mainly observed, with the strength of the joints significantly affecting the deformation response. Similar findings have been reported based on the studies by Song *et al.* (2001), Li *et al.* (2010), Hatzor *et al.* (2010), Curran *et al.* (2008) and Jia and Tang (2008).

The above-mentioned findings based on numerical simulations using discrete methods are found to agree well with the observations made at sites – for example, the severe instabilities encountered during the excavation of the desilting chambers of the Naptha Jhakri Hydroelectric Project was closely related to the unfavorable orientation of the discontinuities (Carter *et al.* 2008). Well-defined wedge-shaped rock blocks posed challenges during the excavation phase. Similar problems have been encountered during the construction of the Pir Panjal tunnel which led to delay in the completion of the project.

2.3.1 Major Findings from Literature and Some Limitations

Based on the above-cited literature, it is understood that the parameters characterizing the spatial distribution and shear strength of the discontinuities; and in-situ stress ratio govern the deformation response of excavations. The deformation response is majorly influenced by:

a. Normal displacement of rock blocks which occur due to joint opening and dilation.
b. Movement of rock blocks as a result of sliding action along the joints.
c. Relative size, shape, and position of the blocks and their subsequent interactions.

Surprisingly, the influence of the deformation parameters of the joints, *i.e., joint normal stiffness (k_n)* and *joint shear stiffness (k_s)* have rarely been investigated and reported in the literature. Since these parameters will influence the movement of rock blocks along the joints, either in the normal or shear direction, an investigation into their effects seems crucial.

Also, the majority of the investigations have idealized the distribution of the geological discontinuities with parallel joint sets. Barton (2002) cautions against the

use of parallel idealization of discontinuities with exaggerated continuity, suggesting such idealization to lead to inaccurate predictions. Thus, the influence of the parameters highlighted must be investigated for other joint configurations to advance our current state of understanding about the deformation response of excavation in the fractured rock mass.

2.4 Comprehensive Review of Seismic Performance of Tunnels

Following recent seismic events, the traditional view about earthquake resistant characteristics of tunnels has been challenged. Severe cases of damage of mountain tunnels have been reported follwoing the 1995 Hyogoken-Nanbu (Japan), 1999 Chi-Chi (Taiwan), 2004 Mid-Niigata Prefecture (Japan) and the 2008 Wenchuan (China) earthquakes (Asakura and Sato 1998, Otsuka *et al.* 1997, Wang *et al.* 2001, Shimizu *et al.* 2007a, Shimizu *et al.* 2007b Jiang *et al.* 2010, Li 2012, Chen *et al.* 2012, Shen *et al.* 2014 etc.). Such poor performances have led scholars and engineers to take up research in the area of seismic behavior of tunnels and underground facilities (Kontoe *et al.* 2008, Penzien 2000, Hashash *et al.* 2001, O'Rourke *et al.* 2001, Konagai 2005, Wang *et al.* 2009, Li 2012).

The subsequent sections provide a review of some critical documents dealing with the seismic performance of mountain tunnels. Prominent cases of seismic induced instabilities are discussed with emphasis on the observed damage patterns. Moreover, the factors believed to be responsible for the damages have been highlighted. Based on the damage patterns and the influencing factors, probable mechanisms of seismic damage of mountain tunnels as suggested in the literature have been summarized.

2.5 Overview of Past Seismic Performances of Mountain Tunnels

Some of the prominent work documenting seismic damage of tunnels and underground facilities have been reported by Dowding and Rozen (1978), Owen and Scholl (1980), Sharma and Judd (1991) and Power *et al.* (1998). An investigation of 71 tunnels was taken up by Dowding and Rozen (1978) following earthquake events in America and Japan. Most of the tunnels considered were part of the railway or roadway network with the majority of them passing through rocky

terrain. Based on analysis of the available data, the unstable cases were grouped as damages caused due to – i. Slope instabilities, ii. Poor geology and iii. Shallow overburden. Damage patterns reported were uplift of invert, spalling of concrete at the crown, failures of sidewalls and portal cracking. The relationship between seismic damage and peak ground acceleration was also established. Major damages were found to occur for seismic events with magnitude greater than 0.50g. The database was further enlarged by Owen and Scholl (1980) in which 127 cases of damages of underground facilities were considered.

Subsequently, Sharma and Judd (1991) documented 192 cases of tunnel performance under 85 different earthquakes. Correlation of seismic induced damage was made with six parameters- i. tunnel overburden, ii. type of subsoil, iii. peak ground acceleration, iv. magnitude of earthquake, v. epicentral distance and vi. type of lining support. It was found that the vulnerability of tunnels increased when the depth of overburden was small. Moreover, earthquake parameters like magnitude, peak ground acceleration, and epicentral distance had a significant impact on the overall stability. The damage levels decreased for tunnels constructed in competent rocks, highlighting the role of the geological setting. Similar observations were made by Power *et al.* (1998) about the performance of underground facilities following the 1995 Hyogoken-Nanbu (Japan) and the 1995 Northridge (U.S.) earthquakes. Table 2.1 collates past seismic performances of tunnels highlighting the significant observations and conclusions.

2.6 Specific Discussion on Major Damages

In the present section, case histories of damage of mountain tunnels for earthquakes in Japan, Taiwan, and China are discussed. For each of the case, discussions are made with an emphasis on the earthquake parameters, ground conditions and damage patterns documented by various researchers. Based on these case histories, predominant damage patterns and the factors affecting the seismic behavior of tunnels have been identified.

2.6.1 Damage of Tunnels in Japan

Owing to the mountainous terrain of Japan, there is an extensive use of tunnels for highway and railway networks in the region. A total of about 4500 tunnels for railways and 6500 tunnels for highways are in operation. In addition, tunnels and underground facilities are also utilized for hydroelectric projects, water supply, and storage purpose.

As Japan is situated in a volcanic zone on the Pacific ring of fire, volcanic and earthquake events are quite frequent. Motions arising as a result of movement of Pacific, Philippine, Eurasian and the North American plates results in around 40 earthquake events of magnitude greater than 4.0 per month. As such, seismic damages of the tunnel have been reported extensively. Table 2.2 summarizes cases of tunnel damages following various earthquakes in Japan. Some of the major tunnel damages during some prominent earthquakes are discussed below.

1923 Kanto earthquake: The catastrophic event of Kanto in 1923 caused severe damages to mountain tunnels in Japan. Over 100 cases of tunnel damages were reported out of which 25 needed immediate repair and reinforcement measures. One of the most severely affected tunnels was the Nabuya tunnel which suffered damage from a landslide. The landslide destroyed a portion of the tunnel lining and led to the collapse of a tunnel section making it inoperative.

1930 Kita-Izu earthquake: The 1930 Kita-Izu earthquake of magnitude 7.1 severely affected the Tanna railway tunnel. The earthquake had a focal depth of 11 km. The tunnel was situated at an epicentral distance of 15km (Sharma and Judd 1991). The damages were maximum in the sections where the tunnel passed through the fault-fracture zone of the Tanna basin. A 60m stretch of the tunnel without concrete cover was subjected to large earth pressure during seismic shaking. Consequently, a large volume of the earth (about 1200m^3) fell into the tunnel disrupting the operations. Cracking of the tunnel lining was also observed at various other sections.

1978 Izu-Oshima-Kinkai earthquake: This earthquake severely affected the railway network of the adjacent area as it caused extensive damage to nine railway tunnels

(Kawakami 1984). Among them, the most severely affected was the Inatori tunnel which was a 906m long single track railway tunnel passing through a deposit of volcanic mudflow. The damage was majorly caused due to movement along a fault resulting in damage to tunnel lining and distortion of track alignment. Based on the field survey following the earthquake, relative displacement of 70cm and 20cm in the horizontal and vertical direction respectively was recorded.

1995 Hyogoken-Nanbu earthquake: Asakura and Sato (1998) investigated 100 mountain tunnels following the 1995 Hyogoken-Nanbu earthquake and found 24 tunnels to be affected by the seismic event. Severe damages were sustained by 12 tunnels making them inoperative. In most cases, damages occurred in the form of cracking of the linings in longitudinal, cross-sectional and circumferential direction highlighting the major influence of interaction of the direction of seismic waves with the tunnel axis and cross-section. Shear and compressive failure of the sidewalls and the arch, heaving of the invert, cracking of the portal wall and collapse of portal sections were also reported (Asakura and Sato 1998, Kitagawa and Hiraishi 2004). Table 2.3 summarizes the observations of some severely affected tunnels following this earthquake.

Table 2.1. Past seismic performances of tunnels

Reference	Main Event(s)	Observations	Major Conclusions
Dowding and Rozen (1978)	San Francisco 1906; Kwanto 1923; Idu Peninsula 1930; Fukui 1948; Off Tokachi 1952; Kern County 1952; Niigata 1964; Great Alaska 1964	• Caving in of rock near roof and arch shoulder. • Upward heaving of invert • Spalling of concrete at crown • Crushing of bottom sidewalls • Cracking at portal sections	• 71 tunnels investigated following earthquake with classification into three categories based on observations – no damage, minor damage and damage. • Damages are related to peak ground motions • No damage observed for ground motion of up to 0.19g. Minor damage observed in the range of 0.25g - 0.5g. Major damage observed for the high peak values of above 0.5g. • Damage classified into three categories: a. Damage near portals due to slope instability b. Damage in poor ground conditions c. Damage due to shallow depth and unsymmetrical load
Brown *et al.* (1981)	San Francisco (1906)	Lateral movement of 80mm of Bay Area Rapid Transit (BART) tunnels at Hayward Fault.	Fault movement is a very prominent factor in damaging a tunnel.
Murano and Takewaki (1984)	Kanto (1923); Kita-Mino (1961); Izu-Oshima-Kinkai (1978)	• Damages to tunnels and powerhouses in rocks especially in portal regions. • Longitudinal and transverse cracks in lining observed frequently	• Tunnel portals highly vulnerable • Poor geology and inadequate lining thickness lead to higher damages • Intersection of tunnel with faults should be avoided • Amplification of seismic waves in weathered zones increases the vulnerability of portal sections
Yoshikawa (1981); Yoshikawa and Fukuchi (1984)	Kanto (1923); Kitaizu (1930); Fukui (1948); Niigata (1964); Izu-Oshima-Kinkai (1978)	53 cases of heavy damages reported	Damages caused due to poor geology, unstable slopes, fault movement and inadequate lining.

Reference	Main Event(s)	Observations	Major Conclusions
Sharma and Judd (1991)	192 cases from 85 earthquakes around the world	• More damage for shallow tunnels • Greater number of damages for higher peak ground acceleration and smaller epicentral distance • Lower damage for tunnels in competent rocks	• Damages have been correlated to earthquake parameters, depth and geology
Asakura and Sato (1996, 1998)	Hyogoken-Nanbu (1995); Kanto (1923); Kita-Tango (1927); Kita-Izu (1930); Fukui (1948); Tokachi-oki (1952); Kita-Mino (1961); Niigata (1964); Tokachi-oki (1968); Izu-Oshima-Kinkai (1978); Miyagiken-oki (1978); Urakawa-oki (1982); Nihonkai-chubu (1983); Naganoken-seibu (1984); Chibaken-toho-oki (1987); Notohanto-oki (1993); Hokkaido-nansei-oki (1993); Hyogoken-Nanbu (1995)	• Cracking of lining in longitudinal, cross-sectional and circumferential directions • Shear and compressive failure at arch shoulders and sidewalls • Heaving and cracking of tunnel invert • Cracks at the portal wall • Partial/ complete collapse of portal region	• Majority failure confined to sections located in highly faulted/fractured zone • Adverse geological conditions, shallow overburden depth and relative displacement of ground led to failures
Power *et al.* (1998)	Hyogoken-Nanbu (1995)	• Cracking and spalling damages reported	• PGA <0.2g – minor damages • 0.2g< PGA < 0.6g – Slight to heavy damage

Reference	Main Event(s)	Observations	Major Conclusions
	Northridge (1995) Loma Prieta (1989)	• Tunnels with liner performed better during earthquakes • Damages can be correlated to peak ground acceleration	• Heavy damage in case of 1923 Kanto earthquake majorly caused by slope instabilities and shallow overburden
Wang *et al.* 2001	Chi-Chi (1999)	• Damage to unreinforced secondary lining. • Longitudinal, circumferential and inclined cracking • Cave in and collapse at shallow overburden (35-45m) sections. • Support damage due to squeezing ground for deeper sections (>100m)	• The unreinforced secondary lining suffered damages due to excessive earthquake loading • Imperfect backfill, bad geometry of tunnel cross section and poor geological conditions contributed to damage. • Maximum damage in the region passing through Sanyi and Shihliufen fault having shallow overburden highlights the effects of adverse geology and depth of tunnel section from ground.

Table 2.2. Summary of tunnel damages following earthquakes in Japan (Adapted from Asakura and Sato 1998, Otsuka *et al.* 1997)

Earthquake	Magnitude	Tunnel Performance
Kanto (1923)	7.9	Severe damages to over 100 tunnels. Damages caused due to fault intersection, slope instabilities and debris flow.
Kita-Tango (1927)	7.3	Minor damage to two railway tunnels.
Kita-Izu (1930)	7.3	Severe damage arising from fault intersection and movement reported for one railway tunnel.
Fukui (1948)	7.1	Severe damage to two railway tunnels.
Tokachi-oki (1952)	8.2	10 railway tunnels damaged slightly.
Niigata (1964)	7.5	Severe damages to 20 railway tunnels and one road tunnel. Damages occurred due to poor geological conditions and subsequent landslides in the form of cracking of tunnel lining.
Tokachi-Oki (1968)	7.9	Damages to 23 railway tunnels. Constant landslides and increased earth pressure responsible for damages.
Izu-Oshima-Kinkai (1978)	7.0	Very severe damages to about 9 railway and 4 road tunnels. Damages attributed to poor geological conditions, fault crossing and rock falls.
Miyagiken-oki (1978)	7.4	Slight damage to 6 railway tunnels located near epicenter.
Urakawa-oki (1982)	7.1	Slight damage to 6 railway tunnels.
Nihonkai-chubu (1983)	7.7	Slight damage to 8 railway tunnels.
Naganoken-seibu (1984)	6.8	Cracking observed in one head race tunnel majorly caused due to fault crossing.
Chibaken-toho-oki (1987)	6.7	Damage to a railway tunnel.
Notohanto-oki (1993)	6.6	Severe damage to a rock tunnel due to the collapse of rock onto the tunnel lining.
Hokkaido-nansei-oki (1993)	7.8	Rock fall-induced failure at portal sections for one road tunnel

Table 2.3. Summary of few tunnels damaged in 1995 Hyogoken-Nanbu earthquake (Adapted from Asakura and Sato 1998, Otsuka *et al.* 1997)

Tunnel	Overburden (m)	Geology	Epicentral Distance (km)	Damages Observed
Maiko	4-50	Granite, sand-gravel	5	Settlement of crown, exfoliation, and cracking of shotcrete.
Nunobiki	240	Mesozoic granite	18	Exfoliation of concrete lining, development of ring cracks.
Bantaki	20-250	Mesozoic granite	32	Exfoliation of concrete lining, development of ring cracks.
Rokko	0-400	Mesozoic granite	20-30	Damage at 12 locations near fractured zones, heave of invert, shear failure and cracking of lining.

In case of *Nunobiki tunnel,* cracking in the lining both in the cross-sectional and longitudinal directions were observed. Also, spalling of concrete at the junction between the arch and the sidewall was observed. However, the damage was confined to a short zone which was comparatively heavily fractured.

The damages in the case of *Bantaki* road tunnel was also confined to a short section of highly fractured zone. Buckling and bending of steel reinforcements were extensively observed. Strong vertical ground motions and thrusting in the axial direction were held responsible for the uplift of the ground pavement of the tunnel.

The *Rokko* tunnel was a 16km long railway tunnel constructed in Mesozoic granite with the alignment passing through five major faults – Koyo, Ashiya, Gosukebashi, Ohtsaki and Nunobiki faults. The poor geological condition arising from the frequent faulting and fracturing led to different configurations of failures. Some prominent patterns of failures observed included the development of shear cracks and spalling of concrete near the arch shoulders. Bottom heaving and uplift in the vicinity of the invert were also reported. Major damages were reported to occur in the poor and highly fractured geological zone encountered between the Gosukebashi and Ohtsaki faults.

2004 Mid-Niigata Prefecture earthquake: The earthquake occurred on October 23, 2004, severely affecting the rail and road network of the area. The focal depth of the earthquake was about 13 km with a magnitude of 6.8. A series of strong aftershocks followed the main event with four of them having a magnitude of around 6 or greater within a span of 38 minutes (Konagai *et al.* 2005). The earthquake affected 24 railway tunnels and caused the derailment of a train. Among them, five tunnels-Uonama, Myoken, Wanatsu, Tenno and Shin-Enokitoge suffered severe damages and had to be closed for a long time for repair and restoration (Shimizu *et al.* 2007b, Yashiro and Kojima 2007, Jiang *et al.* 2010).

The Uonama tunnel located close to the epicenter (<10km) suffered maximum damage. The damaged section had an overburden of about 60 to 100m. Movement of sidewalls along with the development of diagonal cracks was common. At one location, severe damage to the crown leading to lining collapse and exposure of steel reinforcements was observed. As shown in Fig. 2.1, right lateral shift of about 10-15cm of the center ditch along the rails was also observed (Konagai *et al.* 2005).

Even though landslide was prevalent during the earthquake, it is believed that it was not the major cause as the damaged sections were located at deeper depths. Based on the pattern of cracks observed, it was concluded that the damage was caused by slipping of a fault segment intersecting the tunnel.

Another tunnel to be severely affected was Myoken tunnel. Failures in terms of heaving of the invert and compressive failure at the crown were observed. In case of Wanatsu tunnel, compressive failure at the crown with subsequent exposure of steel supports was observed. For both Tenno and Shin-Enokitoge tunnels, cracking of tunnel lining resulting from the failure of bedrock was reported (Shimizu *et al.* 2007b, Jiang *et al.* 2010). A list of tunnels affected by the earthquake along with the associated geology and damage patterns has been reproduced from the study of Jiang *et al.* (2010) in Table 2.4.

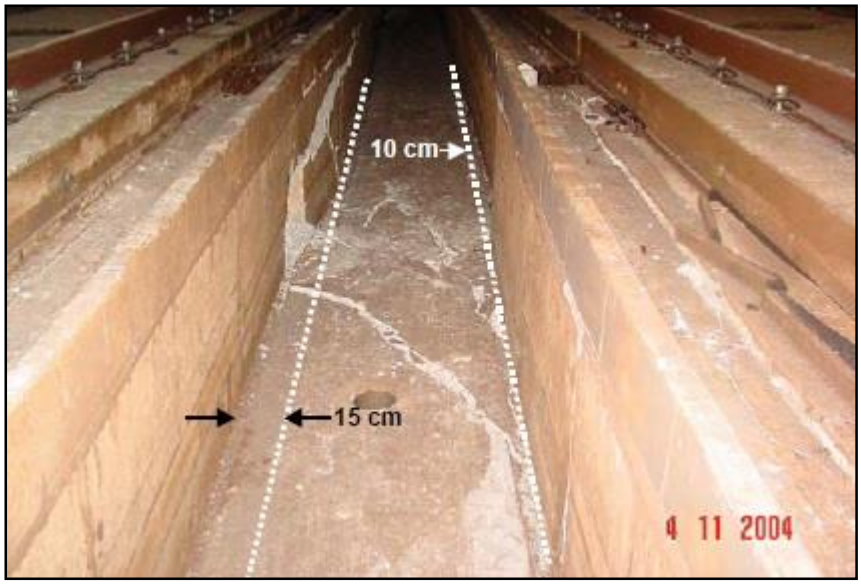

Fig. 2.1. Right lateral shift of about 10-15 cm in Uonama tunnel (Konagai *et al.* 2005)

Table 2.4. Tunnels damaged in Mid-Niigata Prefecture earthquake (After Jiang *et al.* 2010)

Tunnel	Length (m)	Overburden (m)	Width (m)	Height (m)	Geology	Damages
Wanatu	300	40	8.2	4.6	Ss	Side wall deformation and spalling of arch
Kosendani	1088	62	9.5	4.8	Ss	Crack, spalling in arch and sidewall
Yamamotoyama	1839	140	10.2	7.5	Absm	Crack
Yamanaka	1307	200	6.5	4.5	Ss, Ms	Longitudinal crack
Takeisi	331	140	7	7.74	Ss, Ms	Longitudinal crack
Higasiyama	220	35	7	4.7	Ss, Ms	Crack in arch
Siroyama	128	150	7	4.7	Ss, Ms	Longitudinal crack in sidewall
Orinaka	374	60	9.25	4.7	Ss, Ms	Crack in arch and sidewall
Obirou	390	90	9.25	4.7	Ss, Ms	Crack
Sibumi	860	150	6	4.7	An,Tu, Ms	Spalling in arch
Haneguro (roadway)	506	100	5.6	5.2	St	Compressive buckling in bed, crack in arch and sidewall

Tunnel	Length (m)	Overburden (m)	Width (m)	Height (m)	Geology	Damages
Haneguro (pavement)	550	100	2.2	2.85	St	Spalling
Junidaira	210	40	8.5	4.7	St	Spalling, deformation in sidewall
Rangi	590	180	6	4.7	Ss, Ms	Longitudinal crack in arch, upheave in bed
Siotani	512.5	110	7.5	5.85	Ss, Ms	Crack in arch
Kizawa	305	30	6	4.7	Ss, Ms	Deformation, spalling, roadbed opening
Araya	292	45	7.5	5.64	Ss, Ms	Compressive buckling, crack, bed opening
Tochio	854	150	10.35	4.7	An, Ms	Water leakage
Okimitouge	1080	150	8.5	4.7	Ms, Ss	Longitudinal crack in sidewall
Hosa	6087	15	9.6	8.3	Tb	Crack in roadbed
Horinouti	3300	100	9.6	8.3	Cm	Spalling in sidewall
Uonama	8624	70	9.6	8.3	Ms, Absm	Spalling, upheave in bed, crack
Myoken	1459	65	9.6	8.3	St	Crack, upheave in roadbed
Takitani	2673	55	9.6	8.3	St, Ss	Crack
Sinfukuyama	1468	75	4.8	5	Sr	Crack
Fukuyama	1350	7	4.8	5.6	Sr	Crack
Wanatu	725	41	8.5	7.5	St	Spalling, crack, arch-shoulder junction failure
Nakayama	1205	92	8.5	7.5	Sh, Ss	Crack
Usigazima	432	14	8.5	7.5	Sh, Ss	Crack in portal
Tenou	285	11	4.7	5.1	Sh, Ss	Crack
Sintouge	1372	75	4.7	5.1	Sh, Ss	Crack
Touge	641	70	4.8	5.1	Sh, Ss	Crack
Hanada	880	28	8.6	6.3	Sh, Ss	Spalling
Tukayama	1766	150	8.7	6.3	Sh, Ss	Crack
Higasiyama	166	22	8.8	6.4	Ms, Ss	Spalling
Iwayama	652	54	4.7	5.2	Ss	Spalling
Iwazama	203	36	4.6	5.1	St	Spalling

Tunnel	Length (m)	Overburden (m)	Width (m)	Height (m)	Geology	Damages
Myokouzan	1465	151	4.6	5.2	Ar	Crack
Kouyouzan	500	67	4.8	5.1	Sr	Crack
Utigamaki	425	30	4.6	5.2	Ms	Crack
Akakura	10471	440	4.36-8.54	6.16-6.96	Ms, Ss	Spalling, crack in arch and sidewall, water leakage
Jusanmachi	1695	40	5.05	5.68	Cm	Water leakage
Yakusitoge	6199	250	4.36-8.54	5.60-6.96	Ms	Spalling, crack in arch and sidewall, water leakage

Ss: sandstone; Absm: alternating beds of sandstone and mudstone; Ms: mudstone; An: andesite; Tu: tuff; St: siltstone; Tb: tuff breccias; Cm: conglomerate; Sh: shale

2.6.2 Damage of Tunnels in Taiwan

1999 Chi-Chi earthquake: A 7.3 magnitude earthquake struck central Taiwan on September 21, 1999, at a depth of around 7.5km causing catastrophic damage to infrastructural facilities. The earthquake was believed to be a result of reactivation of the Chelungpu fault (Wang *et al.* 2000). The seismic event produced very high ground motion with the free field instruments recording the horizontal motion of 1.0g and 0.8g at two locations (Wang *et al.* 2001). Fig. 2.2 shows the location of the tunnels in the vicinity of the earthquake epicenter and the Chelungpu fault. Following the earthquake, an investigation of 57 tunnels was taken up by Wang *et al.* (2001) based on which 49 cases of damage were reported. Fig. 2.3 presents a number of different damage patterns observed for the 49 cases of instabilities. From Fig. 2.3, it is evident that the damages of tunnel sections are mostly in the form of lining cracks, portal failure and spalling of concrete lining. Fig. 2.4 shows the slope instability induced failure of the Ching-Shue tunnel following this earthquake.

Table 2.5 adapted from Wang *et al.* (2001) lists the 57 tunnels which were investigated providing details about their geometry, epicentral distance, and location with regard to the Chelungpu fault. Greater damages were observed for tunnels located on the hanging wall of the Chelungpu fault which experienced higher ground motion. It was observed that the damages were mainly concentrated in the vicinity of the faulted or fractured region.

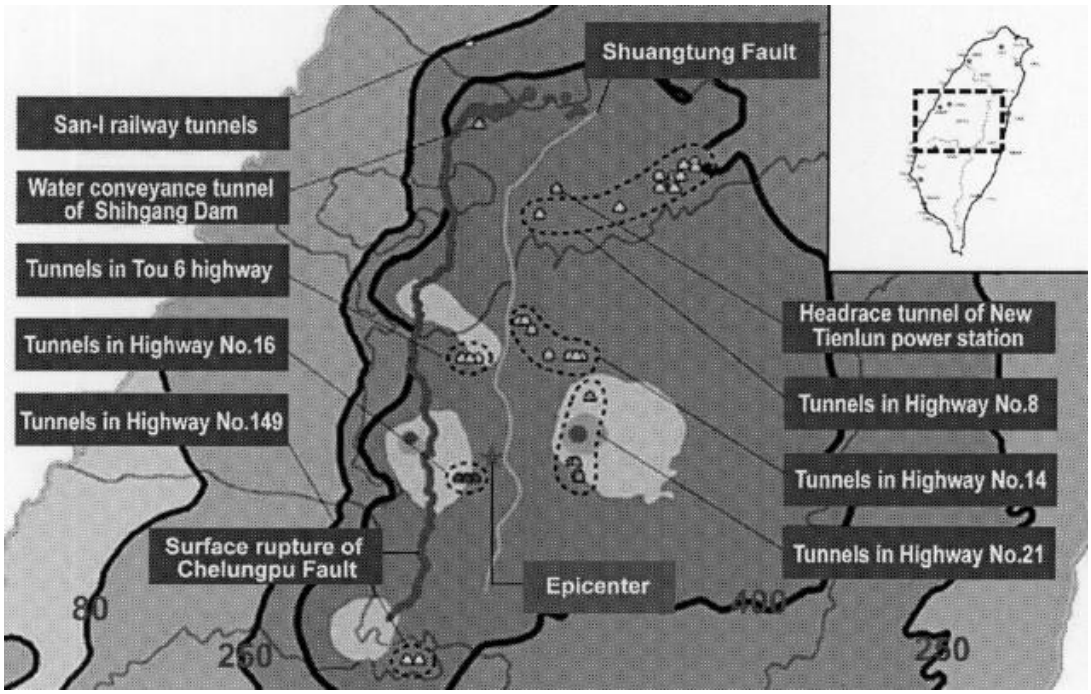

Fig. 2.2. Location of tunnels and Chelungpu Fault in vicinity of epicenter of Chi-Chi earthquake (Wang *et al.* 2001)

2.6.3 Damage of Tunnels in China

2008 Wenchuan earthquake: On May 12, 2008, a strong earthquake having a magnitude of 8.0 on Richter scale struck in the Longmenshan fault zone in the Sinchuan Province of China (Huang and Li 2009, Xu *et al*. 2009, Chen *et al.* 2012,). The focal depth of the earthquake was estimated to be around 15km with the seismic shaking period of 120seconds. This earthquake is believed to be the most destructive seismic event to have struck China in the last 100 years affecting around 87000 people and causing an economic loss of about 845 billion Yuan. Table 2.6 lists 30 tunnels having an epicentral distance less than 50 km which suffered damages during the earthquake (Wang and Zhang 2013, Zhang 2013, Zheng *et al.* 2009, Zheng *et al*. 2012).

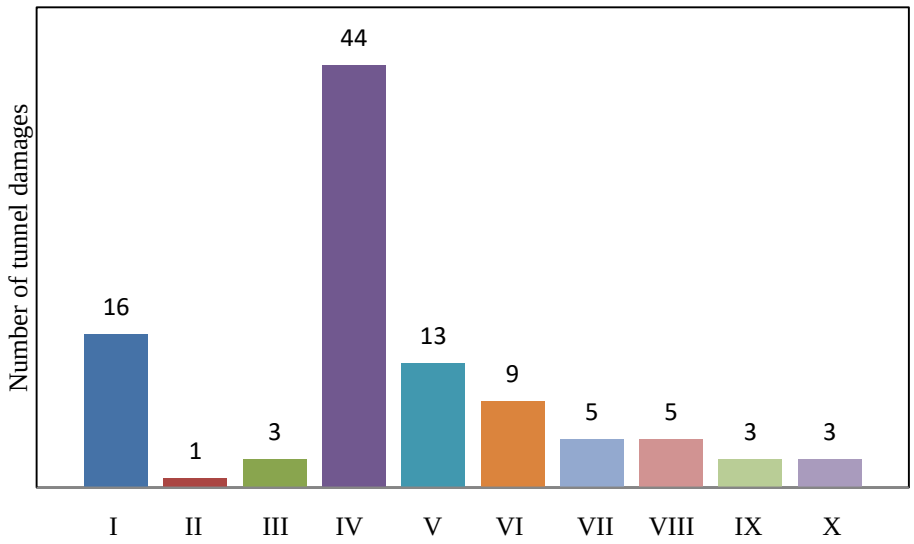

I:Portal failure II: Sheared off lining III: Slope induced failureIV: Lining cracks V: Concrete spalling VI: Water inrush VII: Exposed reinforcement VIII: Displaced lining IX: Pavement cracks X: Rockfalls in unlined section

Fig. 2.3. Various tunnel damages observed in Chi-Chi (1999) Taiwan earthquake

Fig. 2.4. Damage to Ching-Shue tunnel. (a) Tunnel entrance before the Chi-Chi earthquake; (b) Closure and damage of tunnel entrance due to slope instability (Wang *et al.* 2001)

Table 2.5. Tunnel investigated following 1999 Chi-Chi earthquake (After Wang *et al.* 2001)

Tunnel and location	Length (m)	Width (m)	Distance to epicenter (km)	Distance to Chelungpu fault (km)
Shih-Gang Dam, Water conveyance tunnel	-	-	-	0.0
Highway 8, 13k + 381	20	6.5	35.1	12.0
Highway 8, 27k + 710 , Li Lang	30	6.8	38.6	18.6
Highway 8, 34k + 668	50	3.2	44.0	20.1
Highway 8, 34k + 775	41	3.4	44.0	20.1
Highway 8, 35k + 908, Old Ku-Kuan	90	5.1	44.8	19.8
Highway 8, 36k + 908, Ku-Kuan	90	7.5	44.8	19.8
Highway 8, 38k + 500, No.1 old Maa-Ling	150	4.0	45.9	21.5
Highway 8, 38k + 500, No.1 Maa-Ling	365	5.1	45.8	21.5
Highway 8, 39k + 075, No.2 Maa-Ling	60	7.5	46.1	21.6
Highway 8, 40k + 830, No.3 Maa-Ling	245	7.5	46.3	21.6
Highway 8, 41k + 311, No.4 Maa-Ling	100	7.5	47.8	22.1
Highway 8, 41k + 311, No.4 old Maa-Ling	100	4.0	47.8	22.1
Highway 8, 42k + 573	10	6.5	48.3	23.0
Highway 8, 43k + 040	15	6.5	48.3	23.0
Highway 8, 45k + 266	32	6.5	48.5	22.8
Highway 14, 37k + 405, Shuang-Fu	150	7.5	19.7	12.0
Highway 14, 37k + 981(L), Gang-Lin	182	7.5	19.8	12.2
Highway 14, 38k + 000(R), Gang-Lin	249	7.5	19.8	12.2
Highway 14, 39k + 921(L), Yu-Ler	158	7.5	19.0	13.8
Highway 14, 39k + 921(R), Yu-Ler	158	7.5	19.0	13.8
Highway 14, 45k + 182, Pei-Shan	120	7.5	15.9	17.5
Highway 14, 48k + 616(L), No.1 Kuan-Yin	129	7.5	17.1	20.4
Highway 14, 48k + 616(R), No.1 Kuan-Yin	129	7.5	17.1	20.4
Highway 14, 48k + 787(L), No.2 Kuan-Yin	123	7.5	17.5	20.8
Highway 14, 48k + 787(R), No.2 Kuan-Yin	123	7.5	17.5	20.8
Highway 14, 49k + 253(L), No.3 Kuan-Yin	252	7.5	17.6	21.2
Highway 14, 49k + 253(R), No.3 Kuan-Yin	252	7.5	17.6	21.2
Hghway 16, Chi-Chi	238	4.8	6.1	5.5
Highway 16, New Chi-Chi (L)	580	7.5	6.4	5.3
Highway 16, New Chi-Chi (R)	515	7.5	6.4	5.3
Highway 21, 54k + 326 (L), Da-Yuan	462	7.5	14.2	21.8

Tunnel and location	Length (m)	Width (m)	Distance to epicenter (km)	Distance to Chelungpu fault (km)
Highway 21, 54k + 326 (R), Da-Yuan	444	7.5	14.2	21.8
Highway 21, 66k + 940 (L), Shue-Sir	185	7.5	8.5	19.9
Highway 21, 66k + 940 (R), Shue-Sir	185	7.5	8.5	19.9
Highway 21A, 17k + 303, No.1 Huan-Hu	128	7.5	9.3	20.2
Highway 21A, 17k + 253, No.2 Huan-Hu	61	7.5	9.3	20.2
Highway 149, Tsao-Ling	505	7.0	31.1	7.0
Highway 149, Ching-Shue	52	7.5	32.0	3.7
Tou-6 highway, No.1 Tu-Cheng	100	6.5	15.5	7.2
Tou-6 highway, No.2 Tu-Cheng	290	6.4	15.3	7.6
Tou-6 highway, Shuang-Lung (E)	140	5.3	15.2	7.8
Tou-6 highway, Shuan-Lung (W)	90	5.3	15.2	7.8
Tou-6 highway, No.1 Shuang-Tung	80	4.5	15.2	7.8
Tou-6 highway, No.2 Shuang-Tung	120	4.5	15.2	7.8
Chi-Chi line railway, No.1 tunnel	350	5.0	6.1	5.5
Chi-Chi line railway, No.2 tunnel	1400	5.0	<1	11
Chi-Chi line railway, No.3 tunnel	250	5.0	4.5	15.9
Chi-Chi line railway, No.5 tunnel	150	5.0	5.5	16.4
Da-Kuan power station, headrace tunnel	-	-	8.5	19.9
New Tien-Lun power station, headrace tunnel	10600	5.0	40	18.6
Mountain line railway, No.1 San-I tunnel	7540	9.1	55	11.1
Mountain line railway, No.2 San-I tunnel	260	9.1	50	10.1
Mountain line railway, No.3 San-I tunnel	520	9.1	49	10.1
Mountain line railway, No.4 San-I tunnel	455	9.1	49	10.1
Old mountain line railway, No.1 San-I tunnel	230	5.0	59	14.5
Old mountain line railway, No.2 San-I tunnel	730	5.0	58	13.1

Li (2012) has carried out a detailed investigation of the damages to the mountain tunnels of the Dujiangyan Wenchuan highway tunnels following the Wenchuan earthquake highlighting the damage patterns and the factors contributing towards the instabilities. Table 2.7 summarizes the findings of Li (2012) with regard to 11

tunnels of the Du Wen highway network. Details of some of the damaged tunnels are elaborately discussed below.

Table 2.6. Tunnel with an epicentral distance of less than 50 km in the 2008 Wenchuan earthquake (Wang and Zhang, 2013)

Tunnel Name	Length (m)	Epicentral Distance (km)
Longxi	3624	1.6
Zipingpu	4075	7.3
Longdongzi	1051	5
Shaohuoping	450	4.5
Zaojiaowan	1926	8.9
Maojiaowan	399	11.4
Chediguan	403	13
Futang	2365	13
Taoguan	625	7.9
Caopo	759	34.4
Dankanliangzi	1555	24.1
Maanshi	481	7.3
Youyi	962	2.4
Baiyunding	406	6.5
Panlongshan	381	14
Gengda	938	11.4
Niujiaoya	1614	4
Sanpanzi	382	13.2
Jiujiaya	2282	9.6
Longchi	1177	1.1
Xiquanyan	150	28
Xinjiagou	713	45
Guanyazi	639	43
Fenshuiling	1300	22
Shiwenzi	1300	42
Shitigou	371	43
Qujiapo	601	33
Feixianguan	384	37
Minyuexia	1300	38
Qinglinpo	255	40

Table 2.7. Tunnels of Du Wen highway affected by 2008 Wenchuan earthquake (After Li 2012, Wang *et al.* 2009)

Tunnel	Epicenter distance (km)	Adverse impacts
Zipingpu tunnel	50	Transverse and ring fractures of lining, uplift and cracking of invert and partial collapse of portal
Longdongzi tunnel	30	Portal burial, longitudinal cracks (20-35m long), transverse, oblique and ring cracks with 10-20 mm opening
Longxi tunnel	49	Obstruction of tunnel from rock falls, longitudinal, transverse, oblique and ring fractures of lining, distortion of steel beams, opening of construction joints, uplift of invert up to a maximum height of 1.2 m
Shaohuoping tunnel	40	Collapse of slope leading to portal burial, transverse fracture and uplift of invert, water seepage, distortion of steel supports
Zaojiaowan tunnel	42	Leakage of water through construction joints
Maojiawan tunnel	35	Partial burial of portal due to rock fall, cracking of construction joints in portal sections
Chediguan tunnel	32	Partial burial of portal, development of ring cracks at portal sections, cracking of road bed
Futang tunnel	45	Oblique cracks (45^0) in entrance section extending to 30 m, seepage of water through construction joints
Taoguan tunnel	28	Partial burial of portal section due to rock falls
Caopo tunnel	25	Rock falls at portal regions, water seepage through side wall cracks
Dankanliangzi tunnel	10	Minor cracking at portal section

Longxi tunnel: It was a twin tunnel system separated by a distance of 30m. According to the rock mass classification system of Chinese highway tunnel, the alignment passed through two zones. About 29% of the tunnel length passed through sandstone and granite rock which was hard and hence had good overall stability. However, 71% tunnel passed through intensely jointed and fractured rock mass comprising of mudstone, mudstone-siltstone mixture, carbonaceous mudstone and thin coal layers. In such stretches the stability was poor. Following the earthquake, instabilities manifested in terms of portal closure, cracking of pavement and tunnel linings (Li 2012, Chen *et al.* 2012, Shen *et al.* 2014).

Due to the high and steep configuration of the slope, rock falls obstructed the tunnel entrance and destroyed the slope protection works. Fig. 2.5a shows a rock block which fell across the opening during the earthquake. Moreover, five cases of collapse of lining due to the presence of weak mudstone at entrance sections were observed (Li 2012). The tunnel linings were sheared off at some locations as shown in Fig. 2.5b. Also, transverse ring cracks as shown in Fig. 2.5c developed in a particular stretch of the tunnel. A maximum ground bulge of about 120cm with heaving and bulging of tunnel invert was also observed. Fig. 2.5d shows the cracks which developed at the floor as a result of uplift of the bottom pavement.

Fig. 2.5. Damages at Longxi tunnel during 2008 Wenchuan earthquake(Modified after Tao *et al.* 2011): (a) Rockfall obstructing tunnel entrance; (b) Sheared off tunnel lining; (c) Transverse ring cracks; (d) Pavement cracks due to uplift

Baiyunding tunnel: The tunnel had a maximum overburden of 125m and passed through limestone formation which was highly weathered. Intense fracturing in the

area filled with moist and loose gravel soil had led to poor quality of rock mass. A fault belt also existed about 45 m away from one of the portals intersecting the tunnel axis. During the Wenchuan earthquake, widespread damage was reported at the portal sections resulting from a landslide as shown in Fig. 2.6a. Settlement of basement, cracking of the flooring and an average dislocation of around 20cm was noted for a damaged length of about 30m leading to an adverse impact on the functionality of the tunnel (Chen *et al.* 2012). Moreover, spalling of concrete lining and shearing failure was also observed in some sections. Fig. 2.6b shows a section where the reinforcement was exposed as a result of shearing and spalling of the concrete liner.

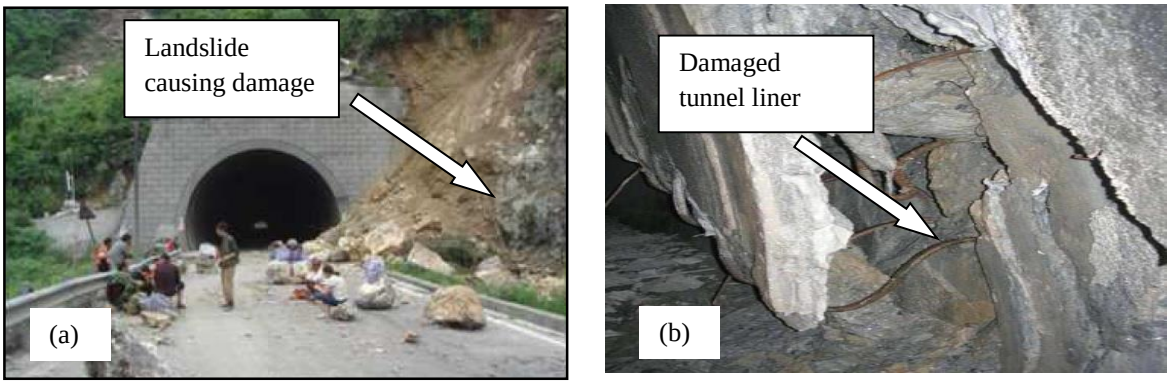

Fig. 2.6. Damages at Baiyunding tunnel (Modified after Tao *et al.* 2011): (a) Portal section damage due to landslide; (b) Sheared off tunnel liner

Longchi tunnel: The tunnel passed through limestone formation having a maximum overburden depth of 345m. The terrain was steep at the portal regions with an overburden of about 50m. Intense weathering of the rock mass and presence of faults near portals contributed adversely during the earthquake leading to failures. Cracking of tunnel lining in transverse, longitudinal and inclined directions as shown in Fig. 2.7a and Fig. 2.7b were noted. Moreover, the cracking and undulation of the bottom pavement were also observed.

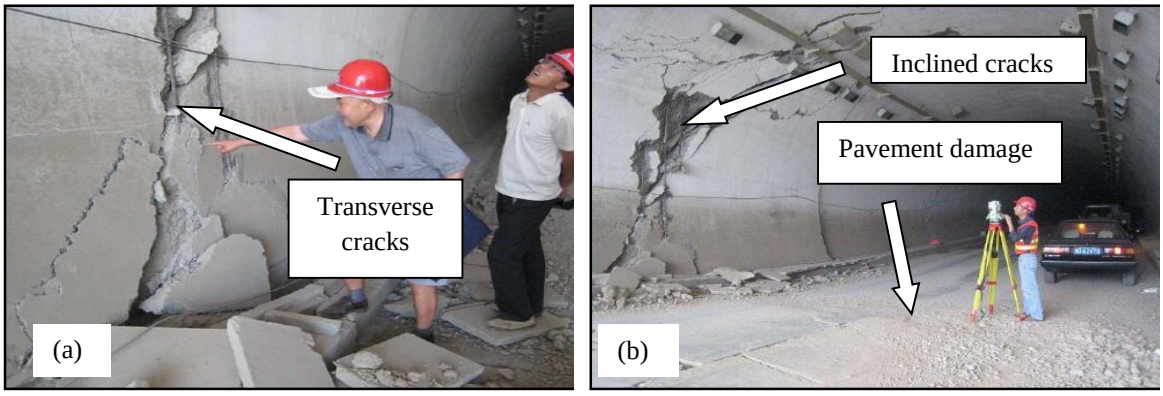

Fig. 2.7. Damages at Longchi tunnel (Modified after Tao *et al.* 2011): (a) Transverse cracking of liner; (b) Inclined cracks and pavement damage

Youyi tunnel: It was a 962m long tunnel having a maximum overburden of 215m with flat terrains at the portal ends. The tunnel passed through carbonaceous shale, argillaceous shale and sandstone with the portal sections located in gravelly soil. Relative movement along the faults caused tunnel liner to be sheared off along with deformation and cracks. Landslide induced failure were widely observed. Fig. 2.8a shows a damaged portal section near one of the tunnel entrance. The exposure of reinforcements as a result of spalling of tunnel lining is shown in Fig. 2.8b.

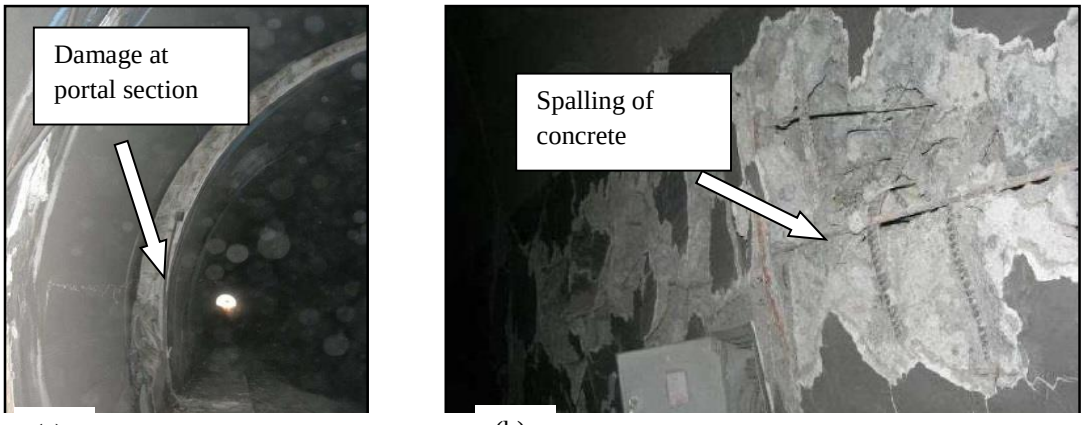

Fig. 2.8. Damages at Youyi tunnel (Modified after Tao *et al.* 2011): (a) Damage at portal section; (b) Spalling of concrete from tunnel lining

Shen *et al.* (2014) compiled the seismic response of 52 tunnels following the 2008 Wenchuan earthquake classifying the observed damage patterns into eight categories. Based on the data, Fig. 2.9 presents a number of different damage

patterns observed following the seismic event. From the figure, it is evident that the damages of tunnel sections are mostly in forms of lining cracks and rock falls.

2.7 Summary of Failure Characteristics

2.7.1 Cracking of Tunnel Lining

The most frequent form of earthquake-induced damage in tunnels is the cracking of the tunnel lining. Based on field observations of tunnel damages, the cracking has been classified as longitudinal, horizontal, oblique breakage, ring breakage and invert cracks. Fig. 2.10 shows some of the crack patterns observed following seismic events. Most of the tunnels which were severely damaged in 1923 Great Kanto earthquake developed longitudinal, horizontal and oblique cracks in the lining. Various forms of cracking have also been reported by Li (2012) for the tunnels of the Du Wen highway following the Wenchuan earthquake of 2008. In some cases, cracks developed on both sides of the arch wall. Moreover, at some sections, collapse of the concrete lining coupled with the exposure and buckling of steel reinforcements compromised the safe operation of the tunnels.

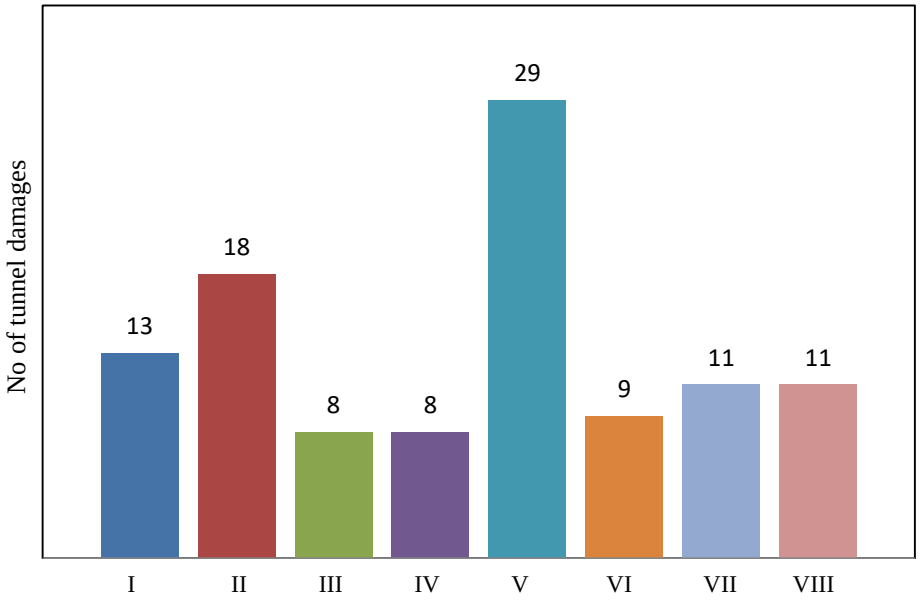

Fig. 2.9. Various tunnel damages observed in Wenchuan (2008) China earthquake

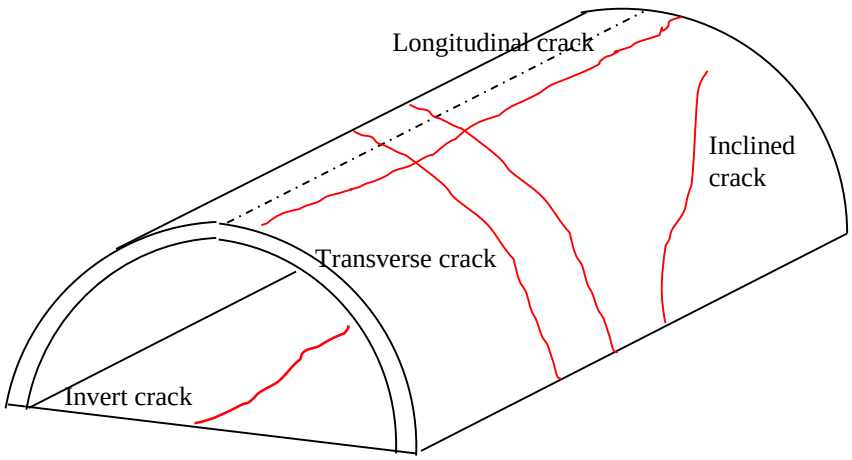

Fig. 2.10. Different patterns of cracks in tunnel lining

2.7.2 Shear Failure of Tunnel Lining

One of the most severe forms of earthquake damages is the shear failure of the tunnel lining. This type of failure results from the shear force acting on the lining near the faults and is characterized by the spalling of concrete coupled with exposure and detachment of steel reinforcements. The Tanna tunnel in Japan was severely affected by the shear failure leading to severe cracks at several locations during 1930 Kita-Izu earthquake. For this particular case, a horizontal displacement of 2.39m and a vertical displacement of 0.6m were observed near the Ena fault zone (Dowding and Rozen 1978).

More recently, the Longxi tunnel was severely affected by the 2008 Wenchuan earthquake and became inoperative following about 1m up and down relative displacement at some locations leading to the collapse of the arch lining. Severe damages to the secondary lining of the Baiyunding tunnel leading to the loss of structural integrity have also been attributed to the shear failure of the lining.

Although the shearing failure of tunnel lining is generally expected for regions crossing the faults, some cases of damage where the tunnel alignment did not cross the fault have also been reported. Prominent among them is the case of the Nagasaka tunnel which was damaged in the 1923 Great Kanto earthquake (Chen *et al.* 2012).

2.7.3 Portal Failure

Review of case histories highlights the fact that the portal sections are the most vulnerable part of the tunnel (Zhao *et al.* 2013). Instabilities in the form of rockfall, avalanches and sliding, cracking of head walls, arch rings, wing walls and expansion joints have been majorly observed following seismic events.

Rock falls occur on steep slopes consisting of relatively strong rock masses. Such damages were observed in case of Longxi tunnel where the rock fall destroyed the slope protection measures (see Fig. 2.5a). In contrast, sliding failure occurs in the vicinity of portal sections where the geological medium consists of highly weathered and fractured rock mass as in the case of the Longdongzi tunnel which suffered damage during 2008 Wenchuan earthquake. The weathered nature of the geological medium coupled with the steepness of the slope and the presence of unfavorably dipping structural planes led to sliding of the rock material burying the right-hand tunnel exit of the Longdongzi tunnel. Spalling and cracking of concrete lining on the arch side wall for the Taoguan tunnel with crack widths reaching up to 50cm are also attributed to the slope instabilities in the portal region (Li 2012).

2.7.4 Heaving and Cracking of Tunnel Invert

Severe cases of heaving and cracking of tunnel invert have been reported (Duke and Leeds 1959, Shen *et al*. 2014). A typical characteristic of this type of failure is the development of transverse cracks. In case of the Longxi tunnel, deformations in both the horizontal and vertical directions of about 30cm were noted. Also, a maximum uplift of 120cm was reported in one of the sections (Shen *et al.* 2014). Following the 1923 Great Kanto earthquake, Namutani tunnel suffered enormous lining distortion due to the uplift of the bottom slab. The displacement ranged between 50cm to 1m along the axis of the tunnel (Duke and Leeds 1959). In case of Longdongzi tunnel also, an uplift of about 2cm was observed (Li 2012).

From a number of case studies, it was concluded that the uplift and cracking of tunnel inverts were more predominant in case of presence of center drainage. This is attributed to the concentration of shear force and stiffness mismatch near the

tunnel invert. Also, the abrupt changes in the cross-section at the invert leading to stress concentration is a major cause for such damages (Shen *et al.* 2014).

2.8 Factors Affecting Mountain Tunnel Damage

2.8.1 Earthquake Parameters

The major earthquake parameters causing seismic damages of mountain tunnels include magnitude, epicentral distance and the depth of the earthquake source. In conjunction, the three parameters define the severity of a seismic event. An earthquake having a higher magnitude, lower epicentral distance and a shallow depth will be more intense and hence will influence the tunnels to a greater extent. Sharma and Judd (1991) collected and analyzed data for 192 tunnels from 85 different earthquakes based on which the influence of magnitude and epicentral distance on the seismic performances were summarized. Table 2.8 provides the effect of Richter magnitude on tunnel damages. It was observed that the number of cases of tunnel damage reached about 50% for magnitudes greater than 6.0. At lower magnitudes, the damage was low. Recent damage of mountain tunnels following 1999 Chi-Chi, 2004 Mid-Niigata Prefecture and 2008 Wenchuan earthquakes also conform to these findings with most of the them associated with magnitude greater than 6.0 on the Richter scale (Wang *et al.* 2001, Shen *et al.* 2014, Shimizu *et al.* 2007a, Shimizu *et al*. 2007b, Jiang *et al.* 2010).

With consideration to the epicentral distance, it is observed that the seismic vulnerability of the tunnels increases when they are situated close to the source of the earthquake. In most of the reviewed cases, it has been found that the epicentral distance for the damaged tunnels was within 70km (Asakura and Sato 1998, Otsuka *et al.* 1997, Wang *et al.* 2001). Table 2.9 summarizes the findings of Sharma and Judd (1991) relating tunnel damages with epicentral distance. However, review of recent case studies does not strictly conform to these observations. In some cases, tunnels located farther away (about 40 km) suffered greater damages in comparison to those located close to the earthquake source (Chen *et al.* 2012).

Table 2.8. Summary relating damage with Richter magnitude (After Sharma and Judd, 1991)

Magnitude	Extent of damage			
	Slight	Moderate	Heavy	None
<4	2	1	1	3
4-<5	1	2	0	8
5-<6	2	2	1	12
6-<7	17	3	6	33
7-<8	13	8	6	17
>8	10	7	6	22

2.8.2 Overburden Depth

Sharma and Judd (1991) analyzed the effect of depth of overburden for 132 cases and concluded that overburden has a major role in influencing tunnel damages. Based on the analysis of available data, they concluded that the damages are more for the tunnel having a depth of less than 50m. However, in contrast, few cases of instabilities of mountain tunnels show deviation from the conclusion mentioned above. Prominent among these are the damage sustained by the Rokko tunnel and the Longxi tunnel. In fact, in the case of the Longxi tunnel, severe damage were observed at a depth of 500m in terms of the collapse of a portion of the secondary concrete lining during 2008 Wenchuan earthquake (Li 2012).

2.8.3 Fault Location

Permanent ground displacements resulting from fault movements during earthquakes have caused a number of failures. In such events, large shear forces act on the tunnel sections and cause relative movement in both horizontal and vertical directions. Some of the prominent cases of fault-induced damages include the case of Uonama (2004 Mid-Niigata Prefecture), Inatori (1978 Izu-Oshima-Kinkai) and the Tanna (1930 Kita-Izu) tunnels.

Table 2.9. Summary relating damage with epicentral distance (After Sharma and Judd, 1991)

Epicentral distance (km)	Extent of damage			
	Slight	Moderate	Heavy	None
<25	30	13	7	20
25-<50	2	7	8	25
50-<100	10	1	2	26
100-<150	2	1	1	9
150-<200	1	0	0	6
200-<300	0	0	0	3

A total of more than 40 tunnel damages related to fault movement have been identified following the 1999 Chi-Chi Taiwan earthquake (Wang *et al.* 2001, Chen *et al.* 2012). In addition, fault movements have also caused damages to tunnels situated in the vicinity of faults by inducing permanent deformations of the surrounding ground. Such damages have been reported for the Longxi, Longdongzi and Zipingpu tunnels of the Du Wen highway network (Li 2012). Even though these tunnels did not cross the main fault, secondary effects of fault movement of 2008 Wenchuan earthquake led to severe instabilities. The cases of damage for Shanglongshan, Shaohuoping, Jiujiaya and the Jiangejianmen tunnels are also related to ground deformation induced by fault movement.

2.8.4 Geology

The geological configuration through which the tunnel passes has a significant impact on its stability during seismic shaking. It is observed that seismic damages of mountain tunnels are concentrated at zones which are weathered and fractured. However, tunnel passing through competent rock mass seldom suffer any significant damage.

Observation of instabilities at the portal sections arising due to rockfalls, and sliding and collapse of the geological medium have been widely documented. The high

vulnerability of portals is attributed to the poor geological conditions and shallow overburden depth.

The portal sections are located in highly weathered rock formation or relatively loose quaternary deposits. Such ground conditions lead to amplification of seismic waves resulting in higher ground deformations. The increased seismic demand at these locations generally exceeds the tunnel liner capacity leading to various forms of damages.

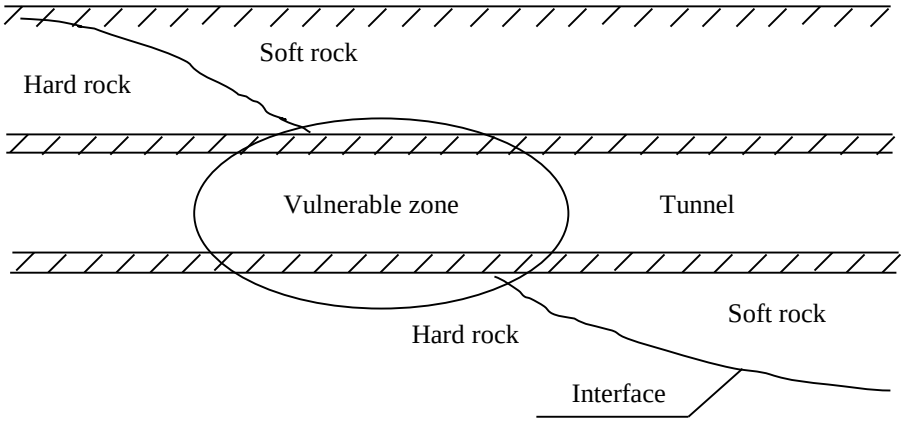

Fig. 2.11. High vulnerability at interface between two types of rock mass

Seismic vulnerability also increases when the tunnel passes through a transition zone between hard and soft rocks. For example, in case of Longxi tunnel, greater seismic damage occurred for the portal region situated in mudstone in comparison to the zone passing through granite rock. Fig. 2.11 illustrates the vulnerability of tunnel passing through a transition zone. In such geological condition, a mismatch in both stiffness and seismic impedance leads to differential kinematic movement. This kinematic movement coupled with amplified ground motion due to the softer strata results in an additional horizontal force on the tunnel liner. This leads to the development of cracks at the junction between the arch shoulder and the sidewall as shown in Fig. 2.12. Such a mechanism is believed to have caused major damage to mountain tunnels as reported by Miyabayashi *et al.* (2008).

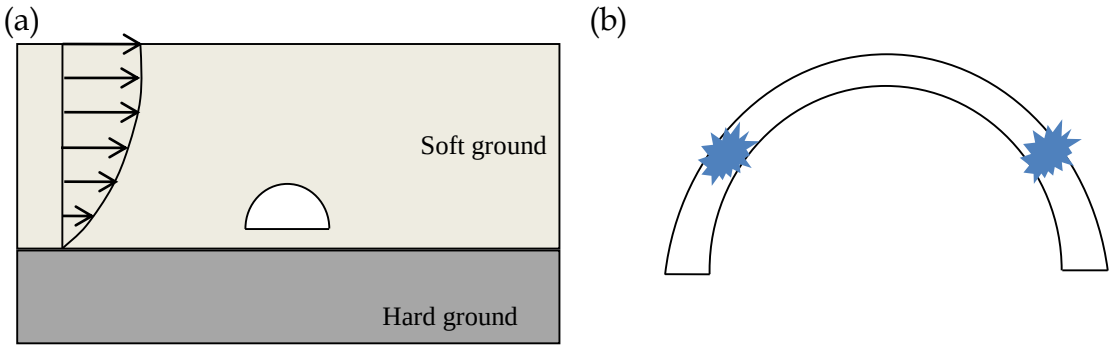

Fig. 2.12. Vulnerability near junction of hard and soft ground (a) Amplified ground movement in softer strata; (b) Development of crack at junction of shoulder and sidewall

The influence of geological conditions has also been recognized for deeper tunnel sections. Damages observed for the Rokko tunnel during 1995 Hyogoken-Nanbu earthquake at sections having comparatively larger overburden depth are also attributed to the prevailing geological conditions. One of the major findings of the investigation was the fact that almost all the damaged sections were located in highly fractured and discontinuous rock mass.

2.9 Plausible Mechanisms of Seismic Damages from Literature

A wide range of tunnel lining failures has been identified based on the case studies of damaged mountain tunnels. A few mechanisms proposed to explain some of them are presented in this section. Fig. 2.13 presents the case of a seismic shear wave propagating along the diagonal directions which causes shear stresses on the tunnel cross-section as shown by dashed lines. These shear stresses can be resolved into a set of horizontal and vertical stresses subjecting the tunnel cross section to compressive and tensile action. As a result of such an action, compressive failure at the arch crown and shear failure at the arch shoulder may occur.

Fig. 2.14 shows a case in which the diagonal stresses give rise to tensile and compressive forces in the horizontal and vertical direction respectively. Such an action causes the vertical compression of the tunnel cross section coupled with an extension of the sidewalls. Spalling of concrete at the sidewalls may be observed in such a scenario resulting in exposure of lining reinforcements.

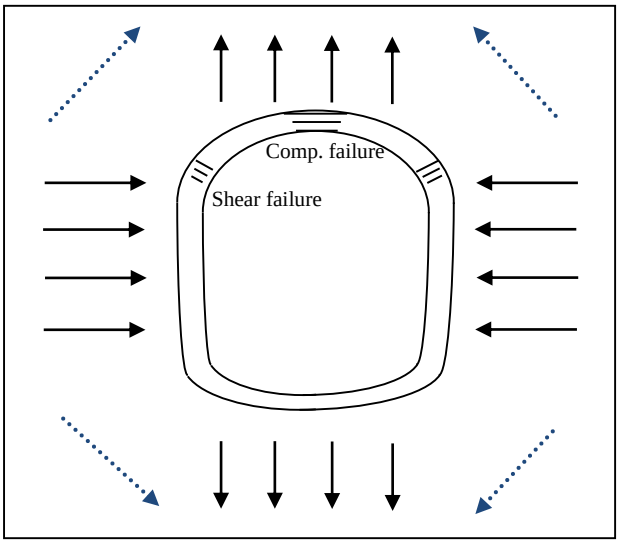

Fig. 2.13. Mechanism of compressive and shear failure of tunnel lining

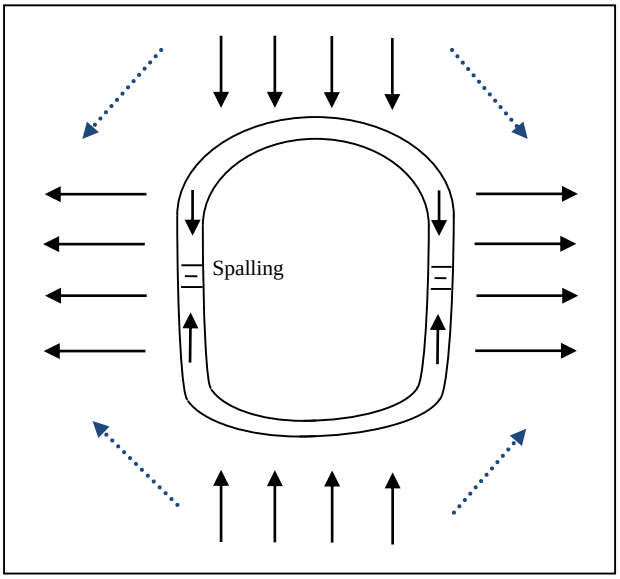

Fig. 2.14. Mechanism of spalling of tunnel lining

With these basic understanding of the mechanism of damages, different failure patterns of tunnel lining may be summarized considering seismic wave propagation as discussed below.

2.9.1 Longitudinal Cracks at Arch Shoulder

The cracking of tunnel lining along the arch shoulder in the longitudinal direction results from vertical propagation of S-waves parallel to the tunnel cross-section. It causes particle movement in a horizontal direction as shown in Fig. 2.15 resulting in stress concentration at the junction of the sidewall and the arch.

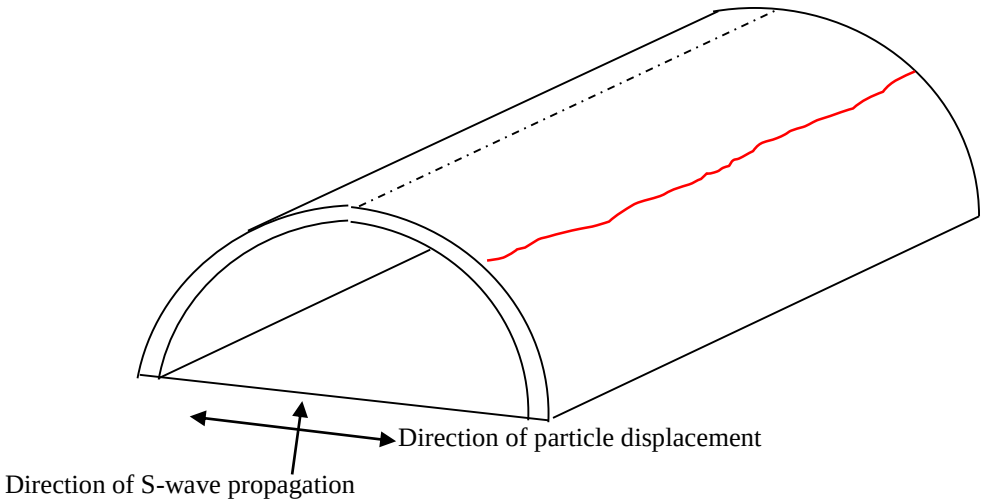

Fig. 2.15. Longitudinal cracks of tunnel lining

2.9.2 Transverse / Circumferential Cracks

Transverse cracks are a result of propagation of P-waves along the direction of tunnel axis. Under this condition, alternate tension and compression along with the pounding of construction joints lead to the development of cracks along the circumference of the tunnel as shown in Fig. 2.16.

2.9.3 Inclined Cracks

Propagation of S-waves in the vertical direction in a plane parallel to the longitudinal axis of the tunnel results in the development of tensile forces resulting in inclined cracks as shown in Fig. 2.17.

2.9.4 Pavement Cracks

The pavement cracks are a result of vertical propagation of high frequency P waves parallel to the cross section. Under such wave propagation pattern arching or bending of the bottom pavement occurs as shown in Fig. 2.18.

2.9.5 Shear Failure of Lining due to Fault Movement

The shearing failure of tunnel lining results from a relative movement of adjacent parts of the tunnel intersecting the fault plane. Generally the damages sustained in such cases are very severe and may result in complete collapse of the tunnel. Fig. 2.19 illustrates the shear failure of lining induced due to fault movement.

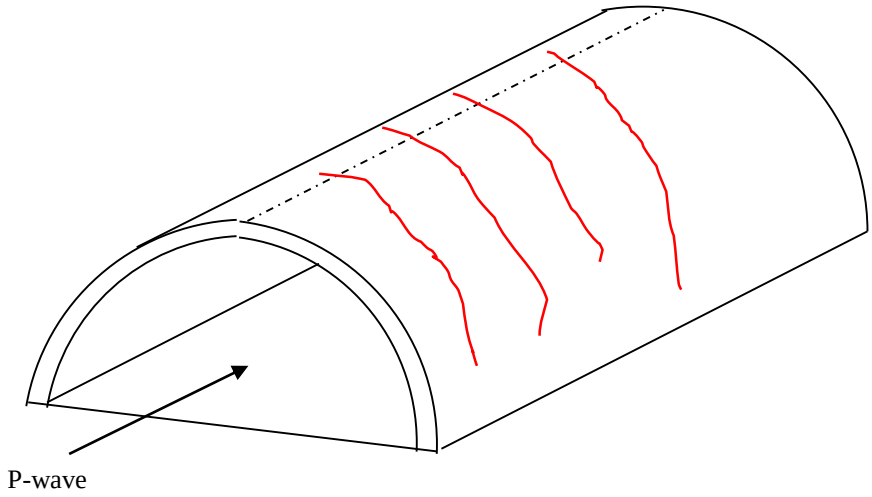

Fig. 2.16. Transverse crack due to propagation of P-wave along longitudinal direction

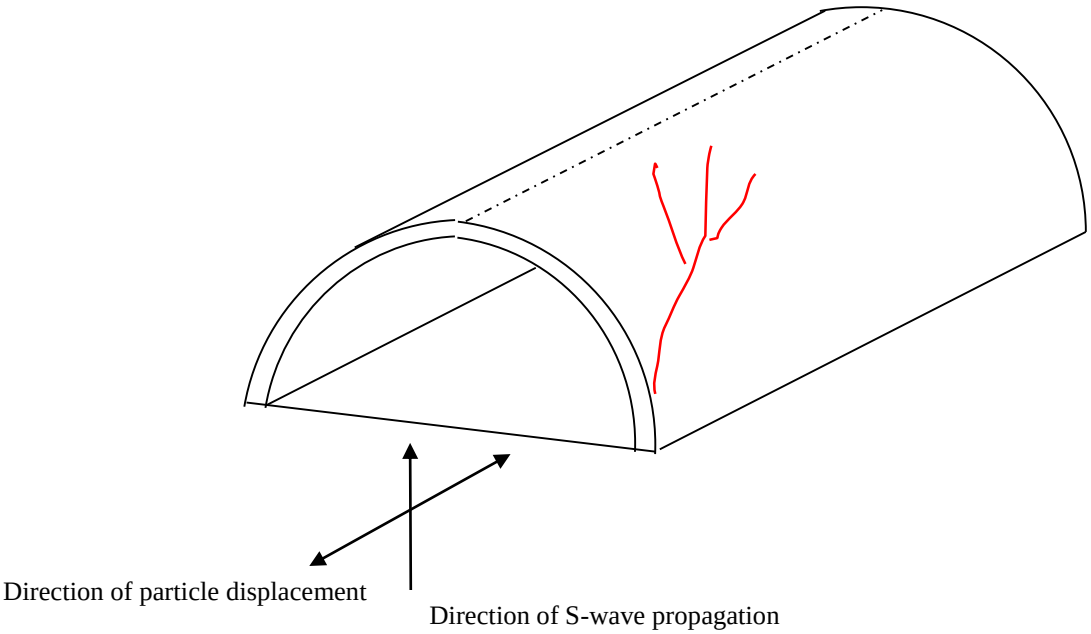

Fig. 2.17. Inclined cracks due to propagation of S-wave

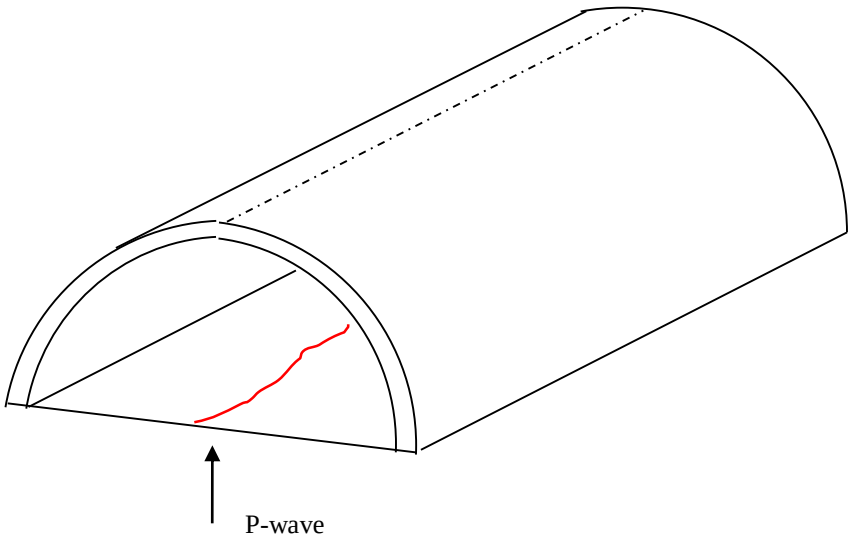

Fig. 2.18. Cracking of bottom pavement under action of P-wave

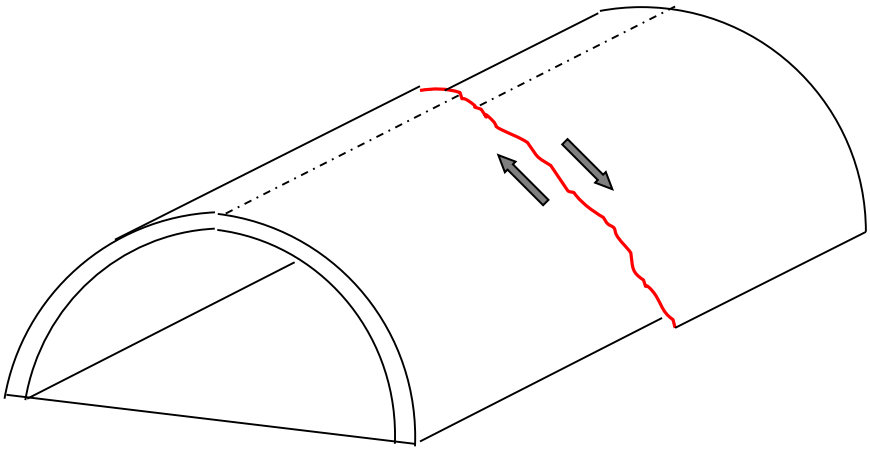

Fig. 2.19. Shear failure of tunnel lining due to fault movement

2.10 Wave Propagation in Discontinuous Medium and Its Implications on Assessment of Dynamic Behavior of Tunnels

The detailed review of seismic damages sustained by tunnels suggest the vulnerable sections to be majorly located in highly fractured and weathered geological region. Such discontinuous geological medium possesses low self-arching capability and a high possibility of developing loosened blocks of rocks under dynamic action. In

fact, the interaction of the waves with the discontinuous medium may significantly influence the response of the tunnel excavations.

Some prominent studies and findings documented in the literature dealing with wave propagation across joints have been reported by Pyrak-Nolte *et al.* (1990), Boadu and Long (1996), Cai and Zhao (2000) and Zhao *et al.* (2006) among others. Pyrak-Nolte *et al.* (1990) derived an expression for transmission and reflection coefficients for wave propagation across a single discontinuity, accounting for the effect of the discontinuity stiffness and wave frequency. Furthermore, the case of wave propagation across a number of parallel fractures with multiple reflections and refractions has been reported by Zhao *et al.* (2006). In case of multiple joints, it has been observed that the ratio of wavelength to joint spacing has a prominent effect on wave propagation. Moreover, the results suggest that the discontinuous medium act as a low pass frequency-filter and has a strong influence on wave transmission across the discontinuous medium. These findings may have a severe implication with regard to the dynamic stability of tunnels in discontinuous rock mass and needs further investigations.

2.11 Gap Areas

The use of discrete methods for the evaluation of deformation response of tunnel excavation in jointed rock mass has been a welcome step. This approach has advanced our current understanding and has provided useful insights into the role of various parameters on the deformation response. However, in most of these studies, the discontinuities have been idealized with parallel joint sets. It has been suggested that such idealization may not always hold true. Hence, a more realistic idealization is necessary to make reliable and accurate predictions. In addition, an investigation into the role of the deformation parameters of the joints *i.e. joint normal stiffness* (k_n) and *joint shear stiffness* (k_s), which has been rarely reported in the literature, needs further attention.

In contrast to the static case, the use of the discrete method for dynamic analyses of tunnels in jointed rock mass has been rare. Mostly, the dynamic analyses have been performed by idealizing the geological medium as being continuous, thereby

neglecting the interaction between the dynamic waves and joints. Such approximation fails to accurately capture the mechanical and kinematic response of discontinuous rock mass, such as the structurally controlled movement of rock blocks, dissipation of energy along the joints, multiple reflection and refraction of seismic waves and the frequency filtering effect. Since seismically induced tunnel damages have been found in the weathered and fractured zone, having a blocky rock mass structure, an assessment of the dynamic behavior of tunnels using discrete method is necessary.

2.12 Objectives

Based on the gap area identified from the review of the literature, the main objectives of the present study are: i. to identify the parameters which have a major influence on the deformation response of tunnel excavations and ii. assess the dynamic behavior of lined tunnel in the blocky rock mass considering the interaction between waves and joints. To meet the objectives, the consideration of the following salient points is required.

1. More accurate idealization of the blocky structure of the rock mass as against the widely adopted parallel joint set idealization.
2. Assess the contribution of various parameters on the deformation response of tunnel excavations and identify the probable mode of rock block movement.
3. Investigate the influence of frequency of input motion on tunnel response taking into account the interaction of dynamic waves with the randomly oriented joints.
4. Evaluate the effect of tunnel depth, in-situ stress ratio, type of waves and PGA on the dynamic response of lined tunnel in the blocky rock mass.
5. Corroborate the observations obtained from the discontinuum based numerical model with the pattern of damages reported in the literature.
6. Propose an effective measure to improve the seismic performance of tunnels in the discontinuous rock mass.

…

Chapter 3

MODELING AND METHODOLOGY

3.1 Introduction

The present chapter provides an introduction to the Distinct Element Method, highlighting its robust capability in simulating the response of discontinuous medium such as jointed and blocky rock mass. An overview of the commercial software package, Universal Distinct Element Code (UDEC) is provided. The various boundary conditions available in UDEC for performing the dynamic analysis is presented. Detailed description of the numerical models and boundary conditions adopted in the present study are discussed. The statistical method employed for assessment of significant parameters affecting the deformation response of tunnel excavations has been explained.

3.2 Distinct Element Method

The origin of the Distinct Element Method draws heavily from the requirements of simulating engineering problems falling within the domain of rock mechanics (Jing and Hudson 2002). In this modeling approach, the entire problem domain to be numerically simulated is treated as an assemblage of blocks, which may be rigid or deformable. Interfaces exist between these blocks which replicate the geological discontinuities. Since the interface is treated as a boundary condition, simulation of large-scale movement of the rock blocks, including rotation and complete detachment is possible, making it versatile and robust for investigating the response of structures built in or on the jointed rock mass (Jing 2003).

3.2.1 Universal Distinct Element Code (UDEC)

In the present study, the distinct element based commercial software *Universal Distinct Element Code (UDEC)* has been used. This software has been extensively utilized for various rock mechanics application such as stability analyses of jointed rock slopes, underground excavations, dams and dam foundations, and masonry structures. The software facilitates the simulations of intact rock and rock joints

considering the widely used constitutive laws suggested in the literature. Apart from routine analysis, an inbuilt programming language FISH is also provided which enables the users to perform customized numerical analysis (*Itasca Inc.* 2004).

3.2.2 Solution Procedure in UDEC

The solution of a numerical simulation in UDEC is based on a series of calculations which alternates between the application of the force-displacement law at all the contacts and Newton's second law of motion for all the blocks. A flowchart depicting the solution process is shown in Fig. 3.1. During a single calculation cycle, the contact forces are evaluated, and the out of balance forces are transferred to the respective blocks. In case of rigid blocks, Newton's law of motion is utilized to evaluate the velocities and displacements. For deformable blocks, the gridpoint velocities and displacements are evaluated, which are subsequently utilized to work out the zone stresses and gridpoint forces. These forces are used to update the position of the blocks which lead to the completion of a single cycle of calculation. At the end of the cycle, the configuration of the individual blocks change, resulting in new contact forces to be generated. The entire process is repeated for the next cycle. The process continues till a stable state is achieved.

The equations utilized in the solution process is discussed here. Considering the 1-dimensional case, the resultant force $F^{(t)}$ acting on a mass m produces acceleration which may be expressed using Eqn (3.1),

$$\frac{d\dot{u}}{dt} = \frac{F^{(t)}}{m} \qquad \text{Eqn (3.1)}$$

where $\dot{u}$ is the block velocity and t is the time.

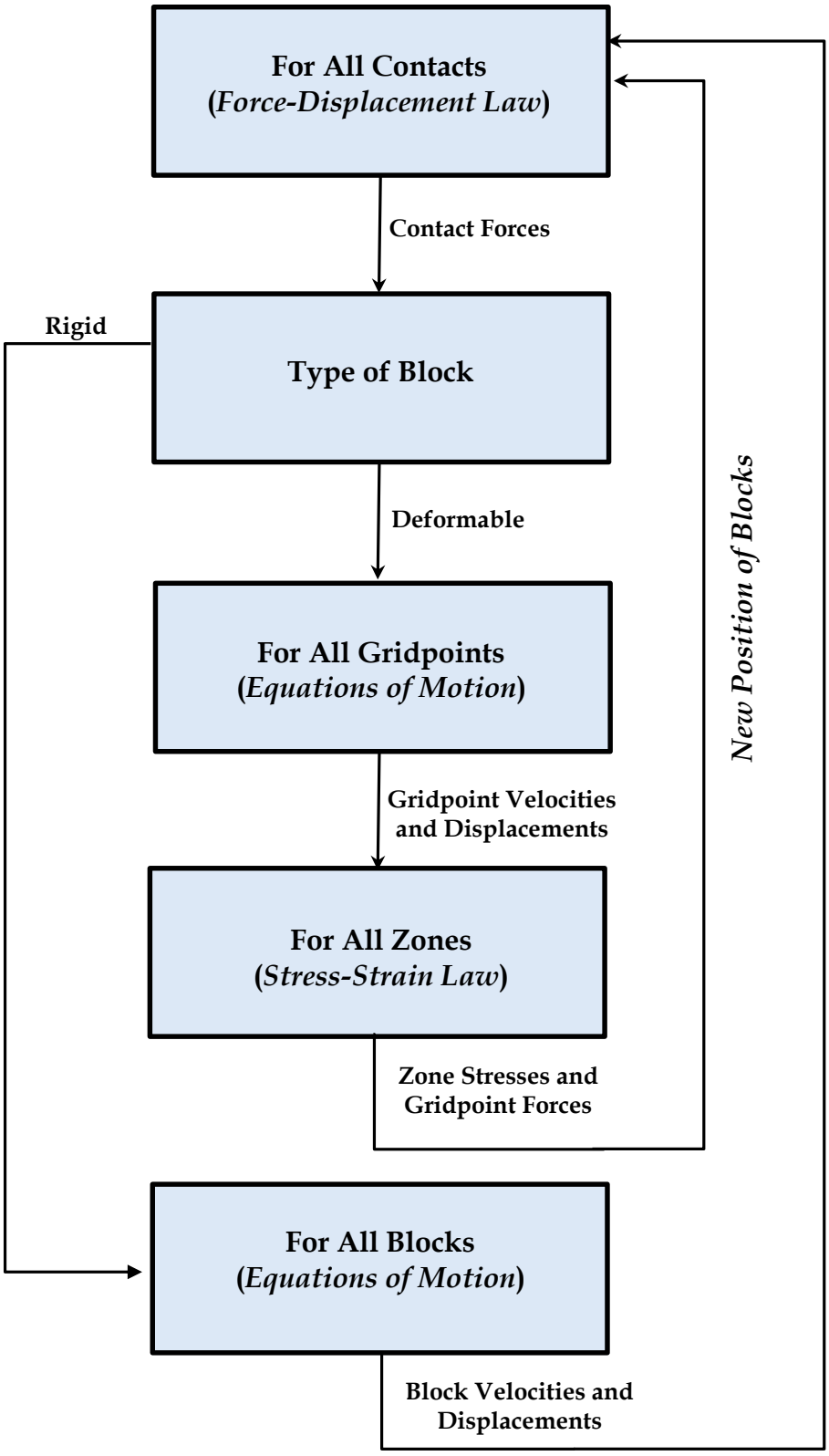

Fig. 3.1. Solution Cycle of a problem simulated in Universal Distinct Element Code (UDEC) (adopted from *Itasca Inc.* 2004)

Using the central difference scheme, the left-hand side of Eqn (3.1) can be expressed as

$$\frac{d\dot{u}}{dt} = \frac{\dot{u}^{(t+\Delta t/2)} - \dot{u}^{(t-\Delta t/2)}}{\Delta t} \qquad \text{Eqn (3.2)}$$

Substitution of Eqn (3.2) in Eqn (3.1) leads to Eqn (3.3)

$$\dot{u}^{(t+\Delta t/2)} = \frac{F^{(t)}}{m}\Delta t + \dot{u}^{(t-\Delta t/2)} \qquad \text{Eqn (3.3)}$$

Since velocities are stored at the half-timestep point in UDEC, it becomes possible to express displacement using Eqn (3.4). Thus, the positions of the blocks are updated at the end of a single cycle.

$$u^{(t+\Delta t/2)} = u^{t} + \dot{u}^{(t+\Delta t/2)}\Delta t \qquad \text{Eqn (3.4)}$$

For the general case of two-dimensional problems, which are acted by large number of forces and gravity, Eqns (3.5) and (3.6) gives the velocity and rotation respectively,

$$\dot{u}_i^{(t+\Delta t/2)} = \dot{u}_i^{(t-\Delta t/2)} + \left(\frac{\sum F_i^{(t)}}{m} + g_i\right)\Delta t \qquad \text{Eqn (3.5)}$$

$$\dot{\theta}_i^{(t+\Delta t/2)} = \dot{\theta}_i^{(t-\Delta t/2)} + \left(\frac{\sum M^{(t)}}{I}\right)\Delta t \qquad \text{Eqn (3.6)}$$

where $\dot{\theta}$ is the angular velocity, I is the moment of inertia, $\sum M$ is the total moment on the block, $\dot{u}_i$ are the velocity components and g_i are the components of the gravitational acceleration.

Thus, the solution of a UDEC simulation follows a time stepping algorithm. The time step for a single cycle is evaluated by UDEC, which is kept very small to ensure that velocities and displacements are constant within a single timestep. In case of rigid blocks, the timestep is evaluated based on the block mass and the stiffness of the interface between the blocks. For deformable blocks, the time step is decided based on the zone size and the stiffness contribution from the intact rock blocks and the contacts between them.

3.2.3 Boundary Conditions in UDEC for Dynamic Analysis

Underground excavations involve geological medium which is unbounded and extends up to an infinite extent. However, only a finite volume of the geological

medium can be considered in a numerical model, which requires the use of proper boundary conditions at the artificial boundaries. In case of static analysis, the use of stress or displacement boundary condition, placed at a sufficiently large distance away from the tunnel excavation holds good for making reliable numerical predictions. However, in case of dynamic analysis, these boundary conditions reflect the outward propagating waves back into the model and fail to simulate the necessary energy radiation. To overcome this issue, UDEC offers additional boundary conditions, *i.e., quiet (or absorbing)* and *free field*, for dynamic numerical simulations.

The quiet boundary condition uses independent dashpots attached in normal and shear directions at the artificial boundaries, which provide viscous normal and shear tractions as per Eqn (3.7) and Eqn (3.8),

$$t_n = -\rho C_p v_n \qquad \text{Eqn (3.7)}$$

$$t_s = -\rho C_s v_s \qquad \text{Eqn (3.8)}$$

where ρ is the mass density of the medium, C_p and C_s are the p-wave and s-wave velocities, v_n and v_s are the normal and shear components of velocities at the boundaries.

The viscous terms can be incorporated directly into the equations of motion for the gridpoints which lie on the artificial boundaries. Alternatively, in UDEC, these traction forces are applied at each time step at the boundaries to replicate the energy radiation.

UDEC also provides the option of free field boundary conditions for dynamic numerical analysis. In this, a one-dimensional column of unit width is attached to the main numerical model at a number of gridpoints along the artificial boundary of the main model, using dashpots in the normal and shear directions. The one-dimensional column replicates the response of an extended medium. Based on the mismatch between the velocities of the main numerical model and the one-dimensional free field column at the shared gridpoints, additional forces are invoked by the dashpots. Eqn (3.9) and Eqn (3.10) are used to invoke forces at the lateral boundaries which ensure that no distortion of outward propagating waves occur.

$$F_x = -\rho C_p (v_x^m - v_x^{ff}) + \sigma_{xx}^{ff} \Delta S_y \qquad \text{Eqn (3.9)}$$

$$F_y = -\rho C_s (v_y^m - v_y^{ff}) + \sigma_{xy}^{ff} \Delta S_y \qquad \text{Eqn (3.10)}$$

where ρ is the mass density of the medium, C_p and C_s are the p-wave and s-wave velocities, v_x^m and v_y^m are the x and y velocities at the gridpoints of the lateral boundary of the main model, v_x^{ff} and v_y^{ff} are the x and y velocities at the gridpoints of free field column, σ_{xx}^{ff} and σ_{xy}^{ff} are the mean free field horizontal stress and mean free field shear stress at the gridpoints and ΔS_y is the mean vertical zone size at the boundary gridpoint.

3.2.4 Voronoi Tessellation Scheme in UDEC

To simulate the response of an excavation in the blocky rock mass, the Voronoi tessellation feature has been utilized in the present study. This feature allows the creation of randomly sized polygonal blocks, thereby dividing the entire model into a number of rock blocks as shown in Fig. 3.2. Strength and deformation properties are specified to the edges of these blocks to simulate the mechanical response along the geological discontinuities such as joints.

3.3 Modeling of Tunnel Excavation in Rock Mass

In the present study, the assessment of the deformation response of tunnel excavation has been studied with two different idealizations of the discontinuities. The first idealization corresponds to the parallel joint sets, which has been extensively adopted in a number of investigations reported in the literature. The second scheme of idealization corresponds to the use of Voronoi polygonal blocks, and corresponds to a blocky rock mass structure. A discussion of the model configuration for both the cases follow.

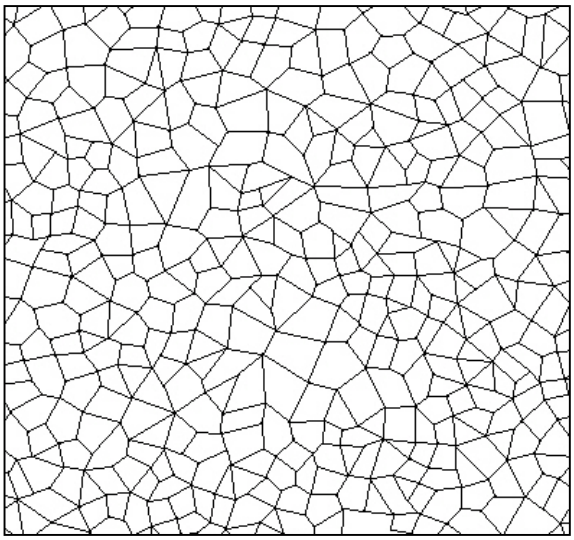

Fig. 3.2. Illustration of the polygonal structure used to simulate blocky rock mass using Voronoi tessellation

3.3.1 Parallel Joint Sets

The first case corresponds to the idealization of the discontinuities with two sets of parallel joints. The two sets of joint J1 and J2 have identical dips (α and β respectively) of 30^0 with a spacing (S1 and S2 respectively) of 3m. A circular tunnel having a diameter of 10m is excavated at a depth (d) of 100m below the ground surface. The width and height of the model are kept as 20 times the diameter of the tunnel opening, to eliminate any unfavorable boundary effects (Kulhawy 1974). In-situ stress has been considered due to the weight of the overlying rock mass with the vertical stress varying linearly with depth. The lateral boundaries are considered to be on rollers, restricting movement in the horizontal direction. The bottom boundary is also specified as a displacement boundary, which is fixed in both the horizontal and vertical directions. A schematic view of the tunnel profile with joint sets J1 and J2 is presented in Fig. 3.3. Intact rock between the joint sets J1 and J2 has been modeled as an elastic-perfectly plastic material following Mohr-Coulomb failure criteria. The constitutive law for joints also follows the Mohr-Coulomb criteria.

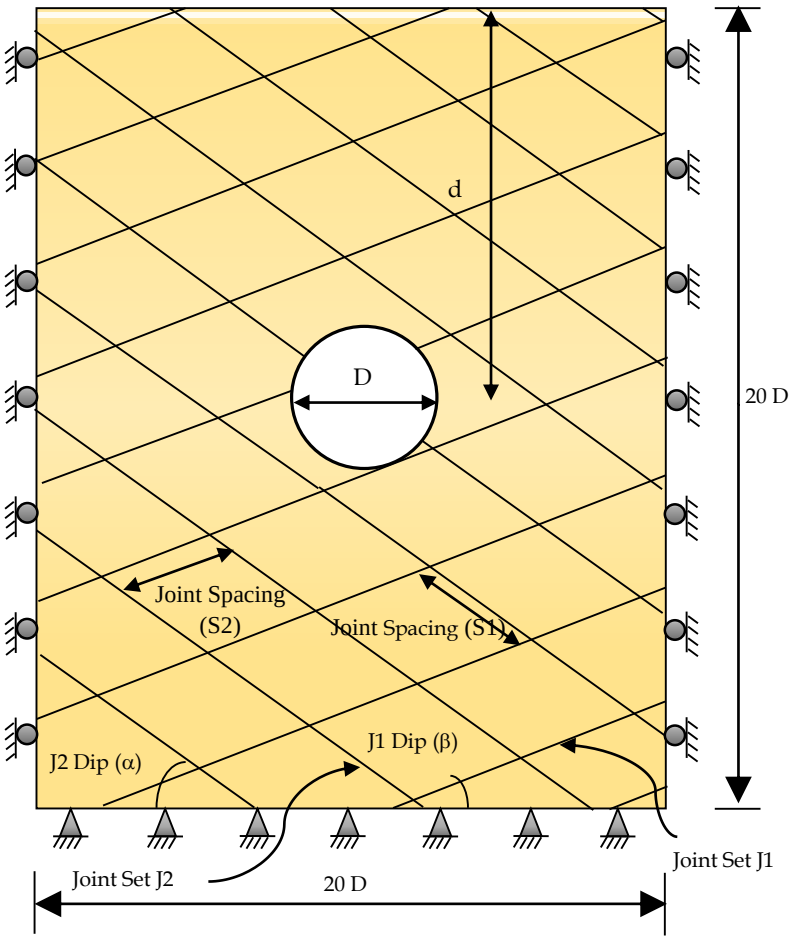

Fig. 3.3. Schematic of considered tunnel in rock mass with the discontinuities idealized with parallel joint sets

3.3.2 Blocky Rock Mass

The schematic representation of the numerical model is shown in Fig. 3.4. As with the previous case, the circular tunnel has a diameter (D) of 10m which is located at a depth (d) of 100m below the ground surface. To simulate the fractured and blocky nature of the rock mass, Voronoi tessellation scheme has been adopted to idealize the discontinuities. The feature creates randomly sized polygons representing the blocky nature of the medium around the tunnel. The dimension of the model has been kept as 20D in both horizontal and vertical direction to ensure that no adverse boundary effects occur. Regarding the boundary conditions, the lateral sides have been restrained in the horizontal direction whereas the bottom boundary has been restrained in both the horizontal and vertical direction. Mohr-Coulomb constitutive law is utilized for both the intact rocks and the joints. Brittle fracturing is allowed to

occur along the edges of the Voronoi blocks in the event of the strength of the joint is exceeded.

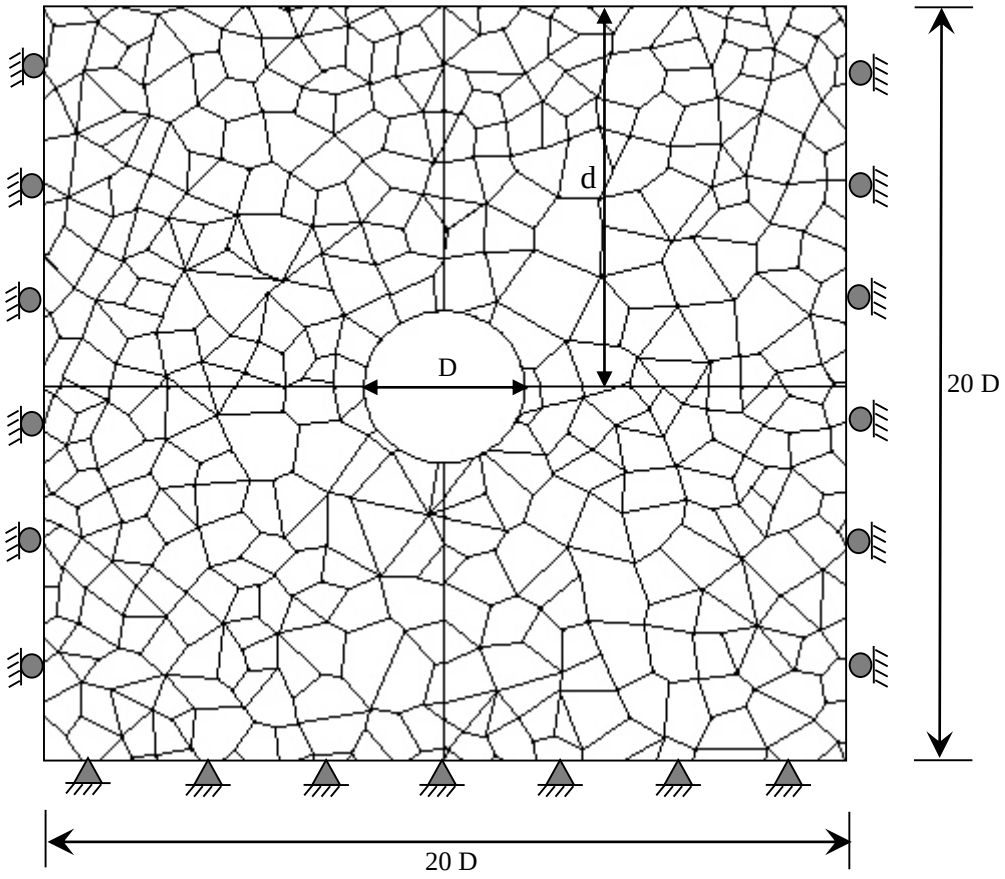

Fig. 3.4. Schematic view of considered tunnel in blocky rock mass

3.4 MODELING FOR DYNAMIC ANALYSES

To investigate the dynamic response of the lined tunnel, the model considered in *Section 3.3.2* has been adequately modified, with regard to the boundary conditions. Fig. 3.5 shows a schematic representation of the circular lined tunnel having a diameter D (10m). The tunnel is considered to be located at variable depths d (50m, 75m, and 150m) below the ground surface. The tunnel liner has been simulated using two-dimensional beam elements. The liner, having a thickness of 0.4m, is assumed to be perfectly bonded to the surrounding rock mass, which is achieved by setting the properties of the interface to very high values to effectively glue them together (*Itasca Inc.*, 2004). This condition is similar to most of the investigations reported in the literature. An elastic behavior has been assumed for the liner in all

the analyses carried out in the present study. The density of the liner is 2500 kg/m^3, having an elastic modulus of 30GPa and Poisson's ratio of 0.2.

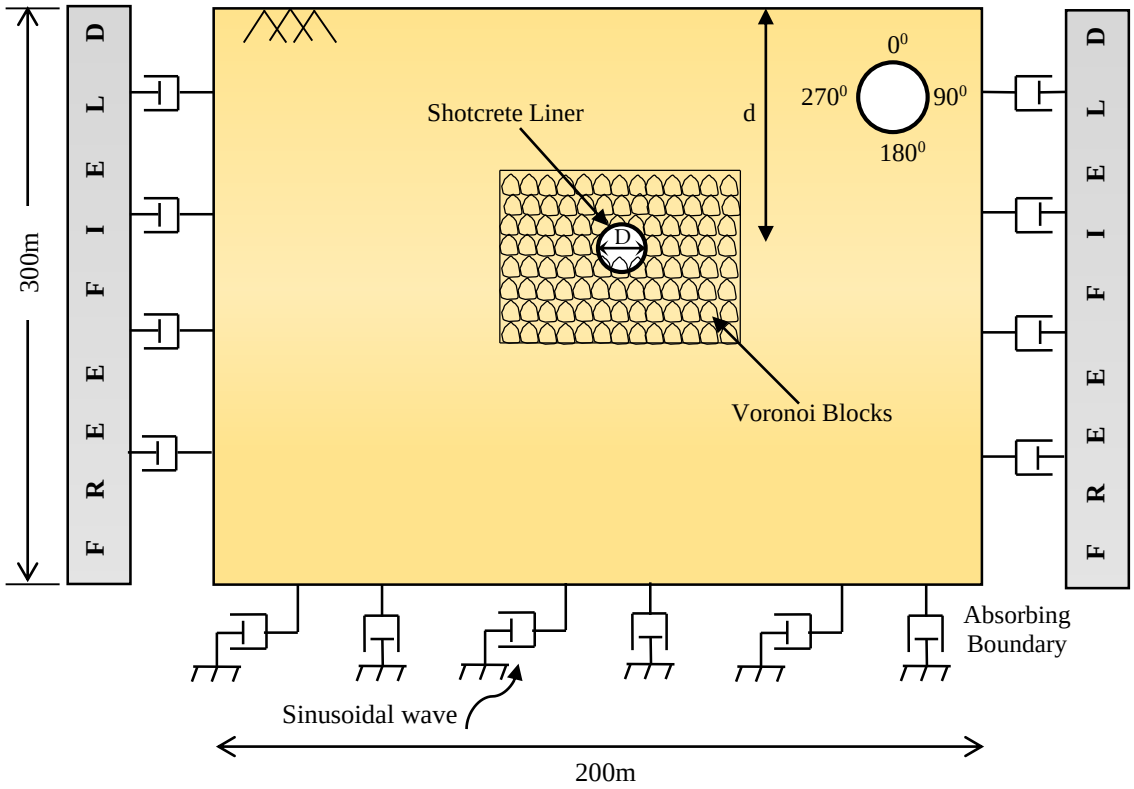

Fig. 3.5. Schematic view of circular lined tunnel in the blocky rock mass for dynamic analysis

The mesh size adopted for the model has been finalized based on the following considerations:

1. Ensuring the efficient propagation of waves of dominant frequencies considered in the present study.
2. To capture the stress gradient in the geological medium in the vicinity of the circular lined tunnel.

To meet the above requirements, graded meshing has been utilized in the numerical model. The first condition has been met by keeping the mesh size smaller than 1/10th of the smallest wavelength of the sinusoidal wave and earthquake time history considered. The second requirement has been met by incorporating a finer discretization in regions close to the tunnel which gradually becomes coarser with increasing distance from the tunnel periphery. It is ensured that the maximum size

does not violate the conditions necessary to meet the requirements of effective wave propagation.

To minimize the influence of the artificial boundaries during dynamic analyses, free field boundary conditions have been invoked at the lateral sides. Also, viscous dashpots have been attached to the bottom boundary to ensure the effective application of dynamic waves and efficient absorption of reflected waves. Moreover, the dimensions of the numerical model have been kept as 200m (20D) x 300m (30D) in all the analyses minimizing the boundary effects on the response of the tunnel. Analyses have been carried out for both S and P waves. In addition, an earthquake time history has also been considered.

The use of dashpots at the bottom boundary requires the dynamic input to be converted into stress waves. This has been achieved through Eqn. (3.11) and Eqn. (3.12),

$$\sigma_s = 2\rho C_s V_s(t) \qquad \text{Eqn (3.11)}$$

$$\sigma_n = 2\rho C_p V_n(t) \qquad \text{Eqn (3.12)}$$

A factor of two is applied as the dashpots provide viscous normal and shear stresses as per Eqn (3.13) and Eqn (3.14),

$$\sigma_s = -\rho C_s V_s(t) \qquad \text{Eqn (3.13)}$$

$$\sigma_n = -\rho C_p V_n(t) \qquad \text{Eqn (3.14)}$$

where σ_s is applied shear stress, σ_n is applied normal stress, ρ represents the mass density of the material, C_s is the shear (S) wave velocity, C_p is the compression (P) wave velocity, $V_s(t)$ is the instantaneous horizontal input motion velocity and $V_n(t)$ is the instantaneous normal input motion velocity. Before every dynamic analysis, an initial static in-situ stress state has been invoked to establish the initial equilibrium. The results of the dynamic numerical simulations have been expressed in terms of the dynamic axial force and bending moment developed in the tunnel liner for various angles along the tunnel periphery as shown in the inset of Fig. 3.5.

3.5 Statistical Approach for Identification of Influencing Parameters

The methodology followed to identify the effect of various parameters on tunnel excavation deformation is based on the application of the concepts of *Design of Experiments* (DOE) (Montgomery 2013). DOE provides a powerful tool to evaluate the cause-and-effect relation between the system response and the input parameters by conducting limited number of numerical simulations. Thus, it brings down the computational burden, especially when the effect of a large number of parameters is to be considered. For efficient implementation of the DOE approach in UDEC, the factorial design concept has been adopted to establish the combination of input parameters to be numerically simulated. Based on the results of the analyses, the influence of each of the considered parameters on the deformation response has been quantified. A concise discussion of the methodology is provided in subsequent sections.

3.5.1 Concept of Factorial Design

The implementation of Design of Experiments (DOE) requires numerical simulations to be performed with certain combinations of input parameters. To frame the combinations, the factorial design has been utilized in the present study. Among various cases of factorial designs, the 2^k designs, where k denotes the number of parameters, have found wide application in engineering studies. In such design, each parameter is assigned two levels: low and high. Thus for a system dependent on k factors, 2^k number of experiments is required to be conducted (Montgomery 2013).

Figure 3.6 presents a flowchart which summarizes the major steps adopted for the identification of the parameters affecting the deformation response of tunnel excavations. Since the present study assesses the influence of five parameters *viz.*, cohesion, friction angle, normal stiffness and shear stiffness of joints and the in-situ stress ratio, a total of 32 combinations of input parameters have been selected using the Point Estimate Method (Rosenblueth 1975). ANOVA (Analysis of Variance) has been performed on the obtained results and the influence of each parameter has been identified.

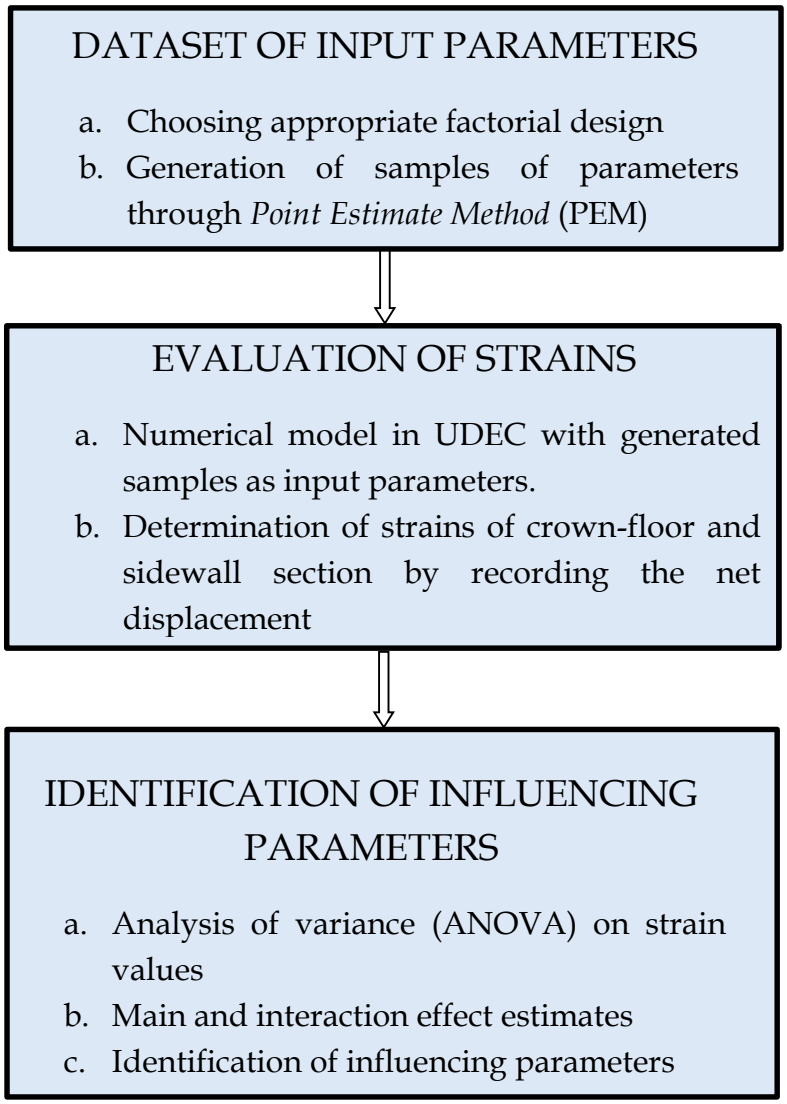

Fig. 3.6. Flowchart depicting the steps adopted for identification of the influencing parameters

3.5.2 Assessment of Influence of Various Parameters

The effects of individual parameters on the response of a system are summarized in the form of main and interaction effect estimates. For clarity, a brief discussion dealing with the evaluation of these estimates is provided below.

Suppose the system response is dependent on three factors A, B and C each at two levels: low and high denoted by - and + respectively. In such case, 2^3 factorial design may be adopted with total eight runs and parameter combinations as illustrated in Table 3.1. In any combination, the high level of a factor is defined by the corresponding lower case letter. By convention, (1) denotes the case where all

the parameters are at their respective low levels. Thus, ab represents the case where factors A and B are at their corresponding high level and factor C is at a low level. Similar convention may be extended for other labels. Fig. 3.7 provides the various combinations possible in case of 2^3 factorial design with an illustration of the meaning of various labels.

The average effect of a factor on the response of a system is defined as the change in the response arising as a result of a change in the level of that particular factor averaged over the levels of all other factors involved in the system. Thus, by definition, the average effect of A, also known as the main effect, may be evaluated using Eqn. (3.15). The interpretation of each term of Eqn. (3.15) is explained below.

The effect of A when both B and C are at low levels is given by $[a-(1)]/n$. Similarly, the effect of A when B is at a low level, and C is at a high level is given by $[ac-c]/n$. $[ab-b]/n$ represent the effect of A when B is at a high level, and C is at a low level. Finally, the effect of A when both B and C are at high levels is given by $[abc-bc]/n$. It should be noted that the term n denotes the number of replicates of the experiment. In the case of no replication, the value of n becomes 1.

Similarly, the equations for main effects of factor B and C are given by Eqn. (3.16) and Eqn. (3.17) respectively.

Table 3.1. Combination of parameters in 2^3 factorial design

Run	A	B	C	Label
1	-	-	-	(1)
2	+	-	-	a
3	-	+	-	b
4	+	+	-	ab
5	-	-	+	c
6	+	-	+	ac
7	-	+	+	bc

8	+	+	+	*abc*

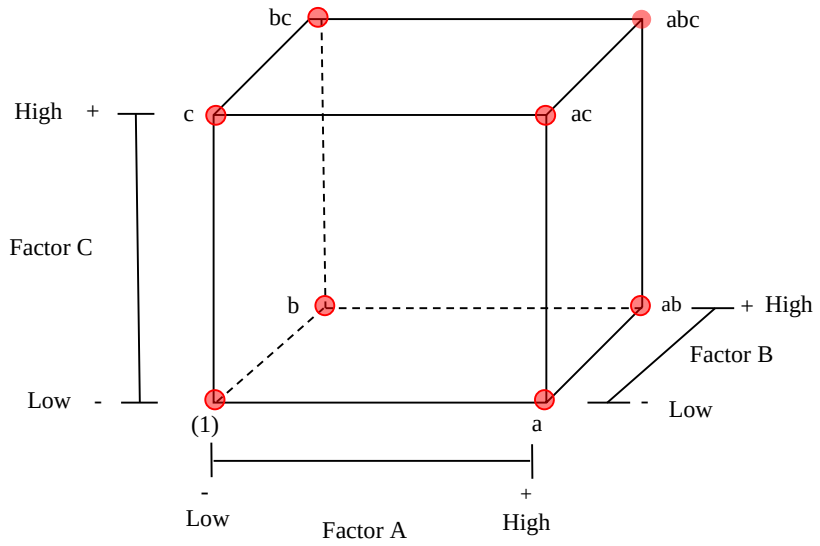

Fig. 3.7. Various combinations of experiment run in a 2^3 factorial design

$$A = \frac{1}{4n}\left[a - (1) + ab - b + ac - c + abc - bc\right] \qquad \text{Eqn (3.15)}$$

$$B = \frac{1}{4n}\left[b + ab + bc + abc - (1) - a - c - ac\right] \qquad \text{Eqn (3.16)}$$

$$C = \frac{1}{4n}\left[c + ac + bc + abc - (1) - a - b - ab\right] \qquad \text{Eqn (3.17)}$$

For interaction between two factors say AB, Eqn. (3.18) is used. The interaction AB is the difference between the average effects of A at two levels of B. Similarly, Eqn. (3.19) and Eqn. (3.20) are used for estimating the interaction effects of BC and AC respectively.

$$AB = \frac{\left[abc - bc + ab - b - ac + c - a + (1)\right]}{4n} \qquad \text{Eqn (3.18)}$$

$$BC = \frac{1}{4n}\left[(1) + a - b - ab - c - ac + bc + abc\right] \qquad \text{Eqn (3.19)}$$

$$AC = \frac{1}{4n}\left[(1) - a + b - ab - c + ac - bc + abc\right] \qquad \text{Eqn (3.20)}$$

For three-factor interaction ABC, Eqn. (3.21) is applicable which denotes the average difference between the interaction term AB at two different levels of C.

$$ABC = \frac{[abc - bc - ac + c - ab + b + a - (1)]}{4n} \qquad \text{Eqn (3.21)}$$

The terms in the brackets of Eqn. (3.15) to Eqn. (3.21) are also known as the contrasts in the treatment combinations (Montgomery 2013). Using the contrasts, the sum of squares for the effect estimates may be evaluated as per eqn. (3.22). Based on the sum of squares of various terms, the percentage contribution towards the response may be evaluated.

$$SS = \frac{(Contrast)^2}{8n} \qquad \text{Eqn (3.22)}$$

The concept discussed for three parameters may be extended for any number of parameters.

The present study has made use of the *Point Estimate Method* (PEM) for the generation of samples required in the implementation of factorial design discussed above. A brief discussion on PEM in generating samples of random parameters is presented next.

3.5.3 Generation of Samples through Point Estimate Method

As discussed in the previous section, the factorial design approach requires the determination of response at various combinations of factors. One of the efficient ways of forming combinations of factors is the application of point estimate method developed by Rosenblueth (1975). As per the original formulation, each random parameter is represented by two point estimates: high and low, given by Eqn. (3.23).

$$x_i^{\pm} = \mu_{xi} \pm \sigma_{xi} \qquad \text{Eqn (3.23)}$$

where μ_x is the mean and σ_x is the standard deviation of parameter X_i. Ahmadabadi and Poisel (2016) provides a detailed discussion on the application of the point estimate method. The above study highlights and summarizes the advantages, limitations, and modifications to be made to the original formulation depending on

the characteristics of the data considered. In the present study, a minor modification has been made in the original formulation represented by Eqn. (3.23). The point estimates in the present study are evaluated using Eqn. (3.24) for all the random variables considered as they are normally distributed (Zhang and Goh 2012).

$$x_i^{\pm} = \mu_{xi} \pm 1.645\sigma_{xi} \qquad \text{Eqn (3.24)}$$

where, μ_{xi} and σ_{xi} represents the mean and standard deviation of the parameter x_i .

…

Chapter 4

VERIFICATION STUDIES IN UDEC

4.1 Introduction

In the present chapter, the results obtained from the UDEC software has been compared with well-established analytical and field reported results. First, the verification of stress distribution around a circular hole in a bi-axially loaded elastic plate is presented. Subsequently, the verification of problems dealing with wave propagation across a single and multiple joints in a rock column is discussed. The utilization of Voronoi tessellation scheme and its applicability for simulating cracks/fractures is also verified. The feasibility of using the Voronoi approach in capturing field observations, as reported in the literature, for an underground excavation is also presented.

4.2 Tunnel in Elastic Medium

The first verification study deals with the problem of a circular tunnel in an elastic medium. Kirsch solution has served as a benchmark for tunnel excavation in an elastic medium. This solution provides the distribution of stresses around a circular hole in a bi-axially loaded plate composed of homogeneous, isotropic, continuous and linearly elastic material (Goodman 1989). The tangential stress at polar coordinate r and θ near an opening with radius a and subjected to horizontal and vertical compressive stresses P_1 and P_2 respectively, is given by Eqn. (4.1).

$$\sigma_\theta = \frac{P_1 + P_2}{2}\left(1+\frac{a^2}{r^2}\right) - \frac{P_1 - P_2}{2}\left(1+\frac{3a^4}{r^4}\right)\cos 2\theta \qquad (4.1)$$

The schematic of the model considered is shown in Fig. 4.1. A circular opening having a diameter D is subjected to compressive stresses P_1 and P_2 in the vertical and horizontal directions respectively. The diameter is taken as 4m whereas the stresses in both the directions are kept equal to 10MPa. The height H and width W of the model have been taken as 100m. The solution in UDEC has been obtained in two steps. In the first step, initial equilibrium is established before excavating the

circular opening. Subsequently, monitoring points have been incorporated along a vertical line, extending upwards from the crown, to record the tangential stresses. In the second step, the excavation is made. A sufficient number of cycles are then run till the system unbalance force becomes constant. The tangential stress obtained from the analysis is presented in Fig. 4.2 which shows close agreement with the Kirsch solution.

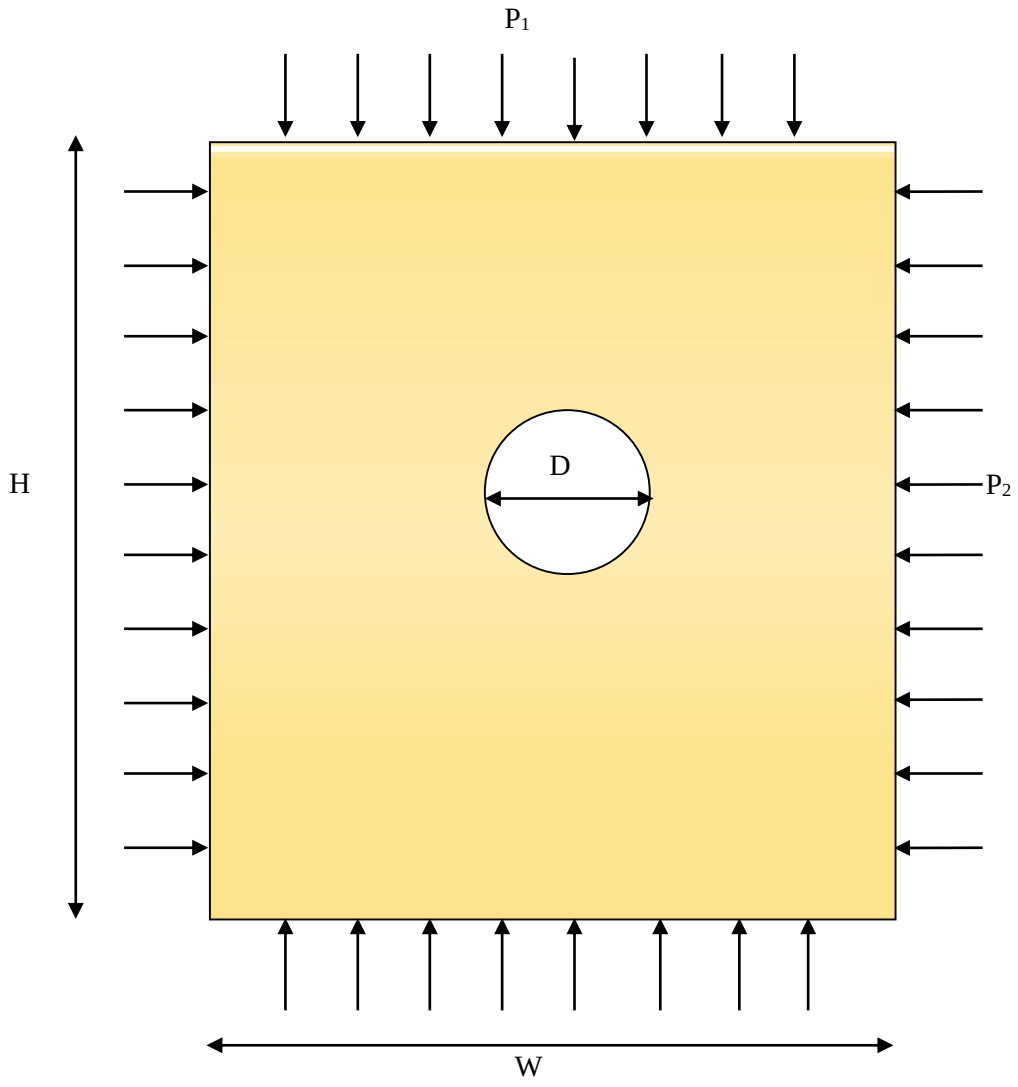

Fig. 4.1. Schematic of circular tunnel in elastic medium

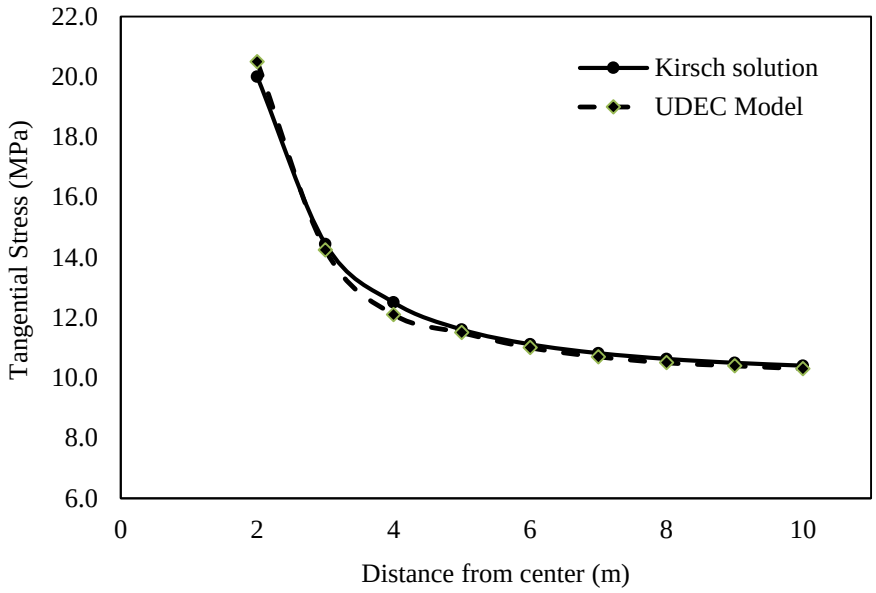

Fig. 4.2. Comparison of results of the UDEC model with Kirsch solution

4.3 Wave Propagation Across Fractures in Geological Medium

4.3.1 Propagation Across Single Joint

For the verification of wave propagation across a fracture in the geological medium, a one-dimensional problem has been considered. A theoretical solution for such a case has been derived by Pyrak-Nolte *et al.* (1990) and Myer *et al.* (1990). As per Pyrak-Nolte *et al.* (1990), the transmission coefficient (ratio of the maximum amplitude of transmitted wave to input wave) for normally incident harmonic P-wave across a single linearly deformable fracture, in an identical rock material is given by Eqn. (4.2).

$$T_1 = \frac{2(K_n/(Z_p\omega))}{-i + 2(K_n/(Z_p\omega))} \tag{4.2}$$

where T_1 is the transmission coefficient across a single fracture, K_n is the normal fracture stiffness, ω is the angular frequency of the harmonic wave, and Z_p is the P-wave impedance, which is equal to the product of P-wave velocity and rock density. The ratio $(K_n/(Z_p\,\omega))$ is known as normalized normal stiffness.

The verification model comprises of a rock column having width W and height H with a single fracture representing a joint as shown in Fig. 4.3. The height and width have been kept as 600m and 1m respectively (Zhao *et al*. 2008). One cycle of

harmonic sinusoidal wave velocity having a peak amplitude of 1m/s and frequency of 50Hz is applied at the bottom boundary which has been kept fixed. The lateral boundaries are restrained in the horizontal direction whereas a dashpot, based on Lysmer and Kuhlemeyer (1969) formulation, is attached at the top of the model to avoid wave reflection. A monitoring point M is specified to record the waves transmitted across the joint.

`

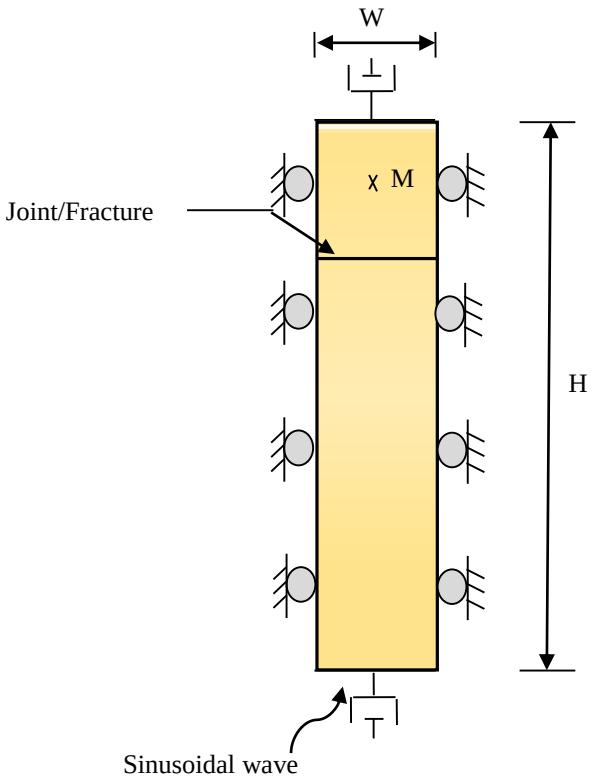

Fig. 4.3. Schematic representation of 1D wave propagation model for a single joint case

The properties of the rock have been adopted from Zhao (1996) which characterizes the rock found at a project site situated in Singapore. The rock density is 2610kg/m^3, Young's modulus is 84GPa and Poisson's ratio is 0.25. The normal stiffness of the joint (K_n) is varied from 0.35GPa/m to 30GPa/m giving normalized stiffness in the range of 0.06 to 5.89.

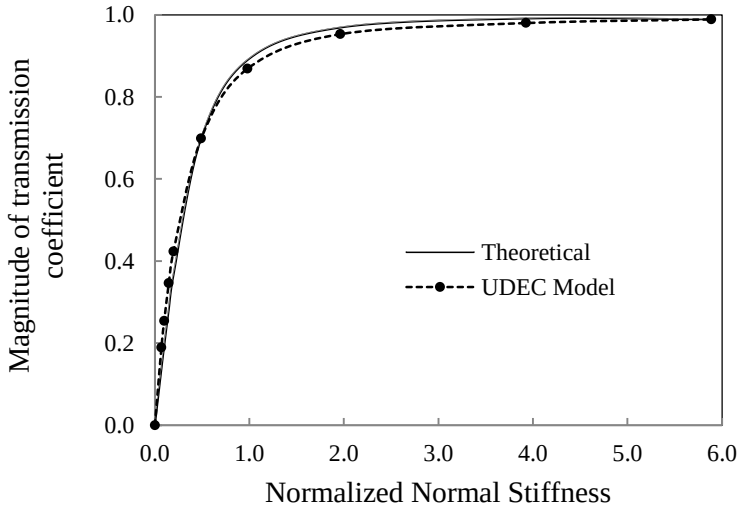

Fig. 4.4. Comparison of transmission coefficient as a function of normalized normal stiffness

Fig. 4.4 compares the transmission coefficient obtained from the numerical analyses with the solution provided by Pyrak-Nolte *et al.* (1990). It may be observed that the results from the numerical model shows good agreement with the theoretical solution.

4.3.2 Propagation Across Multiple Joint

After the verification of a numerical model for wave propagation across a single joint, the case of multiple joints is considered. The configuration of the numerical model is shown in Fig. 4.5. Regarding the boundary condition, the numerical model is similar to the previous case. Two cases of multiple joints (2 and 5) with variable spacing have been numerically simulated. The properties of the rock have been adopted from Zhu *et al.* (2013). The rock density is 2120kg/m^3, Young's modulus is 27.87 GPa, and Poisson's ratio is 0.29. The normal and shear stiffness of the joint is 50GPa/m. The spacing between the joints has been varied to cover a range of non-dimension joint spacing (ζ) between 0 to 0.5, where the non-dimensional joint spacing is defined as the spacing between the joints to the incident wavelength.

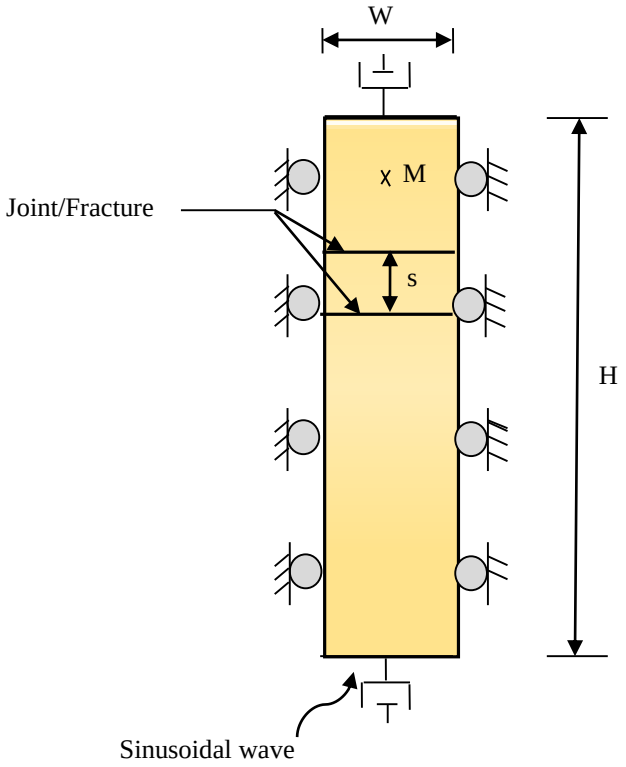

Fig. 4.5. Schematic representation of wave propagation model for multiple joints

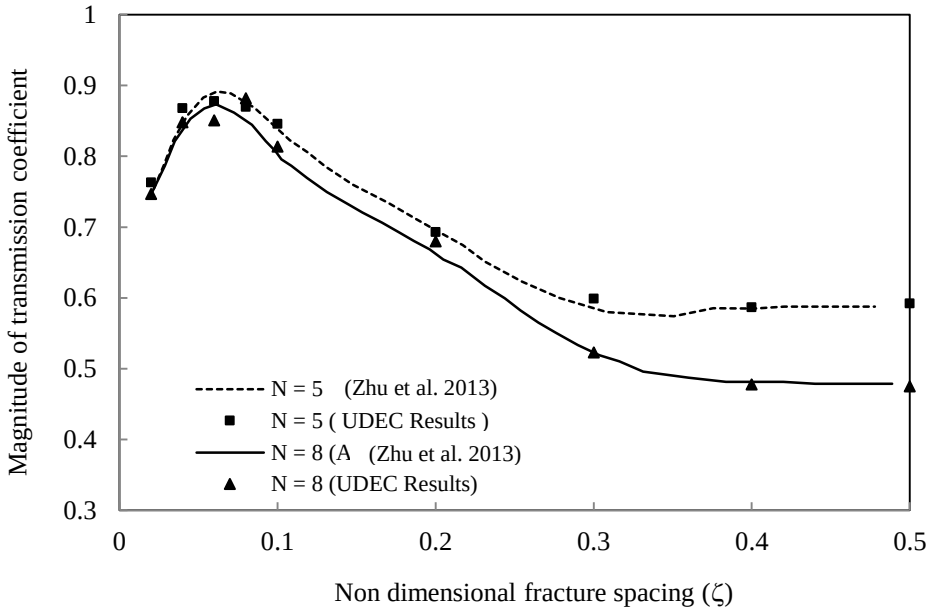

Fig. 4.6. Transmission coefficient versus non dimensional fracture spacing for normally incident P-wave across a joint set for different number of joints

A harmonic P-wave with amplitude 0.1m/s and frequency 1.0kHz is applied at the bottom boundary. The amplitude of the transmitted wave is recorded at point M. Fig. 4.6 shows the magnitude of transmission coefficient as a function of non-

dimensional fracture spacing (ζ) and it is found that UDEC results agree well with the results presented by Zhu *et al.* (2013). The results validate the applicability of UDEC for simulating the wave transmission in multi-jointed rock medium.

4.4 Simulation of Formation of Cracks Using Voronoi Tessellation Scheme

The present section verifies the ability of Voronoi tessellation scheme for simulating the formation of cracks. Voronoi tessellation scheme has been used to study the failure of a simple supported unreinforced concrete beam. Previously, the utilization of the distinct element method in replicating the behavior of unreinforced concrete beam has been reported by Lorig and Cundall (1989).

The schematic representation of the numerical model is shown in Fig. 4.7. The beam is modeled using the Voronoi tessellation scheme which divides the entire problem domain into a number of randomly sized polygons. Thus the beam is composed of an assemblage of intact blocks which are bonded at their interface. Failure of the beam occurs as the bond between the polygonal blocks break.

The schematic representation of the numerical model is shown in Fig. 4.7, which replicates a beam of length of 3.66m and depth of 0.56m. To simulate the conditions of a simple supported beam, zero y-velocity has been specified for a length of 200mm at both the ends on the bottom side of the beam. A constant vertical velocity of 0.01m/step is applied at the mid-span. The properties of the interface of the polygon blocks are as follows: cohesion 8.3MPa, tensile strength 4.1MPa, shear and normal stiffness 2700GPa/m and friction coefficient 0.3. To facilitate the comparison of the results, the properties have been kept the same as reported by Lorig and Cundall (1989).

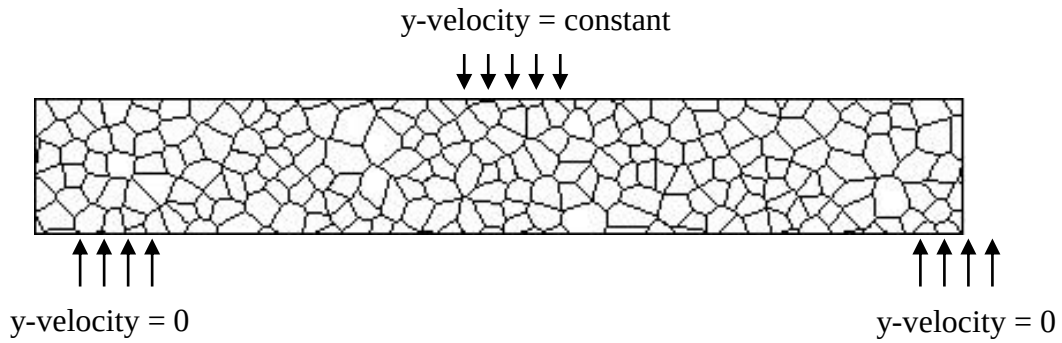

Fig. 4.7. A schematic representation of a simply supported beam modeled using Voronoi tessellation scheme in UDEC

The pattern of crack from the simulation is shown in Fig. 4.8 which shows good agreement with the result reported in the literature. A near vertical centerline crack is observed resulting from tensile failure at the bottom end of the center of the beam.

Fig. 4.8. Development of centerline crack for an unreinforced simple supported beam loaded at the mid-span in UDEC

4.5 Comparison of Field Recorded Convergence Values for Underground Machine Hall

In the present section, results of numerical analyses dealing with the convergence of an underground machine hall of a hydropower project, assessed using both equivalent continuum and discontinuum based approach, are presented. The primary aim is to demonstrate the advantages of the Voronoi tessellation scheme in capturing some of the observed field behavior following the excavation of the machine hall in the blocky rock mass.

The machine hall considered for comparison is a part of the Tala Hydro project, situated in the Himalayas. A schematic representation of the machine hall is shown in Fig. 4.9. The horse-shoe shaped machine hall is located at a depth of 400m, having a width of 20m and a height of 45m. Based on in-situ stress measurements, the

prevailing stresses have been reported as 10.9 MPa in the vertical direction and 9.5 MPa in the horizontal direction (Singh *et al.* 2002). Site investigations further revealed the presence of joints which breaks the rock mass into a blocky structure. During the construction of the machine hall, large convergence along sidewalls coupled with detachment of rock blocks had been observed. Total station measurements had revealed convergence values of around 250-300mm along the sidewall during the construction of the underground facility (Bhasin and Pabst 2015).

The equivalent continuum based numerical analysis has been carried out in the finite element software Phase2 (Rocscience *Inc.,* 2010). The dimensions of the model have been kept as 200m x 200m to eliminate any adverse boundary effects. The properties for the model have been derived from some published literature which are based on extensive geotechnical investigations associated with the Tala hydro project (Sengupta *et al.* 2007; Singh and Goyal 2005, Singh and Sthapak 2007, Venugopala Rao *et al.* 2003a, 2003b; Bhasin and Pabst 2015). Table 4.1 summarizes the rock mass properties adopted for the numerical simulations.

Table 4.1. Rock mass properties adopted in the study (Venugopala Rao *et al.* 2003a, 2003b; Bhasin and Pabst 2015)

Density (kg/m^3)	2650
Cohesion (MPa)	3.41
Friction angle (^{0})	26.2
Elastic modulus (GPa)	6.4
Poisson's ratio	0.335

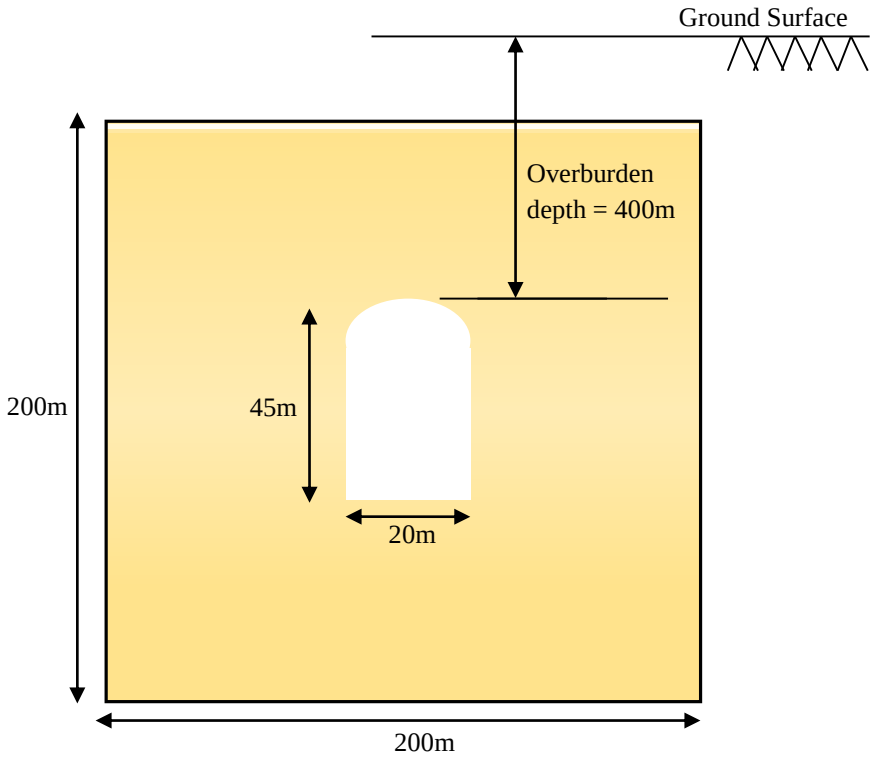

Fig. 4.9. A schematic representation of machine hall utilized for verification

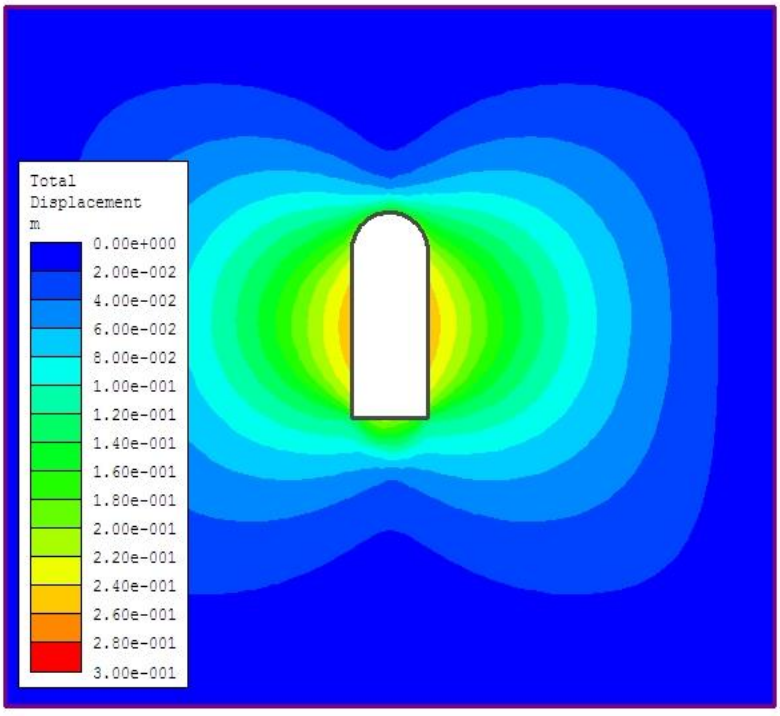

Fig. 4.10. Maximum displacement around the machine hall from equivalent continuum analysis

Before the excavation of the machine hall, in-situ stresses, as reported based on in-situ investigations, have been invoked to establish the equilibrium conditions.

Following the excavation, displacements along the side wall have been noted. The displacement contour obtained from the analysis is shown in Fig. 4.10. It may be noted that the displacement along the sidewalls appears to be symmetric with a maximum value of 255mm. This corresponds well with the field reported convergence values reported in the literature (Bhasin and Pabst 2015).

The discontinuum based numerical simulation has been carried out in the distinct element based software UDEC. To explicitly incorporate the jointed and blocky nature of the rock mass in the numerical model, the Voronoi tessellation scheme has been adopted keeping the average block size as 3m. The properties adopted for the intact rock and the rock block interface have been summarized in Table 4.2.

Table 4.2. Properties for UDEC model (Singh *et al.* 2002; Bhasin and Pabst 2015)

Property	Intact Rock	Rock block interface
Density (kg/m^3)	2740	-
Cohesion (MPa)	6	0
Friction angle (^{0})	52	25
Elastic modulus (GPa)	30	-
Poisson's ratio	0.2	-
Normal Stiffness (GPa/m)	-	25
Shear Stiffness (GPa/m)	-	1

The sequence followed for numerical simulation is similar as described above. Initially, the in-situ stresses are specified and then the model is run to establish the equilibrium. This is followed by the excavation of the machine hall. The model is run till it becomes stable which is monitored based on the unbalanced force (Itasca *Inc.*, 2004).

The result of the analysis has been presented in Fig. 4.11. A closer look reveals that the joint yielding pattern near the sidewall of the machine hall corresponds well with the total displacement contour obtained from equivalent continuum analysis. The maximum sidewall convergence recorded before the detachment of rock blocks is about 290mm An important and interesting observation made is about the rock block movement along discontinuities and their subsequent detachment.

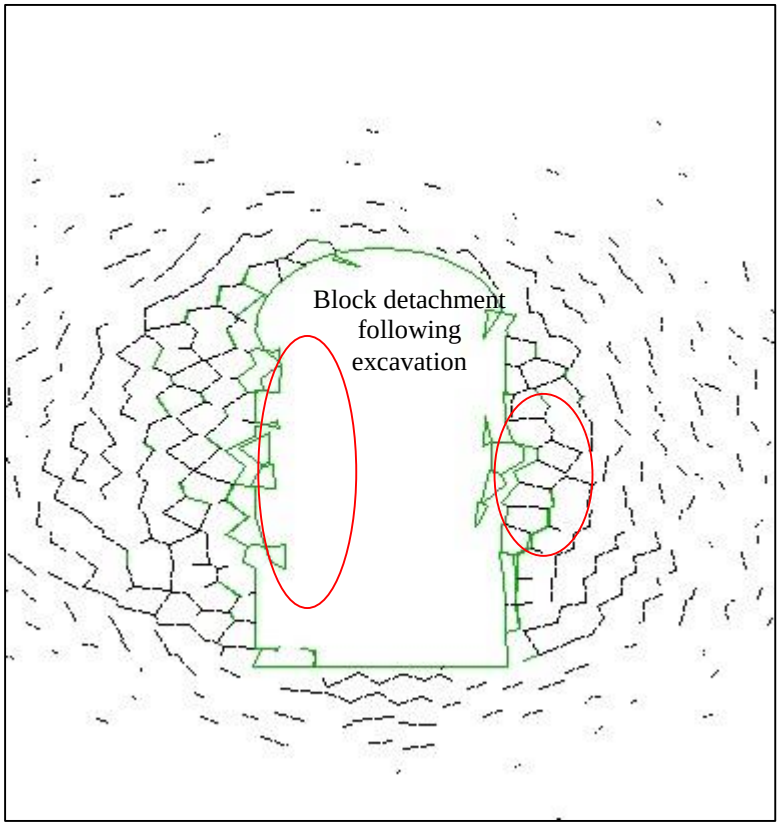

Fig. 4.11. Detachment of rock blocks along sidewall of machine hall

A closer scrutiny of Fig. 4.11, reveals that the discontinuum based Voronoi numerical approach can adequately capture the block detachment from the sidewalls which corresponds well with observations made at the site. Thus it may be stated that the discontinuum based approach used in the present study has an advantage over the continuum-based approach in capturing the discontinuity controlled movement which leads to large convergence and rock block detachments.

…

Chapter 5

INVESTIGATION ON CONVERGENCE OF TUNNEL EXCAVATIONS

5.1 Introduction

The present chapter provides a discussion on the deformation response of tunnel excavation in the jointed rock mass. Two cases of joint idealization – i. Parallel joint sets and ii. Joints idealized with Voronoi polygonal blocks have been considered. For both the idealization, the influence of variability in joint strength and deformation parameters, and in-situ stress ratio has been investigated. The contribution of each parameter on deformation has been assessed, and a discussion on the mode of rock block movement is presented.

5.2 Tunnel Convergence in Rock Mass Idealized with Parallel Joint Sets

The details of the numerical model considered for the case of rock mass idealized with parallel joint sets have been presented in *Section 3.3.1*. For evaluation of convergence strains, four monitoring points have been included in the numerical model as shown schematically in Fig. 5.1. The monitoring points 1 and 3 correspond to the crown and floor, while monitoring points 2 and 4 correspond to the right and left sidewalls respectively. The reduction in the length of the imaginary line joining points 1-3 and 2-4 are noted from the numerical analysis. The convergence strain is evaluated by diving the reduction in the length with the radius of the excavation. This approach is similar to the method reported in earlier studies dealing with the convergence of tunnel (Sakurai 1997a, Hoek 1998a).

5.2.1 Parameters Considered in the Study

To evaluate the effect of the strength and deformation parameters of the discontinuities, and the in-situ stress ratio on the convergence of tunnels, five parameters have been considered. The parameters are listed below:

1. Cohesion of joints, C_{jc}
2. Friction angle of joints, ϕ_{jc}
3. Normal stiffness of joints, K_{nc}
4. Shear stiffness of joints, K_{sc}
5. In-situ stress ratio, K_0

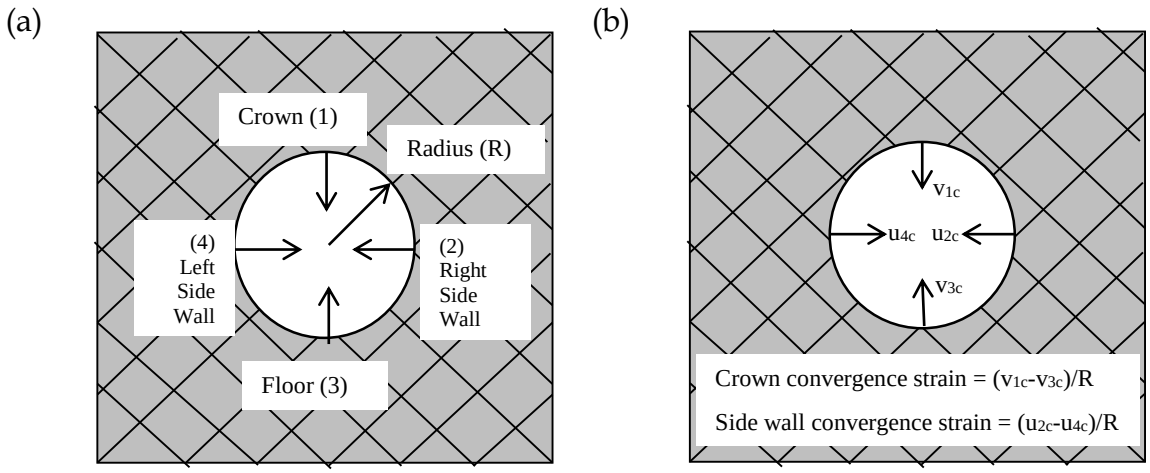

Fig. 5.1. (a) Displacement monitoring points; (b) Notation of displacements and computation of convergence strains for tunnel excavation in parallel jointed rock mass

Since most of the problems experienced during tunnel excavation has been reported to be associated with discontinuities which are filled with clay (Swarup *et al.* 2000, Singh and Goel 2006), similar conditions are simulated here. Hence, the values of parameters have been selected based on the range suggested in the literature for clay filled joints. The cohesion of the discontinuities is reported to have values in the range of 0 to 0.18 MPa, while those for friction angle is between 12^0 to 18.5^0 (Barton 1974). The deformation parameters of the joints, characterized by normal stiffness (K_{nc}) and shear stiffness (K_{sc}) are reported to be in the range of 0.1-5 GPa/m (Kulhawy 1975, Infanti and Kanji 1978). Moreover, these parameters are reported to follow a normal distribution (Mostyn and Li 1993, Nilsen 2000, Pathak and Nilsen 2004, Song et al. 2011).

Based on the range and the statistical distribution mentioned above, Table 5.1 lists the mean value and the low and high estimates of the five parameters. These values have been utilized within the framework of Design of Experiments to assess their

relative contribution on the deformation response of the tunnel excavation. In all the analyses, intact rock with a density of 2300 kg/m^3, cohesion (C_i) 3 MPa, friction angle (ϕ_i) 35^0, and elastic modulus (E) 10 GPa, is considered. These values are representative of the rocks encountered in tunneling projects passing through the fractured zone (Lunardi 2008).

Table 5.1. Parameters adopted for convergence study of tunnels in rock mass idealized with parallel joint sets

Parameters	**Distribution**	**Mean (μ)**	**Standard Deviation (σ)**	**High Point Estimate (+)**	**Low Point Estimate (-)**
C_{jc}(MPa)	Normal	0.1	0.02	0.13	0.067
ϕ_{jc}(in deg)	Normal	18^0	3^0	23^0	13^0
K_{nc}(GPa/m)	Normal	1	0.3	1.5	0.5
K_{sc}(GPa/m)	Normal	0.5	0.15	0.75	0.25
K_0	Normal	1.8	0.3	2.3	1.3

5.2.2 Analyses Performed for Evaluation of Tunnel Convergence

Since five parameters have been considered in the study, 32 number of analysis, corresponding to 2^5 cases of factorial design, has been numerically simulated. In all the analysis, an in-situ stress has been invoked and brought to equilibrium before the excavation of a circular opening. Following the excavation, the model has been allowed to run till the system is stable. From the displacements recorded at the four monitoring points, convergence strains for both the crown-floor and sidewall section have been evaluated. The results of all the 32 analyses are presented in Table 5.2. The low and high point estimates of the parameters are denoted by - and + respectively.

Table 5.2. Model runs and corresponding convergence strain percentage for tunnel excavation in rock mass idealized with parallel joint sets

Model Run	C_{jc}	ϕ_{jc}	K_{nc}	K_{sc}	K_0	Strain (%) (crown-floor)	Strain (%) (Sidewall)
1	-	-	-	-	-	1.51	3.68
2	+	-	-	-	-	1.48	3.32
3	-	+	-	-	-	0.56	1.31
4	+	+	-	-	-	0.56	1.21
5	-	-	+	-	-	0.82	1.96
6	+	-	+	-	-	0.81	1.95
7	-	+	+	-	-	0.31	0.57
8	+	+	+	-	-	0.31	0.55
9	-	-	-	+	-	1.41	3.46
10	+	-	-	+	-	1.39	3.12
11	-	+	-	+	-	0.47	0.86
12	+	+	-	+	-	0.48	0.86
13	-	-	+	+	-	0.74	1.77
14	+	-	+	+	-	0.74	2.07
15	-	+	+	+	-	0.23	0.47
16	+	+	+	+	-	0.23	0.41
17	-	-	-	-	+	15.21	7.22
18	+	-	-	-	+	29.90	6.76
19	-	+	-	-	+	0.93	2.59
20	+	+	-	-	+	0.95	2.56
21	-	-	+	-	+	19.57	6.94
22	+	-	+	-	+	19.60	7.32
23	-	+	+	-	+	0.64	1.81
24	+	+	+	-	+	0.65	1.81
25	-	-	-	+	+	29.20	6.94
26	+	-	-	+	+	31.20	8.80
27	-	+	-	+	+	0.99	2.27
28	+	+	-	+	+	0.92	2.06
29	-	-	+	+	+	23.70	6.96
30	+	-	+	+	+	26.10	8.97
31	-	+	+	+	+	0.50	1.26
32	+	+	+	+	+	0.50	1.25

It may be stated here that for some cases, very high values of crown-floor convergence strain have been observed (refer model runs 17, 18, 21, 22, 25, 26, 29 and 30). Such high values correspond to the case where detachment of rock blocks from the crown is observed. In cases where the detachment of rock blocks at the crown did not occur, the convergence strains are found to be higher for the sidewall section in comparison to crown-floor section.

Figure. 5.2 and 5.3 correspond to model run 17 and 25 respectively, in which high convergence of the crown-floor section is noted. For both the cases, detachment of the rock block at the crown is observed. In fact, for model run 25, the detachment at the crown leads to propagation of disturbance further upwards into the rock mass, which may be noted by the rotation of rock blocks as marked in Fig. 5.3. Also, the six cases of high convergence for the crown-floor section is noted where the in-situ stress ratio is high, and the joint friction angle is low. For cases where the frictional resistance is high, *i.e.*, joint friction angle value is high; the crown-floor convergence strain is reduced. This suggests that sliding of rock blocks along discontinuities precedes the detachment at the crown. In case of high shear resistance along the joints, the detachment is minimized at the crown.

Fig. 5.4 shows the deformation response for model run 7. Block sliding and detachment is noted at the sidewall. However, since the detached block is interlocked, rotation is not possible. The deformation, in this case, is majorly governed by the sliding along the joints and hence on the resistance along the discontinuities. Thus, for cases where the resistance is high, *i.e.*, friction angle is high, the sidewall convergence strain is comparatively low.

5.2.3 Effects of Parameters on Crown-Floor Convergence

ANOVA analysis has been performed on the numerical results for quantifying the effect of the random parameters on the crown-floor convergence. The results are presented in terms of the effect estimate, percentage contribution and p-value for all main and interaction terms in Table 5.3.

From the percentage contribution column of Table 5.3, it can be observed that the major contribution to the strains for the crown-floor section is made by the joint friction angle ϕ_{jc} (33.97%) and the in-situ stress ratio K_0 (32%). The interaction term $\phi_{jc}K_0$ has a percentage contribution of about 30%. In comparison, all other main and interaction factors make a contribution which is less than 1%. Thus it may be stated that out of the five parameters considered in the present study, only two parameters *viz.* joint friction angle (ϕ_{jc}) and the in-situ stress ratio (K_0) make a significant contribution to the crown-floor convergence strain.

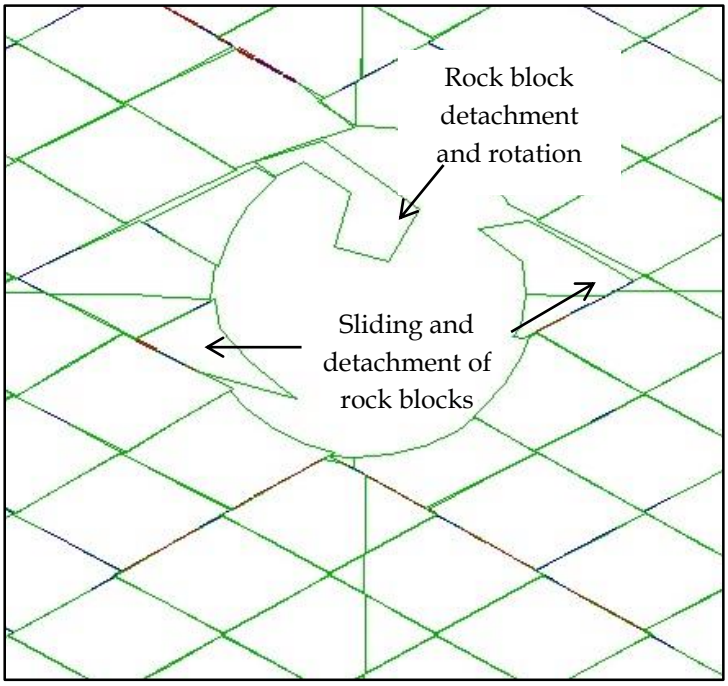

Fig. 5.2. Detachment of rock blocks at the crown and sliding along the left sidewall for model run 17

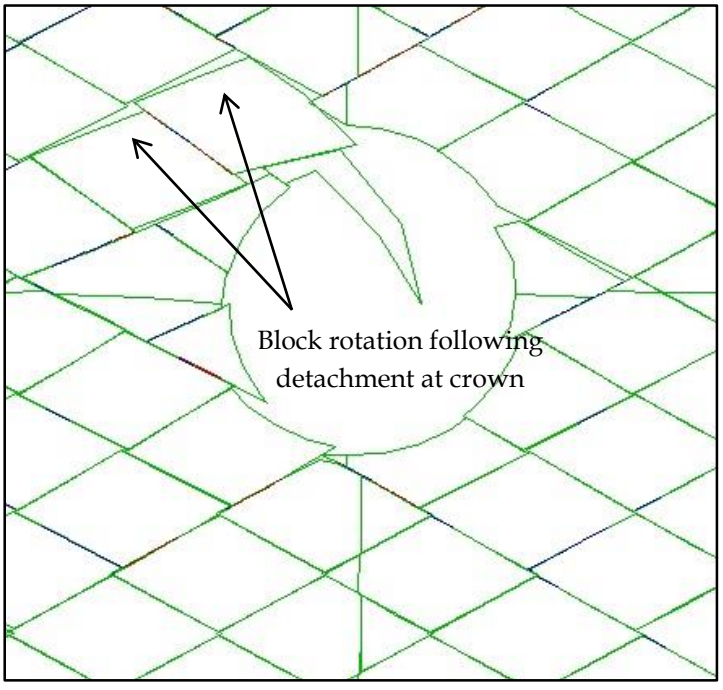

Fig. 5.3. Rock block rotation following detachment at the crown for model run 25

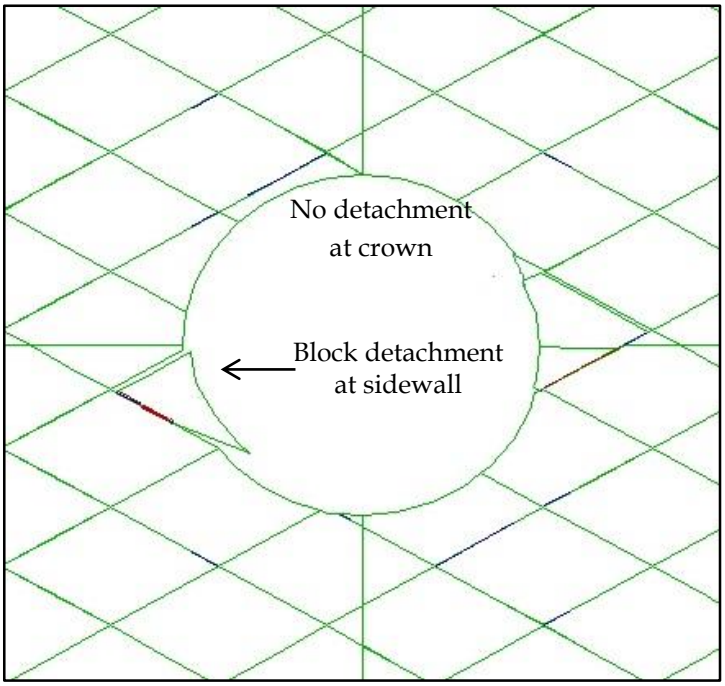

Fig. 5.4. Sliding of rock block at the sidewall for model run 7

Table 5.3. ANOVA analysis on the crown-floor convergence strain for tunnel in jointed rock mass idealized with parallel joint sets

Factor	Effect estimate	Sum of squares	Percentage contribution (%)	p-value
C_{jc}	1.188	11.291	0.326	0.193
ϕ_{jc}	-12.135	1178.066	33.970	0.000
K_{nc}	-1.357	14.732	0.425	0.140
K_{sc}	1.563	19.544	0.564	0.093
K_0	11.781	1110.336	32.017	0.000
$C_{jc}\phi_{jc}$	-1.193	11.386	0.328	0.191
$C_{jc}K_{nc}$	-0.886	6.280	0.181	0.326
$C_{jc}K_{sc}$	-0.650	3.380	0.097	0.468
$C_{jc}K_0$	1.195	11.424	0.329	0.191
$\phi_{jc}K_{nc}$	1.045	8.736	0.252	0.250
$\phi_{jc}K_{sc}$	-1.635	21.386	0.617	0.080
$\phi_{jc}K_0$	-11.416	1042.600	30.063	0.000

$K_{nc}K_{sc}$	-0.307	0.754	0.022	0.730
$K_{nc}K_0$	-0.899	6.466	0.186	0.319
$K_{sc}K_0$	1.644	21.622	0.623	0.078

5.2.4 Effects of Parameters on Sidewall Convergence

Table 5.4 presents the results of the ANOVA analysis quantifying the effect of the parameters on the sidewall convergence. From the percentage contribution column of Table 5.4, it can be observed that the major contribution to the sidewall strain is made by joint friction angle ϕ_{jc} (50.85%) and in-situ stress ratio K_0 (33.18%). The interaction term $\phi_{jc}K_0$ has a percentage contribution of about 12.31%. All other main and interaction factors make little contribution. Thus it may be stated that out of the five random parameters considered in the present study, only two parameters *viz.* joint friction angle (ϕ_{jc}) and the in-situ stress ratio (K_0) make a significant contribution on the sidewall convergence strain.

Table 5.4. ANOVA analysis on the sidewall convergence strain tunnel in jointed rock mass idealized with parallel joint sets

Factor	**Effect estimate**	**Sum of squares**	**Percentage contribution (%)**	**p-value**
C_{jc}	0.185	0.273	0.126	0.348
ϕ_{jc}	-3.711	110.190	50.858	0.000
K_{nc}	-0.682	3.725	1.719	0.003
K_{sc}	-0.001	0.000	0.000	0.995
K_0	2.998	71.894	33.183	0.000
$C_{jc}\phi_{jc}$	-0.239	0.456	0.210	0.229
$C_{jc}K_{nc}$	0.140	0.157	0.072	0.475
$C_{jc}K_{sc}$	0.260	0.541	0.250	0.192
$C_{jc}K_0$	0.258	0.533	0.246	0.196
$\phi_{jc}K_{nc}$	-0.011	0.001	0.000	0.953
$\phi_{jc}K_{sc}$	-0.369	1.092	0.504	0.071
$\phi_{jc}K_0$	-1.826	26.665	12.307	0.000

$K_{nc}K_{sc}$	0.034	0.009	0.004	0.860
$K_{nc}K_0$	0.324	0.842	0.389	0.109
$K_{sc}K_0$	0.188	0.284	0.131	0.339

5.3 Tunnel Convergence in Rock Mass Idealized with Voronoi Blocks

The idealization of the distribution of discontinuities with parallel joint sets may not always hold good. A number of cases are encountered in the field where the joints break the rock mass into a blocky structure. For example, refer Fig. 5.5, where the tunnel passes through a jointed rock mass which is broken down into well-defined discrete blocks of various shapes and sizes. The white lines in Fig. 5.5 roughly correspond to the individual blocks demarcated by the joints. As is evident, the pattern of rock blocks formed cannot be accurately idealized with parallel joint sets as discussed above. Parallel joint set idealization for this particular case may lead to an unreliable assessment of the deformation response.

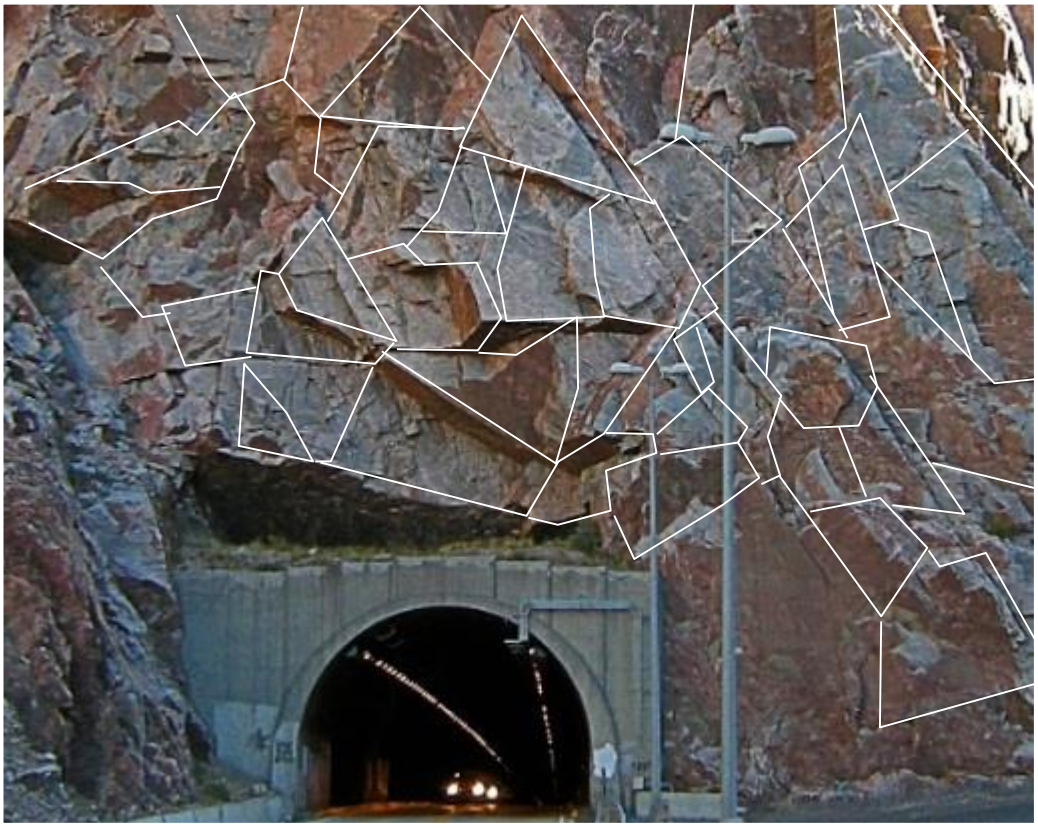

Fig. 5.5. Tunnel passing through a blocky rock mass (white lines demarcate the joints which break the rock outcrop into well-defined rock blocks)

To highlight the importance of proper joint idealization, numerical analyses have been performed in which the Voronoi tessellation scheme is used for representing the joint distribution. This approach divides the geological medium into polygonal blocks, in which the edges replicate the behavior of the joints. As with the previous case, the deformation of tunnel excavation has been evaluated using four monitoring points as shown in Fig. 5.6. To facilitate the comparison of results with the previous case (idealization with parallel joint sets), the simulations have been carried out by adopting similar modeling steps and the combination of input parameters as discussed in *Section 5.2.1*

The results of the analyses are presented in Table 5.5. It is observed that the convergence strains for all combinations of input parameters are comparatively less than those presented in Table 5.1. This demonstrates the significant influence which joint idealization has on the numerical results.

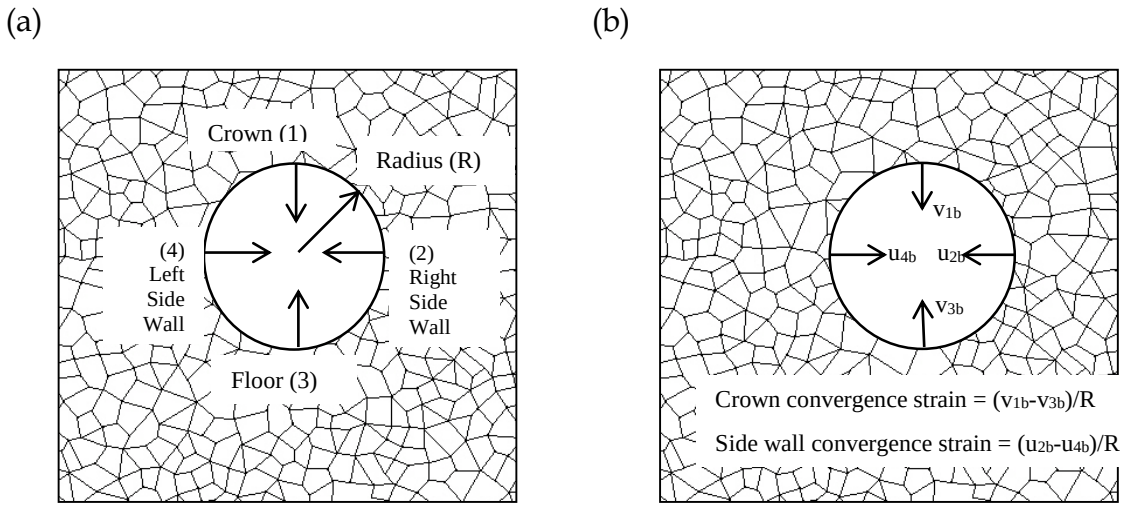

Fig. 5.6. (a) Displacement monitoring points; (b) Notation of displacements and computation of convergence strains for tunnel excavation in blocky rock mass

For the blocky rock mass configuration, the convergence strain for the sidewall section is found to be higher than the crown-floor section for all combination of input parameters, suggesting the movement of rock blocks at the sidewall to

dominate the response. Fig. 5.7 shows the deformation response corresponding to model run 5 of Table 5.5. The blocks at the left sidewall get detached following the excavation. However, the blocky configuration of rock mass leads to interlocking effect and minimizes the sliding and rotation. The deformation response is governed by the detachment action and the subsequent interlocking effect. A comparison of model run 17 and 21 highlights the significance of the joint normal stiffness (k_{nb}) on the convergence strains. A decrease of almost 50% in convergence is observed, for both the crown-floor and sidewall section, when the normal stiffness has a high value. To ascertain the contribution of the parameters, ANOVA has been performed on the numerical results.

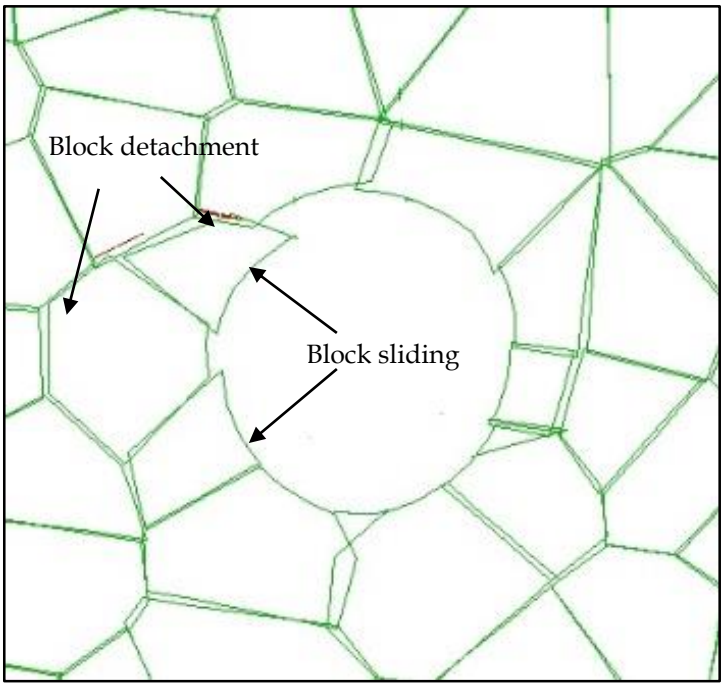

Fig. 5.7. Detachment and sliding of rock blocks at the sidewall for model run 7

Table 5.5. Model runs and corresponding convergence strain percentage for tunnel excavation in rock mass idealized with Voronoi polygonal blocks

Model Run	C_{jb}	ϕ_{jb}	K_{nb}	K_{sb}	K_0	Strain (%) (crown-floor)	Strain (%) (Sidewall)
1	-	-	-	-	-	0.33	0.50
2	+	-	-	-	-	0.33	0.50
3	-	+	-	-	-	0.25	0.41
4	+	+	-	-	-	0.25	0.41

5	-	-	+	-	-	0.16	0.25
6	+	-	+	-	-	0.16	0.25
7	-	+	+	-	-	0.14	0.23
8	+	+	+	-	-	0.14	0.23
9	-	-	-	+	-	0.31	0.44
10	+	-	-	+	-	0.31	0.44
11	-	+	-	+	-	0.20	0.33
12	+	+	-	+	-	0.20	0.33
13	-	-	+	+	-	0.14	0.21
14	+	-	+	+	-	0.14	0.21
15	-	+	+	+	-	0.11	0.18
16	+	+	+	+	-	0.11	0.17
17	-	-	-	-	+	0.25	1.11
18	+	-	-	-	+	0.26	1.10
19	-	+	-	-	+	0.13	0.96
20	+	+	-	-	+	0.13	0.96
21	-	-	+	-	+	0.11	0.53
22	+	-	+	-	+	0.11	0.52
23	-	+	+	-	+	0.07	0.51
24	+	+	+	-	+	0.08	0.51
25	-	-	-	+	+	0.26	1.00
26	+	-	-	+	+	0.27	0.98
27	-	+	-	+	+	0.11	0.79
28	+	+	-	+	+	0.11	0.79
29	-	-	+	+	+	0.10	0.46
30	+	-	+	+	+	0.10	0.45
31	-	+	+	+	+	0.05	0.39
32	+	+	+	+	+	0.05	0.39

5.3.1 Effects of Parameters on Crown-Floor Convergence

Table 5.6 summarizes the results of ANOVA analysis in terms of the effect estimate, percentage contribution and p-value for all the parameters considered in the present study. From the percentage contribution column of Table 5.6, it can be observed that the major contribution to the strains for the crown-floor section is made by in-situ stress ratio K_0 (31.91%), joint normal stiffness K_{nb} (23.19%) and joint friction angle ϕ_{jb} (17.42%). The interaction term $\phi_{jb}K_0$ has a percentage contribution of about 8%. In comparison, all other main and interaction factors make a contribution which is less than 5%. Thus it may be stated that out of the five random parameters considered in the present study, three parameters *viz.* in-situ stress ratio (K_0), joint normal stiffness (K_{nb}) and joint friction angle (ϕ_{jb}) make a significant contribution.

Table 5.6. ANOVA analysis on the crown-floor convergence strain

Factor	Effect estimate	Sum of squares	Percentage contribution (%)	p-value
C_{jb}	-0.067	0.036	2.05	0.168
ϕ_{jb}	-0.194	0.302	17.42	0.001
K_{nb}	-0.224	0.402	23.19	0.000
K_{sb}	0.096	0.073	4.22	0.055
K_0	0.263	0.554	31.91	0.000
$C_{jb}\phi_{jb}$	-0.053	0.023	1.31	0.265
$C_{jb}K_{nb}$	0.009	0.001	0.03	0.856
$C_{jb}K_{sb}$	0.003	0.000	0.00	0.957
$C_{jb}K_0$	-0.073	0.042	2.44	0.135
$\phi_{jb}K_{nb}$	0.010	0.001	0.05	0.830
$\phi_{jb}K_{sb}$	0.001	0.000	0.00	0.975
$\phi_{jb}K_0$	-0.131	0.137	7.92	0.012
$K_{nb}K_{sb}$	0.072	0.042	2.41	0.137
$K_{nb}K_0$	-0.092	0.068	3.89	0.064
$K_{sb}K_0$	0.083	0.055	3.15	0.092

5.3.2 Effects of Parameters on Sidewall Convergence

The results of the ANOVA analysis for the sidewall convergence of tunnel excavation in the blocky rock mass is presented in Table 5.7. From the percentage contribution column of Table 5.7, it can be observed that the major contribution to the sidewall strain is made by in-situ stress ratio K_0 (54.67%) and joint normal stiffness K_{nb} (31.32%). The interaction term $k_{nb}K_0$ has a percentage contribution of 4.24%. All other main and interaction factors make little contribution. Thus it may be stated that out of the five random parameters considered in the present study, two parameters *viz.* in-situ stress ratio (K_0) and joint normal stiffness (K_{nb}) contribute significantly to the deformation.

Table 5.7. ANOVA analysis on the sidewall convergence strain

Factor	Effect estimate	Sum of squares	Percentage contribution (%)	p-value
C_{jb}	-0.002	0.000	0.00	0.891
ϕ_{jb}	-0.115	0.105	3.97	0.000
K_{nb}	-0.322	0.827	31.32	0.000
K_{sb}	-0.113	0.102	3.87	0.000
K_0	0.425	1.443	54.67	0.000
$C_{jb}\phi_{jb}$	-0.002	0.000	0.00	0.873
$C_{jb}K_{nb}$	0.003	0.000	0.00	0.818
$C_{jb}K_{sb}$	-0.001	0.000	0.00	0.919
$C_{jb}K_0$	-0.002	0.000	0.00	0.886
$\phi_{jb}K_{nb}$	0.024	0.005	0.17	0.107
$\phi_{jb}K_{sb}$	0.011	0.001	0.04	0.436
$\phi_{jb}K_0$	-0.050	0.020	0.77	0.002
$K_{nb}K_{sb}$	-0.007	0.000	0.02	0.612
$K_{nb}K_0$	-0.118	0.112	4.24	0.000
$K_{sb}K_0$	-0.055	0.024	0.92	0.001

5.4 CONCLUSIONS AND RECOMMENDATIONS

The present chapter considered two cases of idealization of joints in the rock mass for the evaluation of the deformation response of a tunnel excavation. From the results, the following conclusions has been drawn:

a. The manner of idealization of the joints has a major influence on the mode of rock block movement and hence on the deformation values.
b. Idealization with parallel joint sets leads to comparatively higher deformation values for a given set of conditions. The parallel joints provide pathways along which discrete rock blocks are likely to slide.

c. In parallel joint set idealization, the shear resistance of the joint, characterized by the joint friction angle, has maximum influence on the deformation. This is closely followed by the contribution made by the in-situ stress ratio.
d. The primary mode of deformation is sliding of rock blocks along parallel joints followed by rotation and detachment. As the interlocking effect is low at the crown, the possibility of rotation and detachment of discrete rock blocks is high. In contrast, the interlocking provided by surrounding rock blocks at the sidewall prevents rotation of the rock blocks.
e. The lower deformation values at the crown for excavation in the blocky rock mass (idealized with Voronoi polygonal blocks) is attributed to the interlocking effect and the absence of clearly defined straight path for block sliding.
f. The contribution of the joint friction angle on deformation seems minimal for the blocky rock mass case. Rock block movement appears to be governed by the detachment action and the subsequent interlocking effects.
g. The joint normal stiffness (k_{nb}) has a major effect on the deformation response in the blocky rock mass.

Based on the above-mentioned conclusions, the following recommendations are made:

a. Since the accuracy and reliability of deformation predictions for excavations in the jointed rock mass is significantly influenced by the pattern of idealization of the joints, the use of Discrete Fracture Networks (DFN) using joint set generators is recommended.
b. The present study identifies the joint normal stiffness to significantly influence the deformation response of tunnel excavation in the blocky rock mass. Although well established guidelines *i.e.,* ASTM: 5607-02 and ASTM: 4554-12, elaborately discusses the procedure to determine the strength and stiffness properties of the joints, large-scale field testing are rare. Hence, efforts must be made to evaluate the stiffness properties of the joints for major underground projects.

…

Chapter 6

DYNAMIC BEHAVIOR OF TUNNEL IN BLOCKY ROCK MASS

6.1 Introduction

The traditional belief of underground structures possessing adequate earthquake resistant features has suffered a major setback following observations of damage in some recent past earthquakes. Widespread damage of tunnels has been reported following the 1995 Hyogoken-Nanbu (Japan), 1999 Chi-Chi (Taiwan), 2004 Mid-Niigata Prefecture (Japan) and 2008 Wenchuan (China) earthquakes. In the majority of the cases, the damaged sections are reported to pass through highly weathered and fractured rock mass conditions. Also, large movement and detachment of rock blocks have been noted, suggesting the interaction of waves with the joints to govern the dynamic response. However, a clear understanding of the effect of the discontinuities on the dynamic behavior of tunnels is lacking.

The present chapter provides a discussion on the dynamic response of a circular lined tunnel in the blocky rock mass. Specifically, an assessment of the influence of wave frequency, type of wave action (P and S waves), overburden depth and the in-situ stress ratio on the demand imposed on the tunnel liner is presented. The results of the numerical simulations are utilized to corroborate the damage patterns reported in the literature.

6.2 Numerical Model and Dynamic Analyses

To investigate the dynamic response of tunnels excavated in the blocky rock mass, the numerical model described in *Section 3.4* has been used. Sinusoidal accelerations of amplitude 0.1g with five different frequencies, ranging between 1Hz to 8Hz, have been utilized in this study. For each frequency, five cycles of sinusoidal waves have been incorporated as input. The dynamic simulation is run for sufficient time to ensure that the effect of phase reversal due to the reflection of the waves from the ground surface is taken into account. Before every dynamic analysis, an initial static

in-situ stress state has been invoked. The properties for the rock mass are listed in Table 6.1.

Table 6.1. Properties adopted in present study

Property	Intact Rock	Rock block interface
Density (kN/m^3)	23	-
Cohesion (MPa)	3	1
Friction angle (^{0})	35	20
Elastic modulus (GPa)	10	-
Poisson's ratio	0.2	-
Tensile Strength (MPa)	0.5	0.0005
Normal Stiffness (GPa/m)	-	2.2
Shear Stiffness (GPa/m)	-	1.1

6.3 Results and Discussions

The results of the numerical analyses have been presented in the form of maximum dynamic axial force and maximum dynamic bending moment developed in the tunnel liner due to the wave action. For this purpose, a function was written in FISH to record the time history of the axial force and bending moment, which developed in the liner during the dynamic analyses. It should be noted that the angle along the tunnel liner increases in the clockwise direction, where 0^0 corresponds to the crown. The results of the analyses are presented in the subsequent sections.

6.3.1 Effects of Frequency on Tunnel Liner Response

6.3.1.1 Tunnel at a depth of 50m

The maximum dynamic axial force in the liner for the tunnel located at a depth of 50m, and subjected to S-wave motion is shown in Fig. 6.1a. From Fig. 6.1a, it is observed that the liner is subjected to both compression and tension under the S-wave action, as is evident from the change in sign of the values of the axial force for various angles. It may be noted here that in UDEC, positive values recorded in

structural beam elements correspond to compressive force whereas negative values correspond to tension. Fig. 6.1b presents the peak values among the various maximum compression and tension values shown in Fig. 6.1a, for all the frequencies considered in the study. It is observed that liner axial forces in both tension and compression is maximum when the frequency of input motion is 1Hz. Further, there appears to be a decrease in the maximum axial force with an increase in the frequency of input motion from 1Hz to 2Hz. For higher frequencies of 4, 6 and 8 Hz, the maximum axial force in the liner becomes almost identical and is comparatively less than the lower frequency case.

The variation in maximum dynamic bending moment induced in the liner under S-wave action is shown in Fig. 6.1c, with the peak values highlighted in Fig. 6.1d. Similar to the trend of axial force, a general trend of decrease in bending moment with an increase in the frequency of input motion is observed. Moreover, for higher frequencies of 4, 6 and 8 Hz the bending moment becomes identical.

For the same tunnel configuration at a depth of 50m, the response under the influence of P-wave action, in terms of maximum dynamic axial force is shown in Fig. 6.2a with the corresponding peak values in tension and compression presented in Fig. 6.2b. Similar to the case of S-wave action, maximum liner axial forces are observed to be more, in both tension and compression, when the frequency of input motion is 1Hz. The maximum axial force decreases with increase in the frequency of input motion and becomes almost identical for higher frequencies of 4, 6 and 8 Hz.

Moreover, under P-wave action, the trend of variation in the maximum dynamic bending moment is also similar to that of S-wave action for the same tunnel configuration as is evident from Fig. 6.2c. The corresponding peak values for various frequencies of input motion are shown in Fig. 6.2d. It is noted that the dynamic axial force induced in the tunnel liner is almost identical for both S-wave and P-wave motions for higher frequencies of 4,6 and 8 Hz. However, P-wave motion induces slightly higher values of bending moment, especially in the lower frequency range.

Fig. 6.3 and Fig. 6.4 presents the pattern of Voronoi joints/edges which have yielded either in shear or tension during dynamic analyses. It is observed from numerical simulation that the yielding pattern is maximum for the low-frequency case of 1 Hz as shown in Fig. 6.3. However, for higher frequencies, the extent of yielding of Voronoi joints decreases. The pattern of yielding for the frequency of 6Hz is shown in Fig. 6.4, where no conspicuous yielding in the vicinity of the lined tunnel is observed.

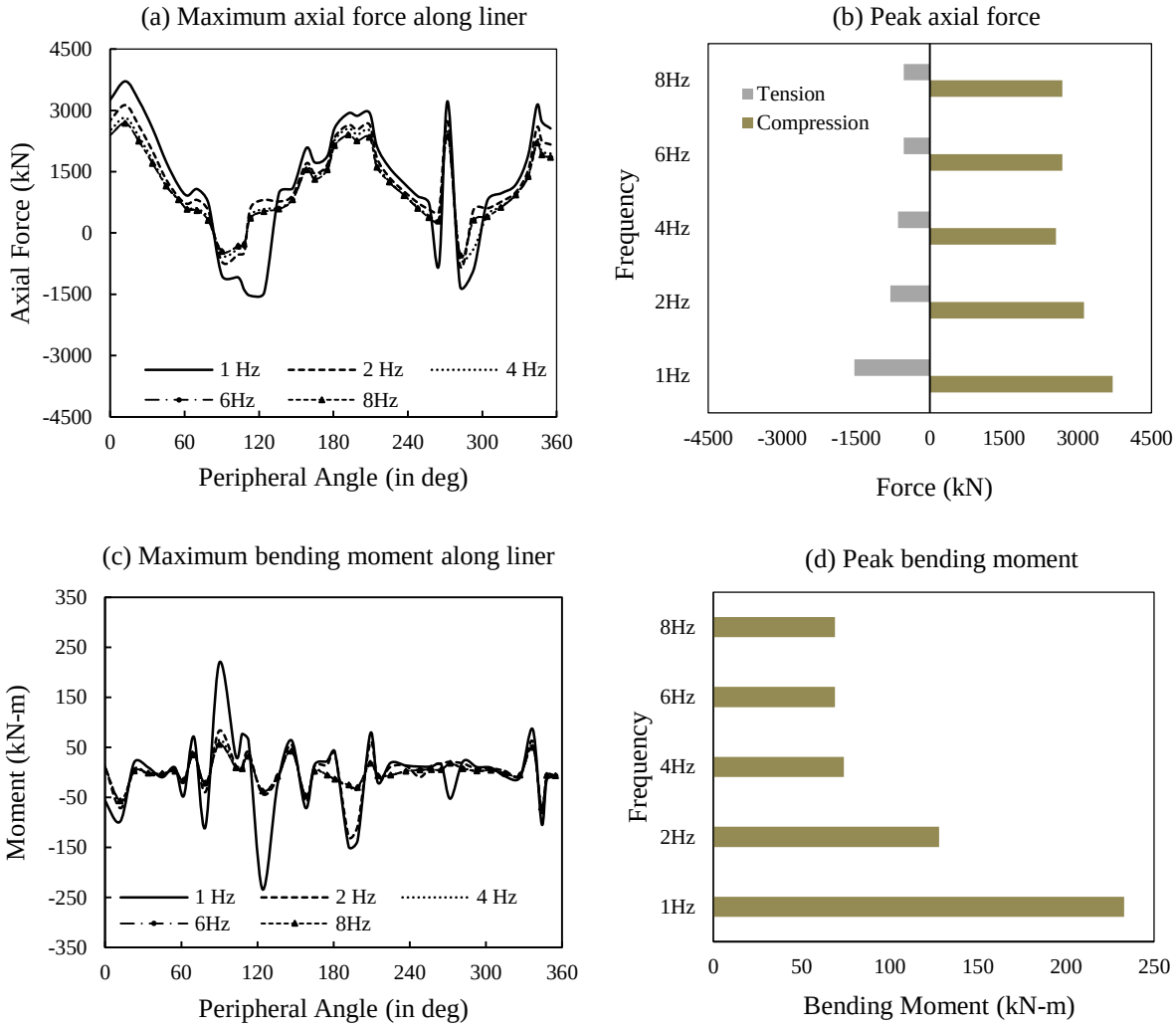

Fig. 6.1. Effect of frequency of excitation on tunnel located at a depth of 50m considering S-wave: (a) Maximum axial force along liner; (b) Peak axial force; (c) Maximum bending moment along liner; (d) Peak bending moment

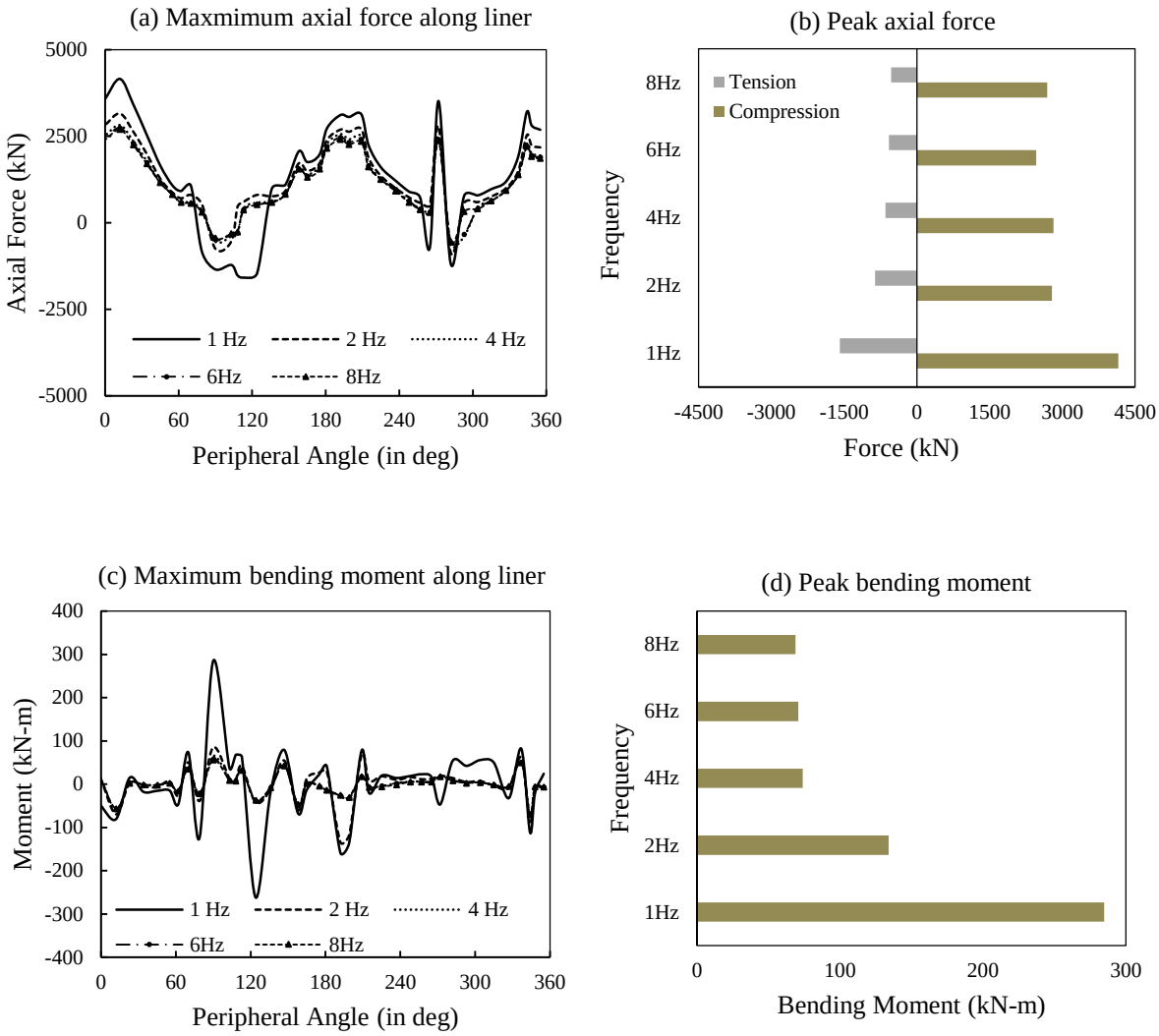

Fig. 6.2. Effect of frequency of excitation on tunnel located at a depth of 50m considering P-wave: (a) Maximum axial force along liner; (b) Peak axial force; (c) Maximum bending moment along liner; (d) Peak bending moment

The difference in the pattern of yielding may be explained by the frequency-filtering effect of the joints. The randomly oriented joints simulated with the Voronoi blocks act as low pass filter. As the transmission of dynamic waves across joints is inversely proportional to the frequency, the filtering effect allows the low-frequency waves to pass through them, while offering resistance to high-frequency waves. Thus, at higher frequencies, the extent of yielding of Voronoi joints is comparatively less. Further, for the case of 1 Hz frequency of input motion, it may be observed that the reflection of waves from the ground surface leads to a pattern of yielding along the Voronoi joints as highlighted in Fig. 6.3. This leads to loosening of the rock blocks,

imparting to them a higher degree of kinematic freedom under wave action. Referring to Fig. 6.3, it may be inferred that the cracks create a wedging action over the roof of the tunnel which allows the rock block to vibrate under the influence of dynamic action. This vibration leads to higher compressive forces (positive) at peripheral angles of 10^0-25^0, as is evident from Fig. 6.1a. Moreover, tensile forces (negative) develop along the sidewall under the action of dynamic forces at peripheral angles of 90^0- 120^0, as may be noted from Fig. 6.1a. The tensile action at the sidewall is the result of the tunnel deformation under the combined influence of the bending, which occurs at the vicinity of the sidewall, coupled with the compressive force over the right shoulder due to the vibration of the rock wedge. The formation of yielded Voronoi rock blocks in the vicinity of the tunnel periphery causes bending to occur more readily at the sidewall under the action of the wave motion.

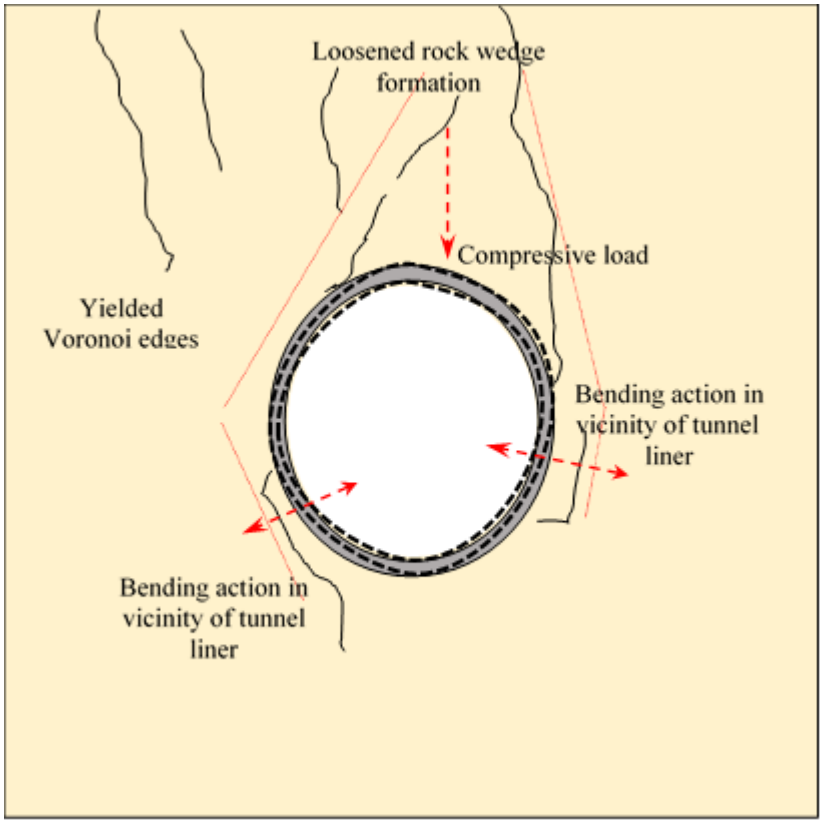

Fig. 6.3. Pattern of yielded joints for 50m depth tunnel under S-wave with 1Hz frequency

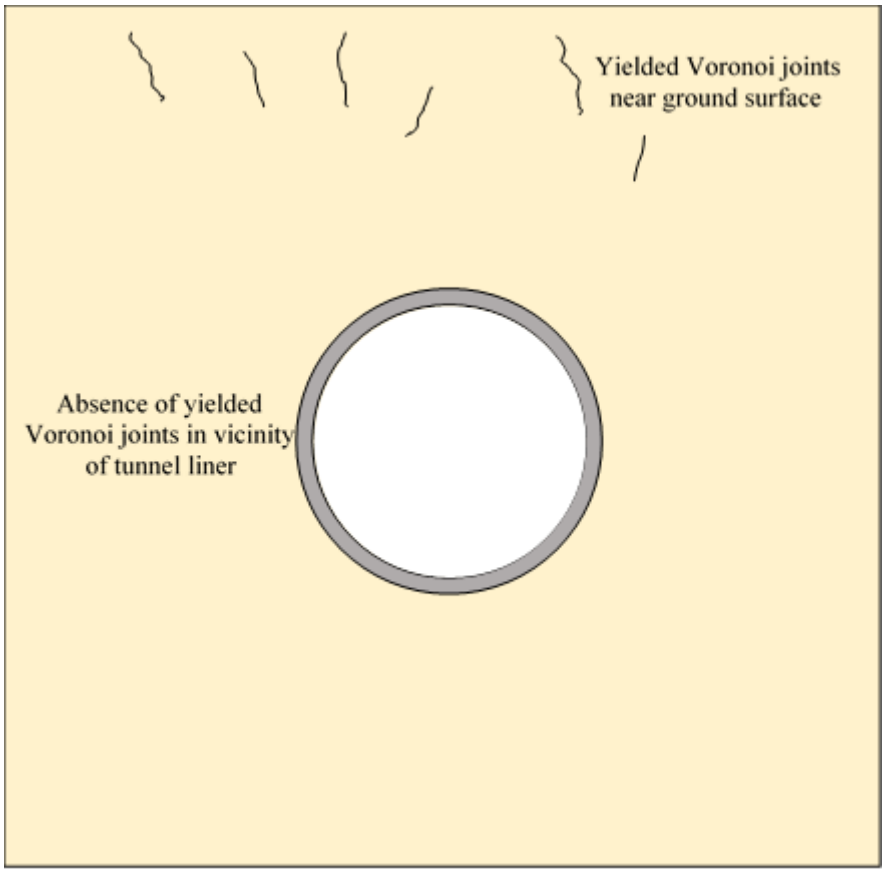

Fig. 6.4. Pattern of yielded joints for 50m depth tunnel under S-wave with 6Hz frequency

These observations correspond well with the damage patterns documented in the literature. It has been widely reported that in most of the cases of damage during the seismic action, spalling of concrete occurred near the crown and arch shoulders, with buckling of steel reinforcements at the sidewalls (Asakura and Sato 1996, Kitagawa and Hiraishi 2004).

6.3.1.2 Tunnel at a depth of 75m

With the increase in the depth of the tunnel to 75m, it is expected that the influence of waves reflected from the ground surface on the tunnel will reduce. Similar observations have been captured from the numerical simulations, which is evident from the yielding pattern of Voronoi joints highlighted in Fig. 6.5 and Fig. 6.6. It may be observed that there has been minimal yielding of Voronoi joints with no conspicuous wedge formation either above the tunnel crown or near the sidewall. Hence, the loosening of the rock blocks in the vicinity of the tunnel is not as

prominent as in the case of tunnel excavated at a depth of 50m. This has major implications on the forces developed in the liner during the wave action.

The variation in maximum dynamic axial force induced in the liner under S-wave action is shown in Fig. 6.7a and the peak values are shown in Fig. 6.7b. For this depth of tunnel also, a general trend of decrease in maximum force with increase in the frequency of input motion is observed. Moreover, it may be pointed out that the peak value of compression and tension forces highlighted in Fig. 6.7b is lesser than the corresponding peak values highlighted in Fig. 6.1b for the tunnel at a depth of 50m.

The variation in maximum dynamic bending moment induced in the liner under S-wave action is shown in Fig. 6.7c with the peak values highlighted in Fig. 6.7d. It may be observed that the bending moments are less than the values recorded for the tunnel at 50m depth. Thus, the absence of clearly defined loose rock blocks leads to lower axial force and bending moment since they are not free to vibrate under dynamic action in case of the tunnel at 75m depth. It is observed from Fig. 6.7b and Fig. 6.7d that the effects of frequency for this particular depth of tunnel on the peak compressive force and bending moment are marginal. However, higher tensile forces are developed for lower frequency of 1Hz highlighting the frequency-filtering effect of the joints.

Considering the P-wave action, the pattern of yielded joints has been found to be similar to those obtained with S-wave motion as shown in Fig. 6.5 and Fig. 6.6. It is observed that the maximum tensile forces recorded are more for input motion having a frequency of 1Hz and 2Hz as shown in Fig. 6.8a and Fig. 6.8b. It may also be noted that the maximum compressive axial force in the tunnel liner is almost identical at all the frequency of input motions considered. Fig. 6.8c shows the variation in maximum dynamic bending moment induced in the liner with the peak value shown in Fig. 6.8d. It may be observed that the axial force under P-wave action are comparatively less to those recorded for the tunnel at 50m depth for lower frequency of 1 Hz. However, for higher frequencies, the P-wave motions seem to have a greater influence on axial force and bending moment as compared to the tunnel located shallower than this depth.

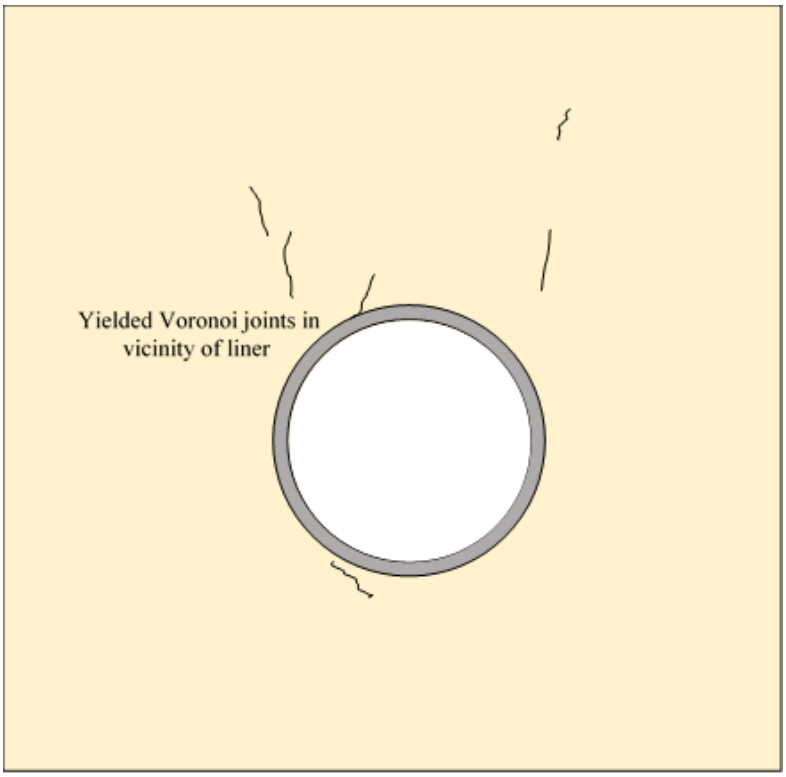

Fig. 6.5. Pattern of yielded joints for 75m depth tunnel under S-wave with 1Hz frequency

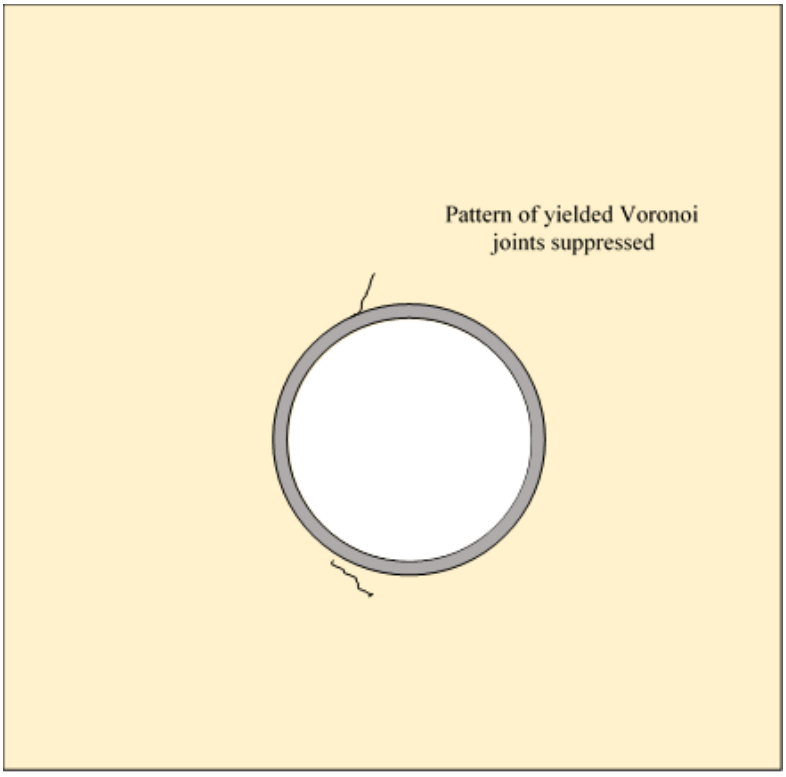

Fig. 6.6. Pattern of yielded joints for 75m depth tunnel under S-wave with 6Hz frequency

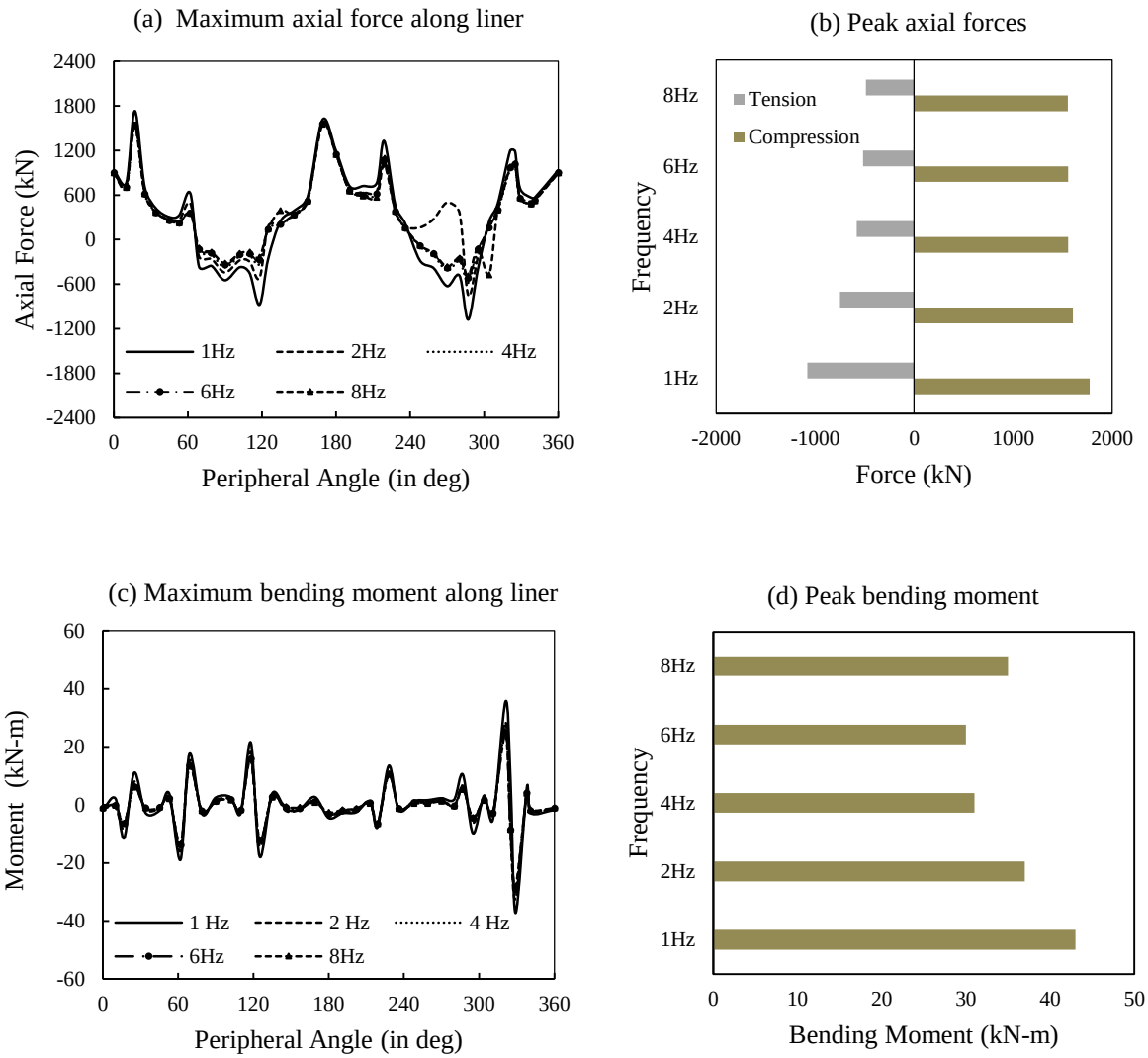

Fig. 6.7. Effect of frequency of excitation on tunnel located at a depth of 75m considering S-wave: (a) Maximum dynamic axial force along liner; (b) Peak axial force; (c) Maximum bending moment along liner; (d) Peak bending moment

6.3.1.3 Tunnel at a depth of 150m

The pattern of yielding of Voronoi joints for the case of the tunnel at a depth of 150m, and corresponding to the frequency of input motion of 1Hz and 6Hz for P-wave motion is shown in Fig. 6.9 and Fig. 6.10 respectively. It may be observed that due to frequency filtering effect, the yielding of Voronoi joints is minimal for the case of 6Hz. However, well-defined yielding pattern is observed for lower frequency of 1Hz. Moreover, at a 1Hz frequency of input motion, a distinct transition in the extent and direction of yielding is observed. The cracks become inclined unlike the earlier case of 50m and 75m. This is attributed to the fact that an

increase in overburden and in-situ stresses affects the mechanical response of the blocky rock mass. Similar results have been obtained under the S-wave action also. The combined effect of increased overburden and development of loose rock blocks results in an increase in tunnel liner forces. The variation in the maximum axial force under S-wave action is presented in Fig. 6.11a and Fig. 6.11b.

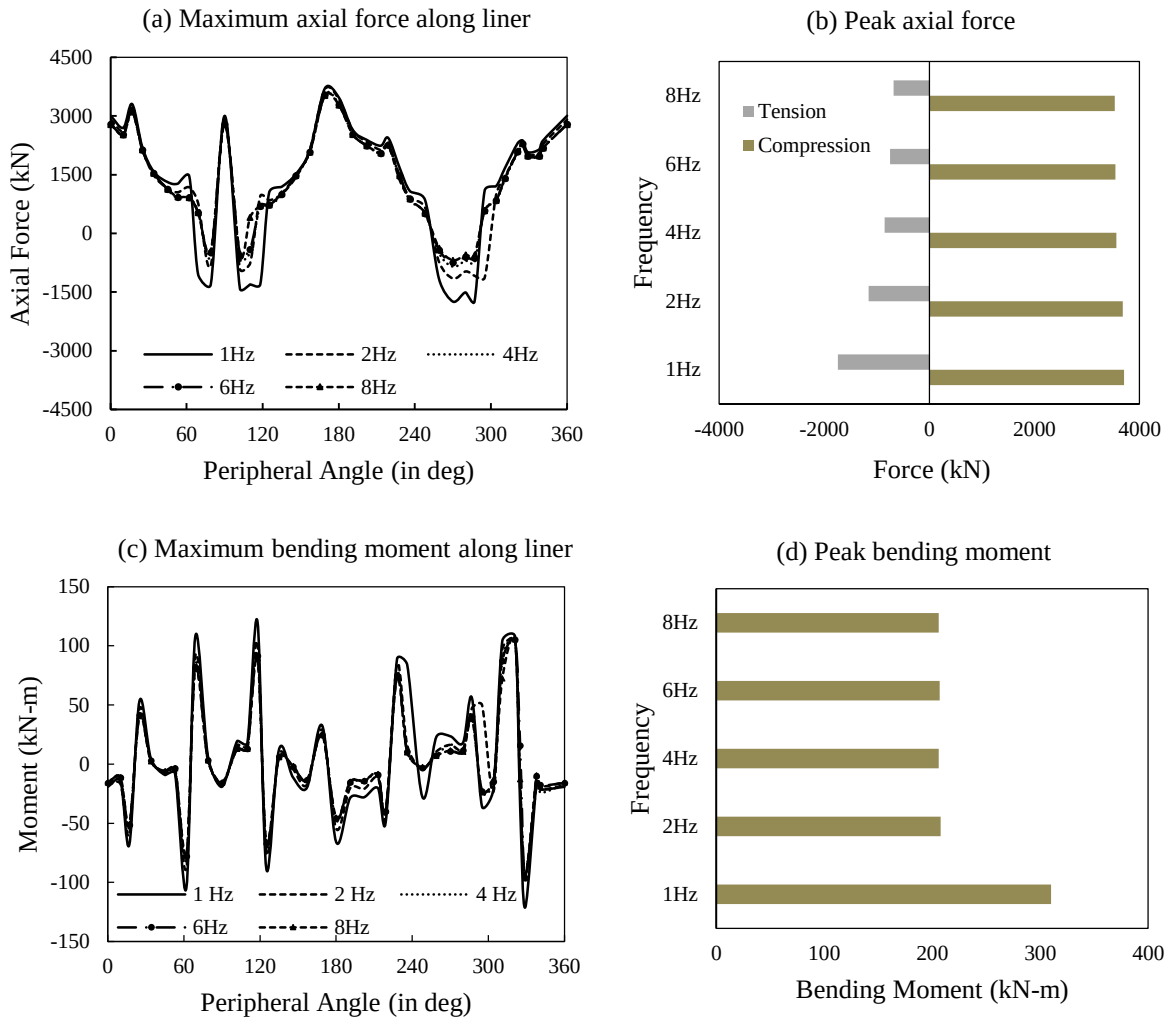

Fig. 6.8. Effect of frequency of excitation on tunnel located at a depth of 75m considering P-wave: (a) Maximum dynamic axial force along liner; (b) Peak axial force; (c) Maximum bending moment along liner; (d) Peak bending moment

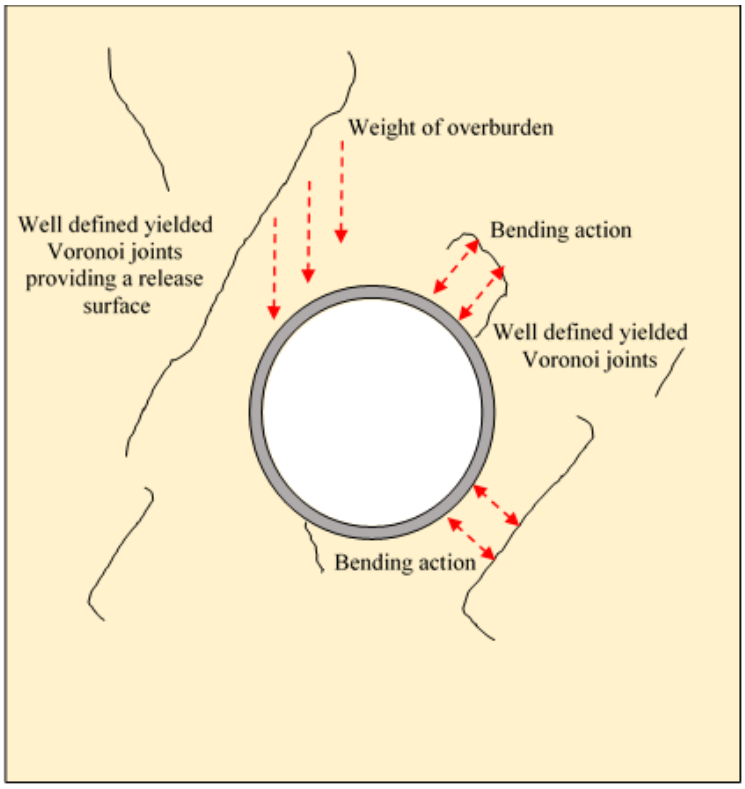

Fig. 6.9. Pattern of yielded joints for 150m depth tunnel under P-wave with 1Hz frequency

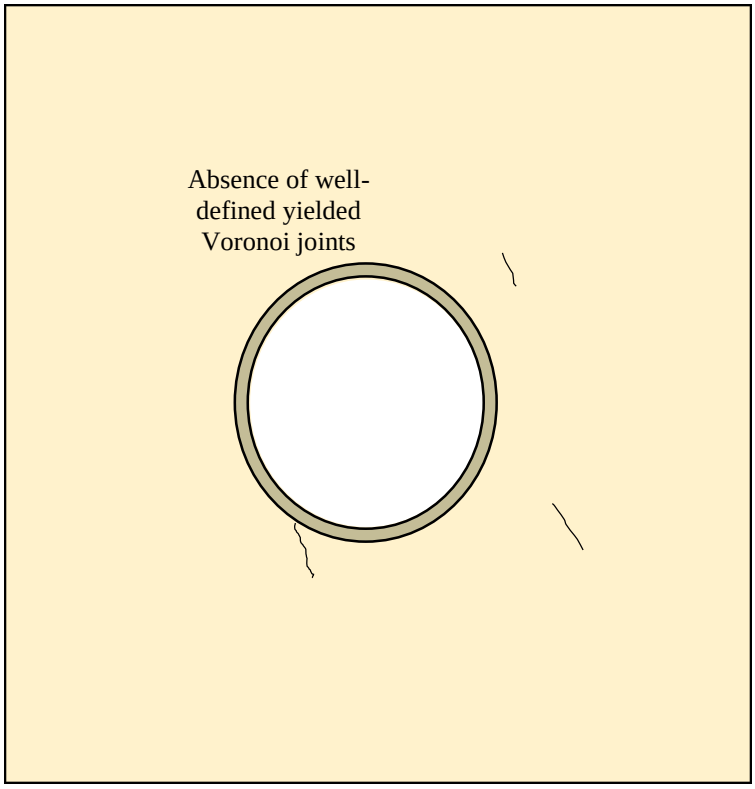

Fig. 6.10. Pattern of yielded joints for 150m depth tunnel for P-wave with 6Hz frequency

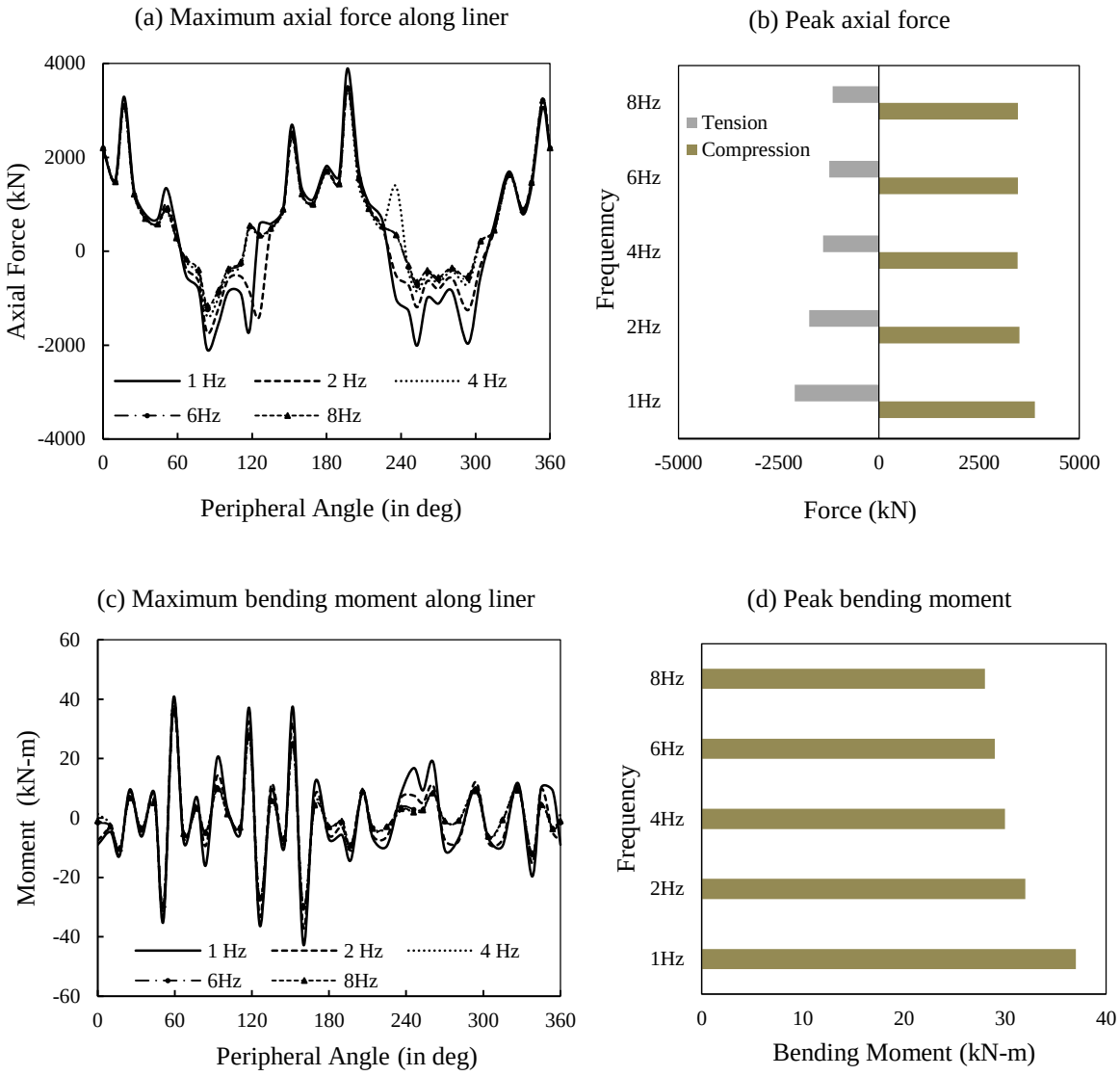

Fig. 6.11. Effects of frequency of excitation on tunnel located at a depth of 150m considering S-wave: (a) Maximum dynamic axial force along liner; (b) Peak axial force; (c) Maximum bending moment along liner; (d) Peak bending moment

The distribution of dynamic bending moment has been shown in Fig. 6.11c while the corresponding peak values are shown in Fig. 6.11d. The dynamically induced axial forces in the tunnel liner are greater under P-wave action as shown in Fig. 6.12a and Fig. 6.12b. Moreover, the bending moment is also more under P-wave action as shown in Fig. 6.12c and Fig. 6.12d. The increase in force and moment in the tunnel liner is attributed to the change in the overburden and hence the stresses at this depth.

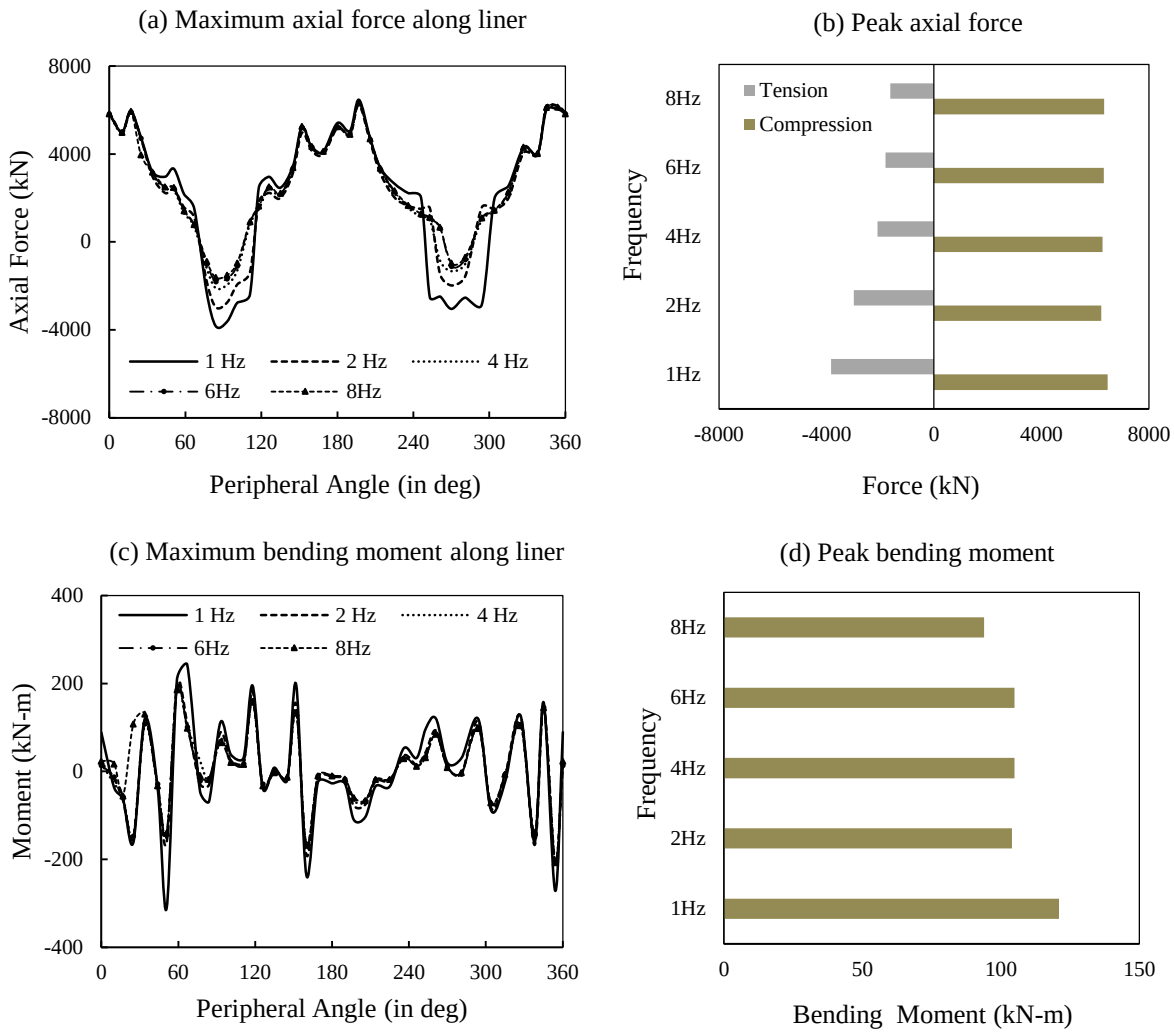

Fig. 6.12. Effects of frequency of excitation on tunnel located at a depth of 150m considering P-wave: (a) Maximum dynamic axial force along liner; (b) Peak axial force; (c) Maximum bending moment along liner; (d) Peak bending moment

Thus, it may be concluded from the above results that the tunnels excavated through blocky rock mass are more vulnerable for the lower frequencies of dynamic waves as the highly fractured and jointed region acts as a low pass frequency filter. At lower frequencies of input motion, the chances of formation of loosened rock blocks are more, and hence the demand on the liners under dynamic action is expected to be high. Also, the depth of the tunnel plays an important role with regard to the creation of loosened rock blocks, which dictate the nature of vibration and hence has a significant effect on the axial force and moment induced in the tunnel liner.

6.3.2 Influence of Depth and Type of Wave Action on Tunnel Response

The present section discusses the influence of depth of the tunnel and the type of wave action on demand imposed on the tunnel liners. As the vulnerability is found to be higher for lower frequencies of input motion, as highlighted in the previous section, the discussion presented here corresponds to the results obtained for input motions with frequency of 1 Hz and 2Hz only.

The peak dynamic axial force and bending moment under the action of S-waves are shown in Fig. 6.13a and Fig. 6.13b respectively. It is observed that both in compression and tension, peak dynamic axial force is more when the tunnel is at a depth of 50m and 150m in comparison to the tunnel at a depth of 75m. Moreover, it may be observed that the peak dynamic bending moment is maximum for tunnel at a depth of 50m. For deeper depths of 75m and 150m, there is a drastic reduction in the dynamic bending moment.

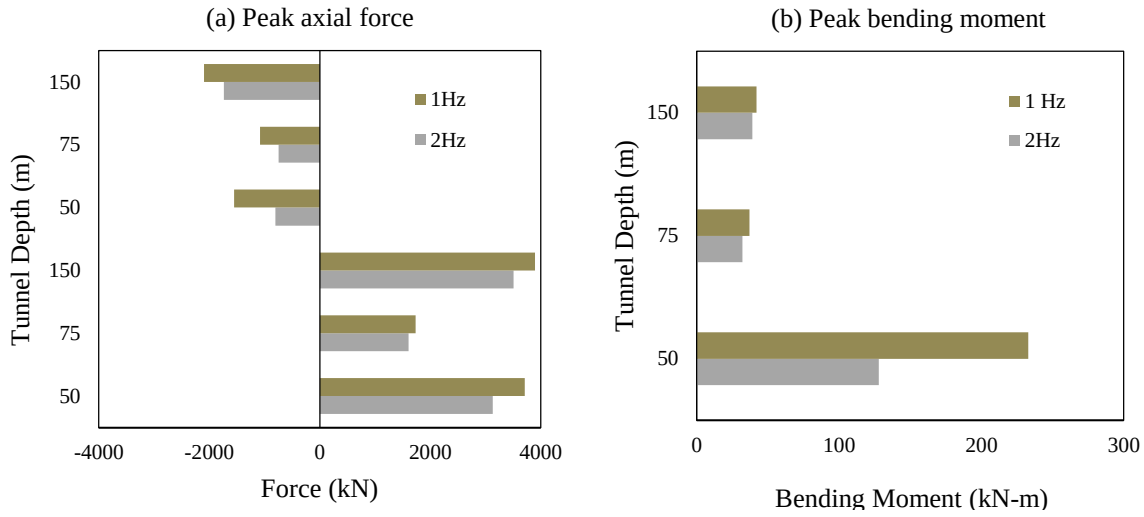

Fig. 6.13. Comparison of tunnel liner forces for different depths under S-wave: (a) Peak dynamic axial force along liner; (b) Peak dynamic bending moment along liner

These observations may be explained on the basis that as the tunnel depth increases from 50m to 75m, the influence of waves reflected from the ground surface reduces. Thus, the Voronoi joints do not yield either in shear or tension resulting in the absence of formation of clearly yielded Voronoi joints (refer Fig. 6.5), along which

the rock blocks could vibrate freely. Hence, the maximum dynamic axial force and bending moment are comparatively less for the 75m case.

Although the influence of waves reflected from the ground surface is minimal for the tunnel at a depth of 150m, the coupled influence of increased overburden and the energy imparted by the passage of the dynamic waves through the blocky region results in the formation of well- defined Voronoi joints which yield in shear and tension. Thus the loosened rock blocks vibrate under the influence of S-wave action leading to high axial forces for this tunnel depth.

The variation in the trend of the dynamic bending moment may be explained on the basis that for 50m tunnel depth, well-defined rock blocks are formed as a result of yielding of Voronoi joints in the vicinity of the tunnel liner. The mode of movement of these rock blocks under S-wave action causes high bending moment in the tunnel liner. However, for the 75m and 150m tunnel depth, there is no conspicuous rock wedge demarcated by yielded Voronoi joints in the vicinity of the tunnel liner. Hence, the bending moments in the tunnel liner are highly suppressed. Thus, it may be stated that the bending action under S-wave decreases with increase in the depth of tunnel.

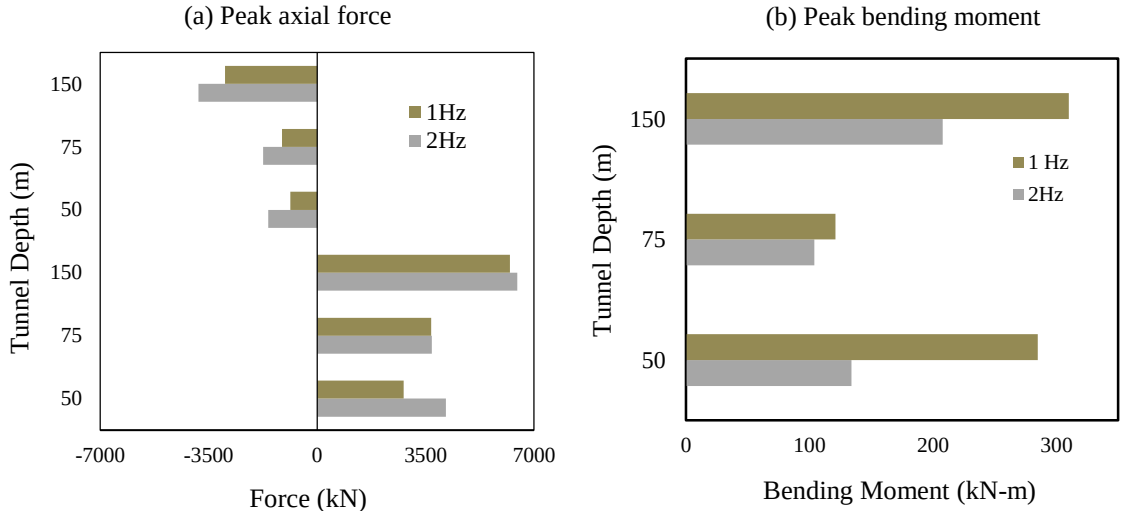

Fig. 6.14. Comparison of tunnel liner forces for different depths under P-wave: (a) Peak dynamic axial force along liner; (b) Peak dynamic bending moment along liner

For the P-wave ground motion, the maximum dynamic axial force in both tension and compression are comparable for 50m and 75m tunnel depths as shown in Fig.

6.14a. However, the recorded force is highest for the case of 150m tunnel depth. Moreover, the highest peak dynamic bending moment is recorded for the tunnel at a depth of 150m below the ground surface as presented in Fig. 6.14b. For the three tunnel depths considered in the present study, the dynamic bending moment is least for the 75m case. Under the influence of P-wave action, the vertical vibrations add to the gravitational overburden. However, the absence of well-defined rock blocks in case of 75m depth does not allow large bending moment to develop in the tunnel liner. But with an increase in tunnel depth to 150m, the vertical vibration (P-wave) coupled with large overburden results in increased demand on the tunnel liner.

6.3.3 Influence of In-situ Stress Ratio K_0

An important parameter governing the behavior of underground excavations is the distribution of stresses in the host material. In this context, the in-situ stress ratio may play a significant role in the dynamic response of tunnels. To evaluate the influence of in-situ stress ratio K_0, numerical analyses have been carried out considering 1 Hz frequency of input motion. Three in-situ stress ratios (K_0) of 1.0, 1.2 and 1.5 have been adopted for all the three tunnel depths considered. Table 6.2 summarizes the results in the form of maximum dynamic axial force and bending moment recorded for the tunnels at three different depths under the action of S-waves. The ratio (R) of the forces for each depth with respect to the values for K_0=1.0 are also presented for a better demonstration of the effect of in-situ stress ratio.

It is observed that for all the three tunnel depths, an increase in in-situ stress ratio leads to a corresponding increase in the compressive axial force. However, the increase is comparatively more in case of the tunnel at depths of 75m and 150m. Regarding tensile force and bending moment, a general trend of decrease in values with increase in in-situ stress ratio is observed for the tunnel of depth 50m. However, for tunnel depth of 75m and 150m, increase in tensile force and moment is observed.

Table 6.2. Maximum dynamic axial force and bending moment for various in-situ stress ratio (K) under the action of S-wave

Tunnel depth (m)	In-situ Ratio K	Compressive (in kN)	R_C	Tensile (in kN)	R_T	Moment (in kN-m)	R_M
50	1.0	3712	1.00	1553	1.00	233	1.00
	1.2	4935	1.33	905	0.58	154	0.66
	1.5	5924	1.60	1063	0.68	162	0.70
75	1.0	1773	1.00	1079	1.00	37	1.00
	1.2	5473	3.09	1829	1.70	163	4.41
	1.5	6810	3.84	1741	1.61	196	5.30
150	1.0	3894	1.00	2098	1.00	42	1.00
	1.2	10419	2.68	4517	2.15	364	8.67
	1.5	13192	3.39	4885	2.33	354	8.43

Similar trends of variation in maximum dynamic axial force and bending moment is observed for tunnels under the action of P-waves as summarized in Table 6.3. The following prominent points are noted.

- The dynamic axial force and bending moment increases under the influence of S-wave action for higher in-situ stress ratio of 1.2 and 1.5. The role of in-situ stress ratio becomes very critical with the increase in the tunnel depth.
- For P-wave action also, an increase in the demand on the liner with increase in the in-situ ratio is observed. However, the increase in ratio is not as high as observed for the case of S-wave action.
- The compressive and tensile axial force developed in the tunnel liner becomes maximum for the tunnel located at a depth of 150m at an in-situ stress ratio of 1.5. This observation holds true for both the S-wave and P-wave action.

Table 6.3. Maximum dynamic axial force and bending moment for various in-situ stress ratio (K_0) under the action of P-wave

Tunnel depth (m)	In-situ Ratio K_0	Compressive (in kN)	R_C	Tensile (in kN)	R_T	Moment (in kN-m)	R_M
50	1.0	4155	1.00	1585	1.00	285	1.00
	1.2	5401	1.30	1470	0.93	164	0.58
	1.5	6070	1.46	1741	1.10	176	0.62
75	1.0	3705	1.00	1741	1.00	121	1.00
	1.2	5554	1.50	2010	1.15	149	1.23
	1.5	6892	1.86	2218	1.27	198	1.64
150	1.0	6464	1.00	3380	1.00	310	1.00
	1.2	6810	1.05	1901	0.56	337	1.09
	1.5	12586	1.95	5782	1.71	358	1.15

From these observations, it may be concluded that the adverse effect of both the S-wave and P-wave increases with an increase in the in-situ stress ratio, especially at a deeper depth of 150m. Thus, it may be stated that the in-situ stress is an important parameter affecting the dynamic response of tunnels. As mountain tunnels pass through variable geological conditions with varying in-situ stress conditions, a due consideration of the same is necessary.

6.3.4 Effect of Intensity of Ground Motion

To evaluate the influence of the peak ground motion on the dynamic response of tunnels, analyses have been carried out by employing sinusoidal motions with PGA of 0.2g and 0.5g for tunnel located at a depth of 150m. The analyses have been run for frequencies of 1Hz and 2Hz considering S-waves. The variation of the dynamic axial force in the liner for the case of 0.2g and 0.5g has been presented in Fig. 6.15 and Fig. 6.16 respectively. Similarly, Fig. 6.17 and Fig. 6.18 highlight the variation of bending moment in the liner for excitations having PGA of 0.2g and 0.5g respectively.

For the case of 1Hz frequency, it is observed that the maximum dynamic axial force increases by 25% as the PGA increases from 0.1g to 0.2g. The percentage increase

becomes 54% when a PGA of 0.5g is adopted. A similar trend of increase in the dynamic bending moment is noted where an increase of 92% and 271% is observed for PGA of 0.2g and 0.5g respectively. A similar trend of increase in the liner forces is observed for the case of 2Hz. However, the percentage increase is lower in comparison to the case of 1Hz frequency. Thus, it may be stated that the vulnerability of the tunnels subjected to dynamic loads is higher in case of low-frequency motions having higher PGA values. Table 6.4 summarizes the maximum forces and percentage change for the cases considered in the study.

6.4 Effect of Intensity of Earthquake (PHA) on Observed Tunnel Damages

Based on the discussions presented in the preceding sections, it can be concluded that one of the major factors affecting the tunnel damages is dependent on the energy reaching the location of the tunnel. To predict the level of ground shaking, a number of attenuation laws have been proposed in the literature (Kramer 1996).

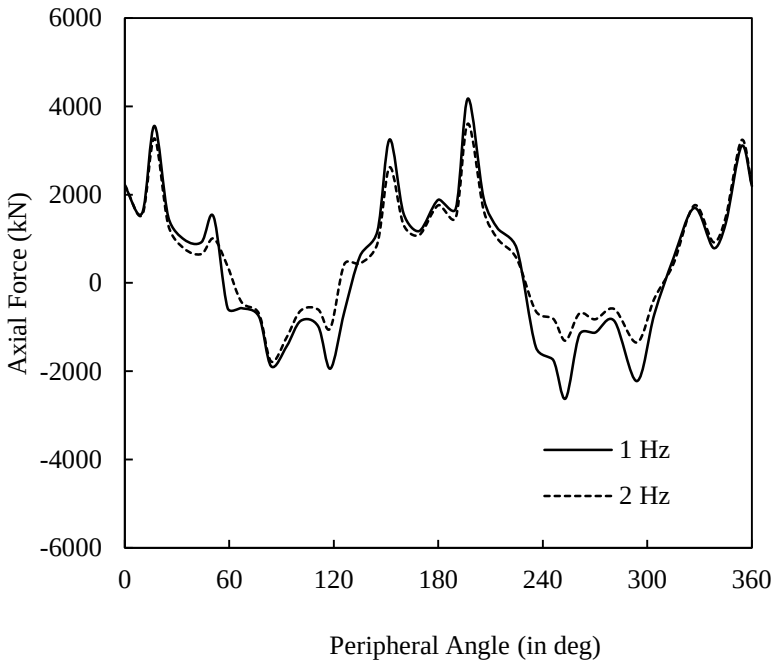

Fig. 6.15. Maximum dynamic axial force along liner subjected to PGA of 0.2g

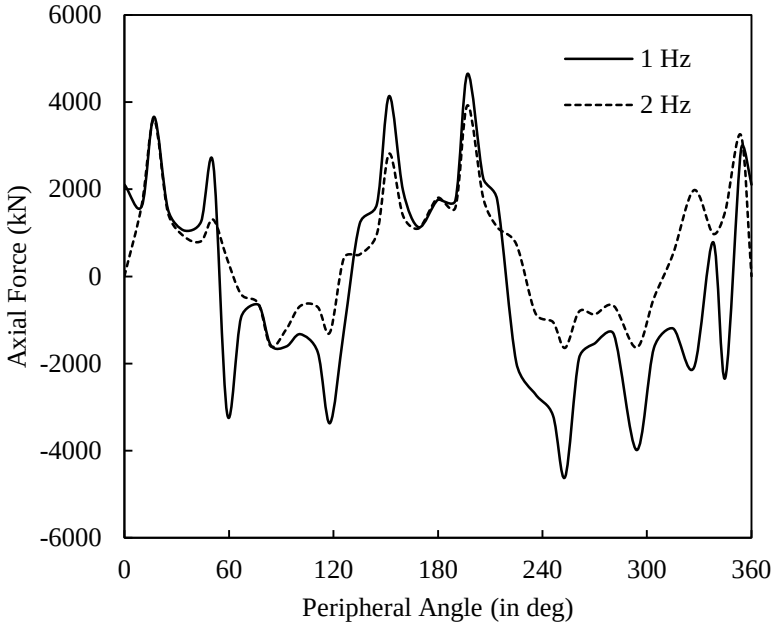

Fig. 6.16. Maximum dynamic axial force along liner subjected to PGA of 0.5g

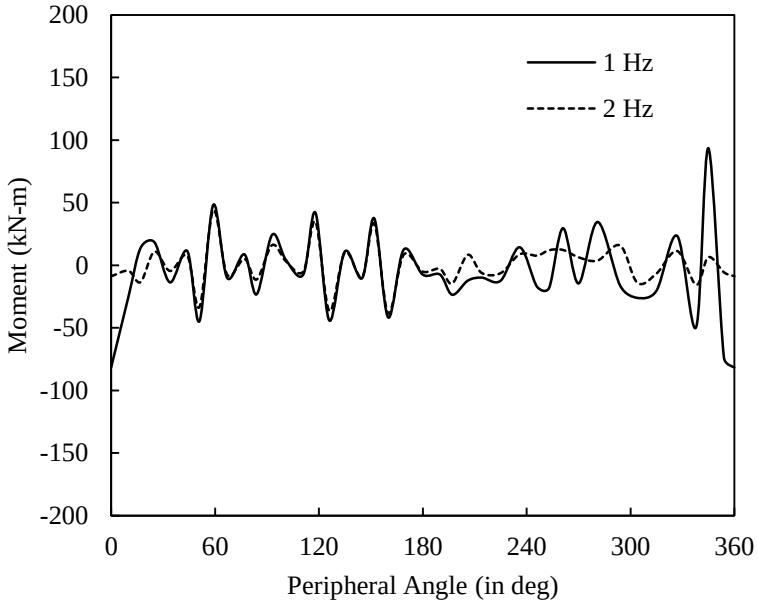

Fig. 6.17. Maximum dynamic bending moment along liner subjected to PGA of 0.2g

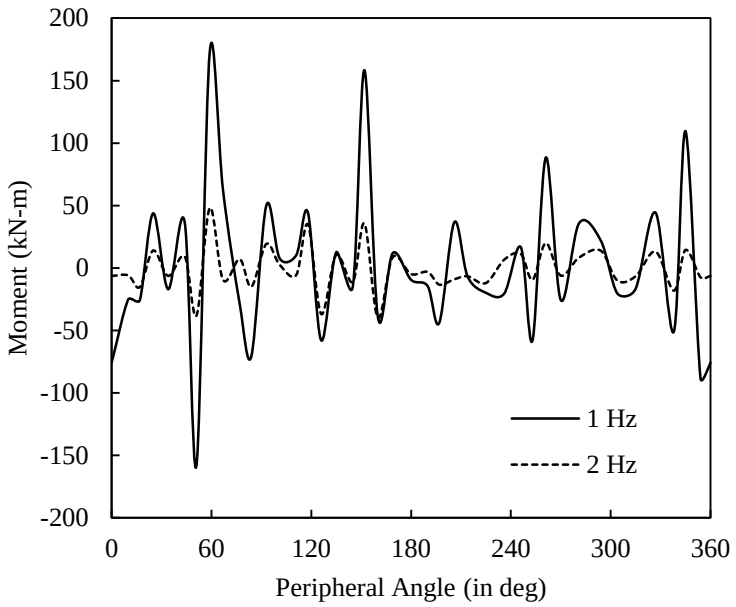

Fig. 6.18. Maximum dynamic bending moment along liner subjected to PGA of 0.5g

In the present section, the attenuation relation suggested by Campbell (1981) has been used to evaluate the peak horizontal acceleration (PHA) at tunnel locations reported to have been damaged following the 1999 Chi-Chi earthquake and 2008 Wenchuan earthquake. Eqn. (6.1) represents the attenuation relation expressing the peak horizontal acceleration as a function of epicentral distance (R) and magnitude (M).

$$\ln PHA(g) = -4.141 + 0.868M - 1.09\ln[R + 0.0606\exp(0.7M)] \qquad (6.1)$$

Table 6.4. Variation in maximum axial force and bending moment with PGA

Freq. (Hz)	PGA (g)	Axial (+) (in kN)	%	Axial (-) (in kN)	%	Moment (+) (in kN-m)	%	Moment (-) (in kN-m)	%
1	0.1	3894		2098		41		43	
	0.2	4175	7	2623	25	93	56	82	92
	0.5	4650	25	4605	54	173	77	158	271
2	0.1	3509		1739		39		37	
	0.2	3606	3	1780	2	44	10	39	4
	0.5	3925	12	1638	-6	48	21	40	7

Using Eqn. (6.1), the PHA at tunnel location for the 57 tunnels listed in Table 2.5 has been evaluated. The results have been summarized in Table 6.5 relating the number of tunnels damaged with the PHA. It is noted that only three tunnels suffered damages in case the PHA predicted from the attenuation relation is up to 0.1g. However, a substantial increase in the number of tunnel damage is noted for higher PHA. Similarly, the PHA for the 30 tunnels of the Du-Wen highway network summarized in Table 2.6 has also been evaluated and summarized in Table 6.6. Similar to the earlier case, it is noted that tunnel damage is not observed in case of PHA being within 0.1g. However, higher PHA of 0.2g and above is associated with greater number of tunnel damage.

Table 6.7 combines the results of both the earthquake events. From Table 6.7, it can be observed that a PHA of 0.1g has caused tunnel damage to 3 tunnels only. In comparison, a substantial increase in cases of tunnel damage is observed for a PHA of 0.2g and higher. These observations compare well with the findings highlighted in the previous section where a substantial increase in tunnel liner forces has been observed with the increase in the PGA level.

Table 6.5. Damage to tunnels for various PHA in 1999 Chi-Chi earthquake

PHA (g)	Number of tunnels damaged	Percent
Upto 0.1	3	5
0.11-0.2	21	37
0.21-0.3	20	35
0.31-0.4	5	9
0.41-0.5	6	11
0.51-0.6	0	-
0.61-0.7	1	2

Table 6.6. Damage to tunnels for various PHA in 2008 Wenchuan earthquake

PHA (g)	Number of tunnels damaged	Percent
Upto 0.1	-	-
0.11-0.2	4	13
0.21-0.3	7	23
0.31-0.4	2	7
0.41-0.5	7	23
0.51-0.6	5	17
0.61-0.7	3	10
0.71-8	2	7

Table 6.7. Summary of damage to tunnels in 1999 Chi Chi and 2008 Wenchuan earthquake

PHA (g)	Number of tunnels damaged	Percent
Upto 0.1	3	3.4
0.11-0.2	25	28.7
0.21-0.3	27	31
0.31-0.4	7	8
0.41-0.5	13	14.9
0.51-0.6	5	5.7
0.61-0.7	4	4.6
0.71-8	3	3.4

6.5 Corroboration of Observed Damage Patterns with Numerical Simulation

In the present section, a brief overview of damage patterns of tunnels passing through the highly fractured zone and subjected to seismic action is presented. Further, the corroboration of the highlighted damage patterns with the numerical simulations carried out in the present study is presented along with a description of the mechanism involved. Thus, the present section highlights the applicability of the present modeling approach to study the dynamic response of tunnels passing through blocky rock mass.

From a detailed review of seismic damage of tunnels reported during 1995 Hyogoken-Nanbu (Japan), 1999 Chi-Chi (Taiwan), 2004 Mid-Niigata Prefecture (Japan) and 2008 Wenchuan (China) earthquakes, the following major damage patterns have been identified.

- Uplift/heaving of bottom invert
- Spalling of tunnel liner at the crown
- Large movement of sidewall leading to large convergence
- Failure of tunnel liner at the arch shoulder regions

Most of the above stated damage patterns have been found to be associated with tunnel sections passing through highly fractured rock mass. Prominent examples include the cases of Uonama and Myoken tunnel which were damaged in the 2004 Mid-Niigata Prefecture earthquake.

6.5.1 Mechanism Leading to Damage of Tunnel Liner

Based on the results of the numerical analyses presented in *Section 6.3.1*, it may be observed that the pattern of variation of maximum dynamic axial force and bending moment is almost similar. Hence, to generalize the discussion for various cases simulated in the present study, the tunnel liner has been divided into four regions as shown in Fig. 6.19. The prominent action to which the various regions of the tunnel liner is subjected under seismic action is demonstrated in Fig. 6.20. It should be noted that in Fig. 6.20, the solid lines represent the original shape of the liner

before being subjected to wave action whereas the dashed lines represent the state of the liners during the wave action.

Referring to Fig. 6.20a, it may be noted that the crown and arch shoulder (section AB) is majorly subjected to overburden load under dynamic vibrations. The weight of the overburden causes compressive forces to develop which concentrates towards the crown and become very high at around 5^0-10^0 resulting in the spalling of tunnel liner. This has been highlighted in *Section 6.3.1* for all three tunnel depths considered in the study.

The region BC is subjected to high bending moment which causes the liner to bend. As a result of the bending action, there occurs a transition in the curvature causing the development of high tensile forces at the sidewall which leads to damage. Moreover, the high bending moment also leads to large convergence which has been widely observed for most of the tunnels under seismic action in the past. However, the continuity of the liner causes a change in the curvature leading to compressive forces directed towards the invert as highlighted in Fig. 6.20b. The concentration of the compressive force leads to a condition facilitating the uplift of the bottom floor.

The region CD is subjected to high bending action leading to a concentration of compressive force near the floor and tensile forces near the left sidewall as shown in Fig. 6.20c. The region DA corresponding to the left sidewall is majorly subjected to tensile forces which results in the spalling of the tunnel liner.

The four major regions highlighted corresponds to the sections where damages have been observed during the past earthquakes. It is observed that the analyses carried out in the present study are able to predict the response of the tunnels to a substantial extent thereby corroborating the damage patterns observed in the field.

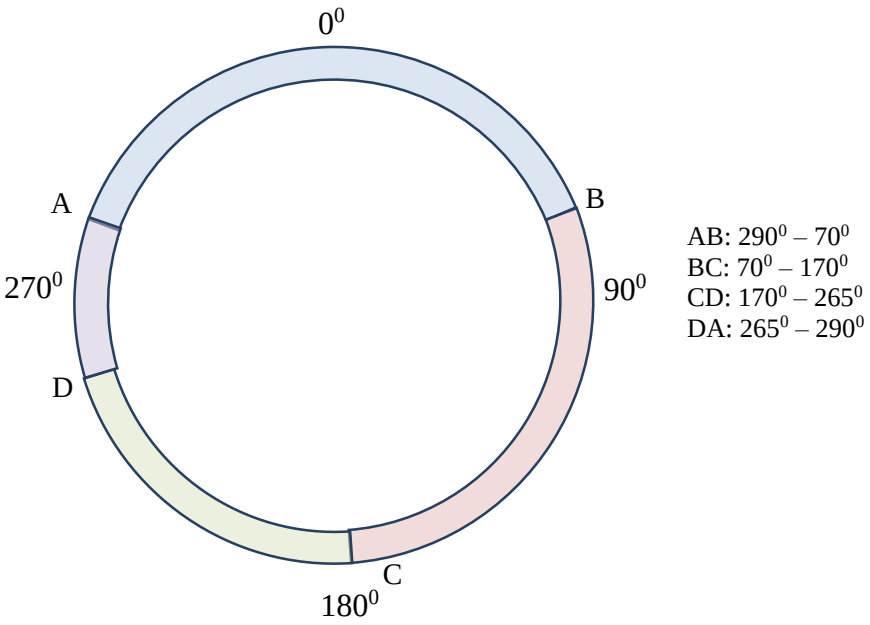

Fig. 6.19. Tunnel liner regions considered for explanation of failure mechanisms

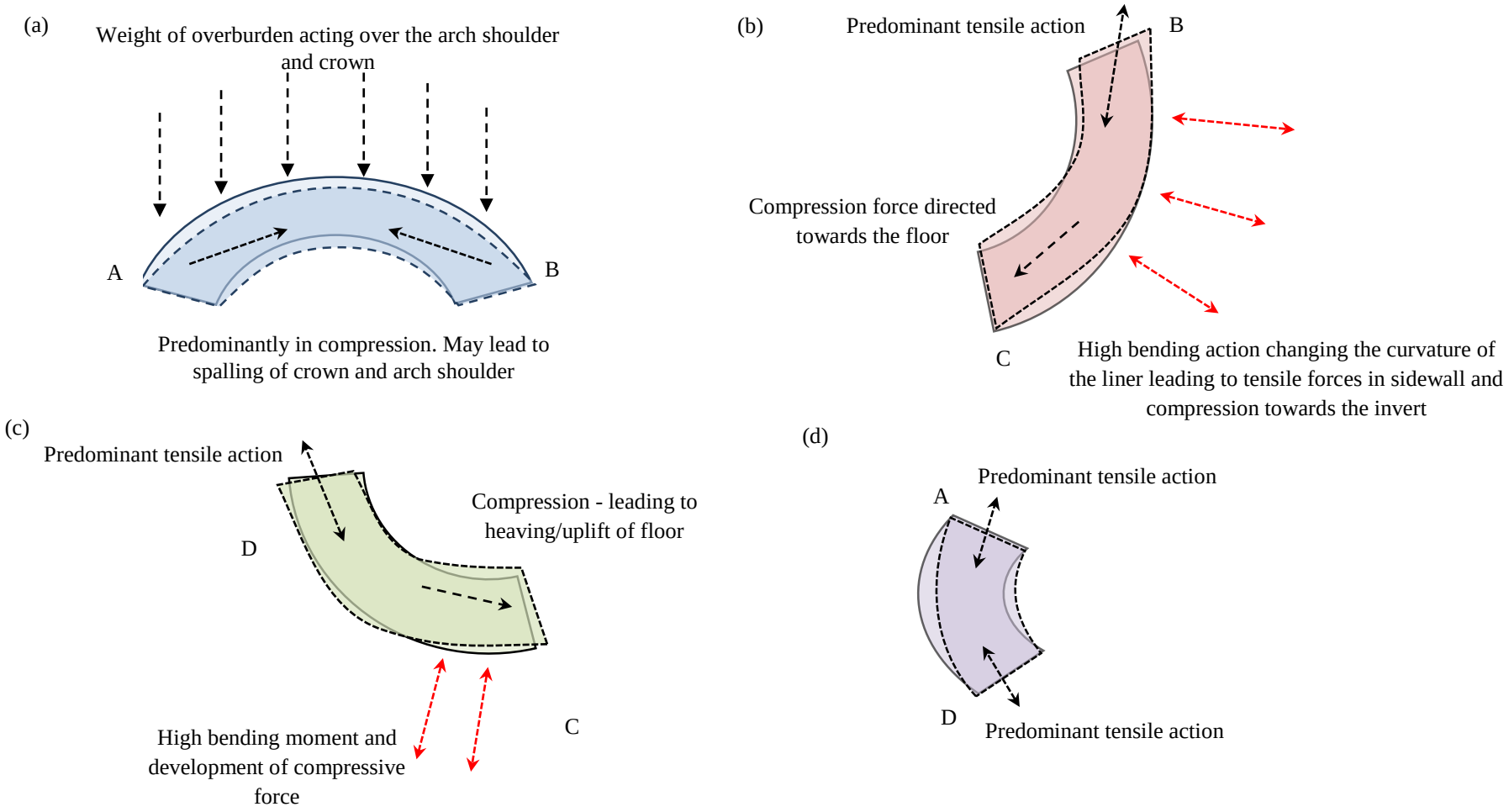

Fig. 6.20. Generalized forces leading to damage acting on different regions of tunnel liners

6.6 Summary

In the present chapter, numerical investigation for the seismic response of a circular lined tunnel in the blocky rock mass has been attempted. To account for the interaction between the dynamic waves and the jointed rock mass, the analyses have been carried out in a distinct element based framework. For a realistic representation of the blocky rock mass, the Voronoi tessellation scheme has been utilized for idealizing the joints.

The influence of the frequency of input motion, depth of tunnel, in-situ stress ratio and type of wave action on the tunnel response has been assessed. The response has been evaluated in terms of the dynamic axial force and bending moment developed in the tunnel liner. Also, an attempt has been made to corroborate the findings of the numerical simulations with the damage patterns highlighted in the literature. The findings of the present study may be summarized as follows.

- The randomly oriented joints, which break the geological medium into blocky rock mass, acts as a low pass filter allowing low-frequency waves to pass through the fractured region and offers resistance to the high-frequency waves.
- As a result of the frequency filtering effect, the dynamically induced axial forces and moments are largest for the case of low frequency of input motion for both S and P-waves. Thus, it may be concluded that low-frequency waves are more detrimental in case of tunnels passing through blocky rock mass.
- The tunnels at shallow depths of 50m are affected by the wave reflected from the ground surface. The reflected waves cause cracks to develop in an almost vertical pattern which provides an added degree of kinematic freedom to the rock blocks to move under the influence of dynamic action. However, such an observation is valid for low-frequency waves only.
- As the tunnel depth increases, the influence of waves from the ground surface decreases. However, the increased overburden may still cause the development of loosened rock blocks under the combined influence of

dynamic action and the in-situ stresses. Thus, tunnels at deeper depths and passing theough the blocky rock mass are vulnerable to seismic damages. This is in contrast to the traditional belief that tunnels at deeper depths are not vulnerable to seismic damage.

- At lower in-situ stress ratio of K_0=1.0, the effect of P-waves is more detrimental to the integrity of the tunnel. However, as the in-situ stress ratio increases, the adverse influence of S-waves increases with increase in the tunnel depth.
- Peak Horizontal Acceleration (PHA) is a critical parameter governing tunnel damage. Using attenuation relationship, PHA values were evaluated for the tunnels damaged in 1999 Chi-Chi and 2008 Wenchuan earthquakes. It shows that PHA has a significant effect on tunnel damage. The numerical investigation also confirmed the same.
- Damage patterns observed in the tunnels during past earthquakes can be comprehensively explained by the numerical approach considered in the study. Based on the present study, generalized seismic forces in various regions of the tunnel liner have been presented.

…

Chapter 7

SEISMIC ISOLATION OF TUNNEL USING EXPANDED POLYSTYRENE (EPS) GEOFOAM

7.1 Introduction

The damage sustained by mountain tunnels in recent earthquakes highlight the high seismic demands imposed on the tunnel liner. Thus, an effective mitigation measure aimed towards the reduction of the demands on the liner is necessary. The present chapter presents the promising capability offered by Expanded Polystyrene (EPS) Geofoam as a potential seismic buffer for lined tunnels in the blocky rock mass.

7.2. Seismic Isolation of Tunnel

Among various mitigation measures, the application of seismic isolation through the incorporation of a protective coating material has shown promising results for some geotechnical structures such as pipelines and retaining walls. Recently, the use of Expanded Polystyrene (EPS) Ggeofoam as an effective buffer material for seismic isolation of retaining walls has been suggested based on the results of a number of shake table tests and numerical investigations. Given the promising capabilities, the effect of inclusion of an EPS Geofoam as an aseismic measure for tunnels is presented here.

7.2.1 Numerical Model and Dynamic Analyses

The present section provides a comparison of the axial force and bending moment developed in the tunnel liner under the seismic action for two cases – i. liner without any isolation layer and ii. liner covered with EPS geofoam. For the first case, the seismic demand on the tunnel liner is evaluated by applying an earthquake time history to the numerical model discussed in Section 3.3. To evaluate the influence of the EPS Geofoam, dynamic simulation has also been performed by incorporating an EPS Geofoam layer of 0.4m thickness around the

liner. The EPS Geofoam is assumed to be elastic having a density of 16 kg/m^3 and an elastic modulus of 4.8 MPa in the analyses.

For each case, two depths of the tunnel, i.e., 75m and 150m, have been considered. The evolution of the axial force and bending moment developed in the liner during the seismic action is presented. The largest axial force and bending moment developed in the liner under the seismic action is also highlighted.

7.2.2 Earthquake Time History

The seismic demand imposed on the tunnel liner has been evaluated under the action of the acceleration time-history recorded during the Kobe earthquake (1995) as shown in Fig. 7.1. The corresponding Fourier amplitude is shown in Fig. 7.2. The acceleration record has a peak value of 0.34g with a predominant frequency of 0.59 Hz which occurs at 6.93 sec after the onset of the earthquake. Since the earthquake time history corresponds to the motion recorded at the ground surface, deconvolution has been performed on the record to arrive at the base motion to be applied for the numerical simulation.

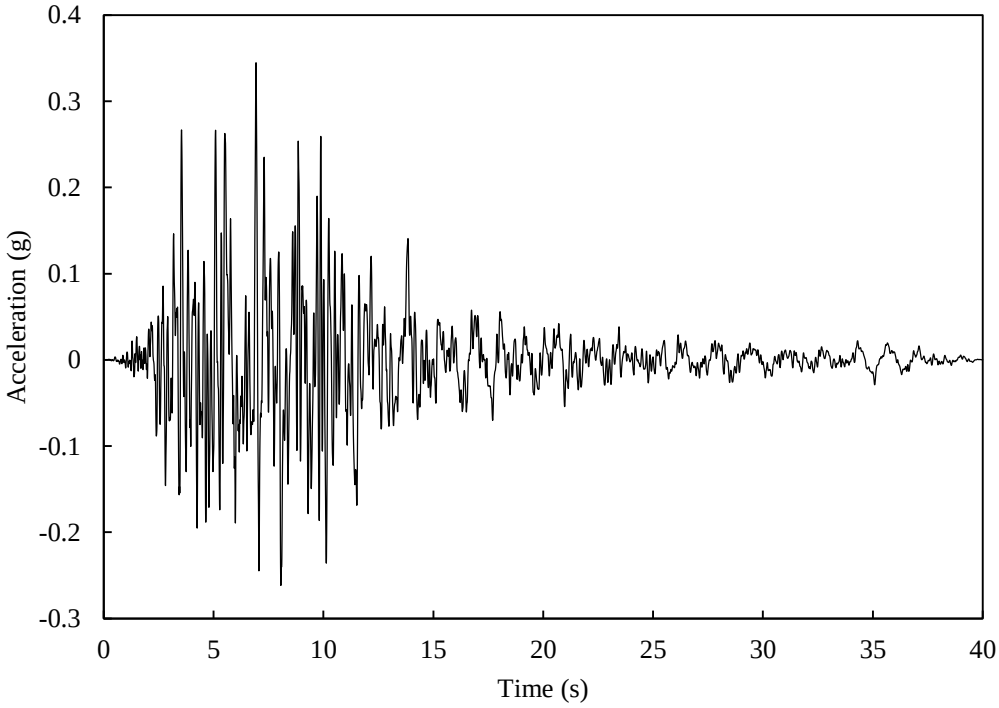

Fig. 7.1. Acceleration time history considered

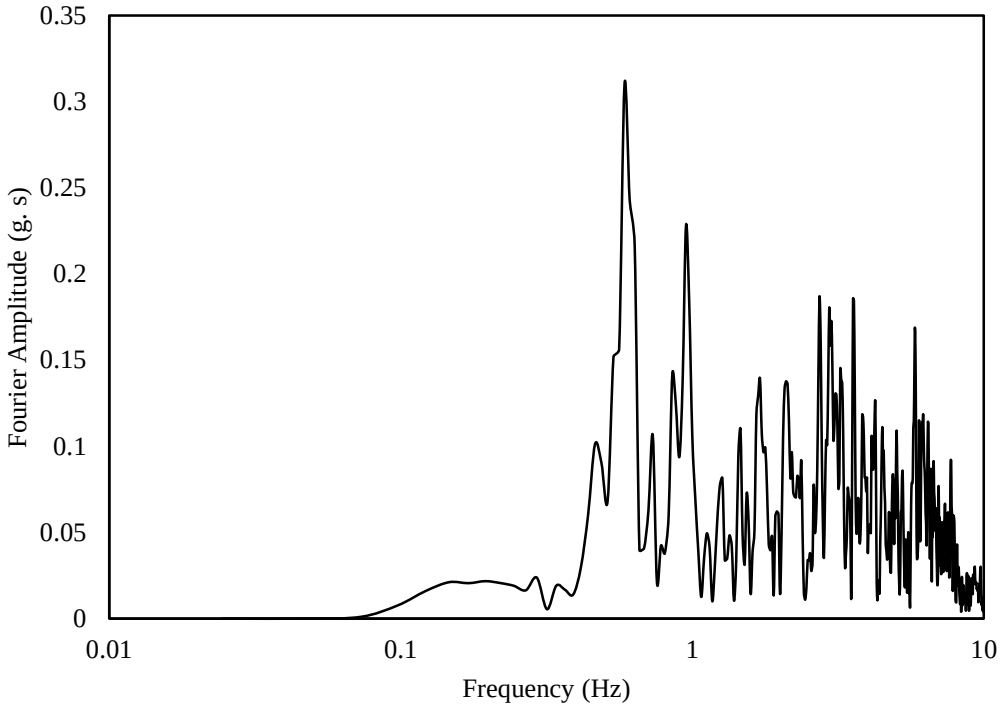

Fig. 7.2. Fourier spectrum of acceleration time history

7.3. SEISMIC DEMAND ON LINER

The maximum seismic demand imposed on the tunnel liner is presented in terms of the axial force and bending moment.

7.3.1. Tunnel at 75m Depth without any Isolation Layer

The distribution of maximum axial force and bending moment developed in the tunnel liner is shown in Fig. 7.3 and Fig. 7.4 respectively. It may be noted that the maximum axial force is recorded at the floor of the tunnel which corresponds to 180^0. High bending moment is recorded at 90^0, 180^0 and 270^0 which correspond to the right and left sidewall respectively. The value maximum axial force and bending moment is 1350 kN and 113 kN-m respectively. This implies that the demand on the tunnel liner will be comparatively high at the sidewall sections and the floor due to the seismic action. In fact, in the majority of the cases of damage reported in the literature, the vulnerability of the sidewalls and the uplift of the floor have also been observed. The evolution of the axial force and bending moment during the application of the acceleration time history is presented in Fig. 7.5. The results are presented for various locations of the tunnel liner.

A distinct change in the axial force and bending moment is noticed at around 3.2 sec from the onset of the dynamic excitation for almost all the positions along the tunnel liner. From the earthquake time history shown in Fig. 7.1, it is to be noted that at 3.2 sec, the peak ground acceleration almost reaches a value of 0.1g which causes the distinct change in the trend. Barring a few cases, the axial force and bending moment in the tunnel liner shows a transient response in the time interval between 5 secs and 15 secs which corresponds to the variations in the acceleration time-history record. At the end of 15 secs, the axial force and the bending moment in the tunnel liner tends to stabilize to a constant value.

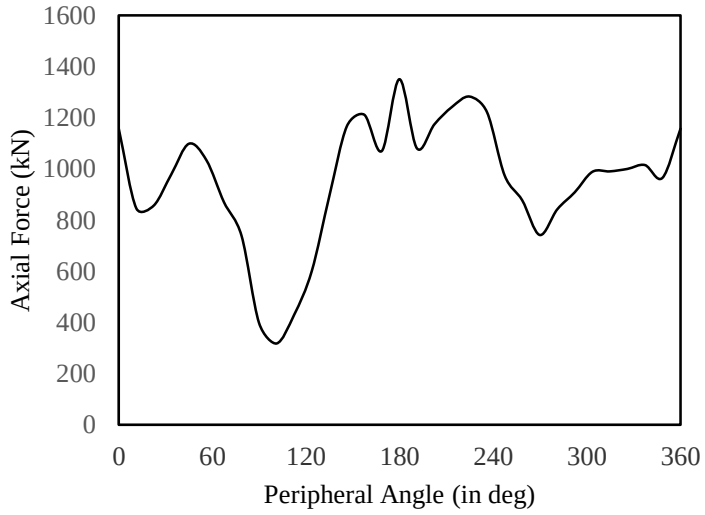

Fig. 7.3. Maximum axial force along liner

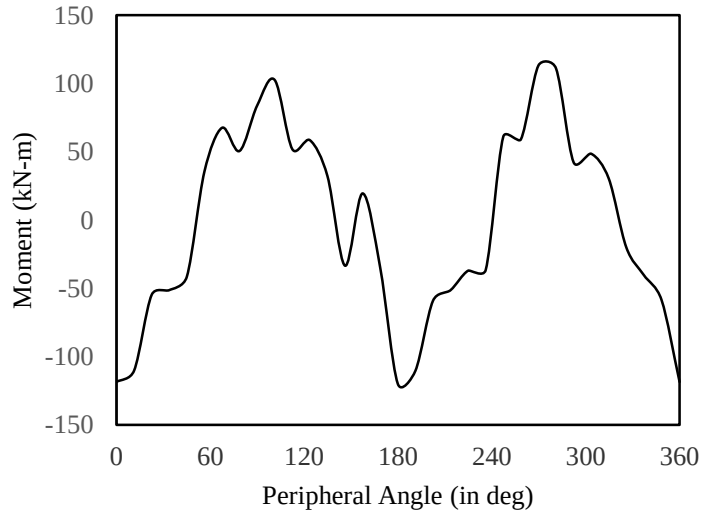

Fig. 7.4. Maximum bending moment along liner

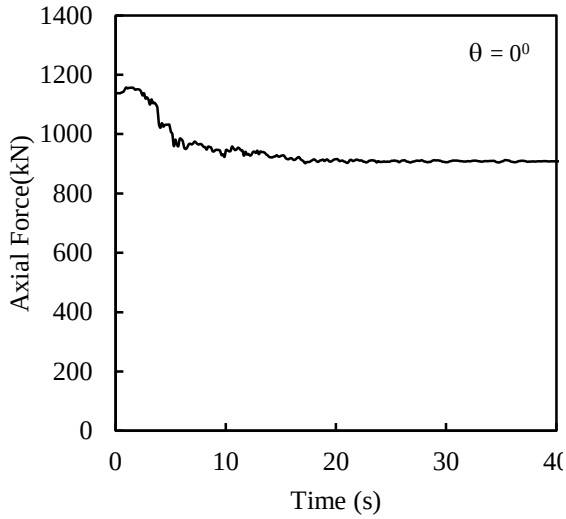
θ = 0⁰
Axial Force(kN)
Time (s)

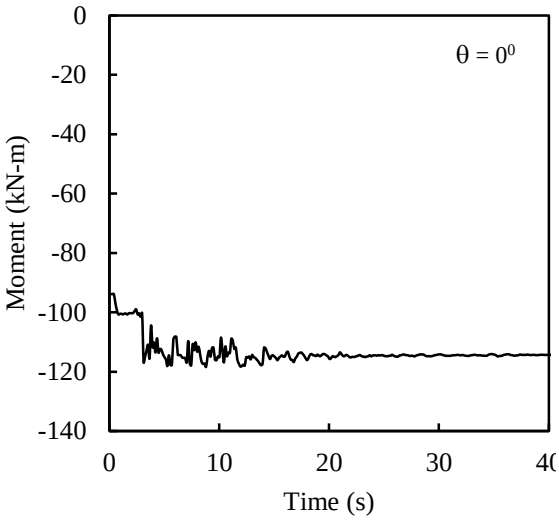
θ = 0⁰
Moment (kN-m)
Time (s)

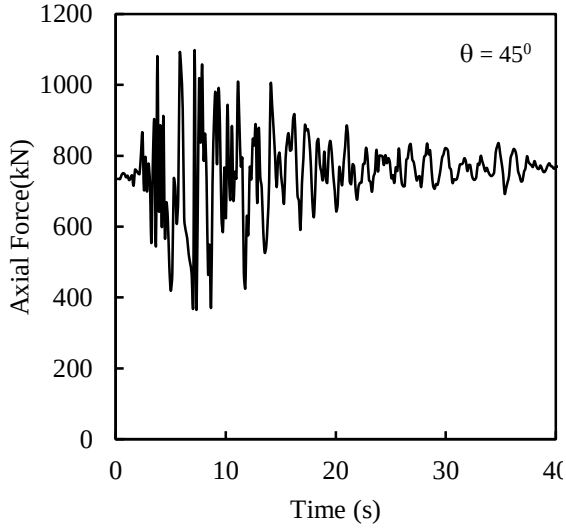
θ = 45⁰
Axial Force(kN)
Time (s)

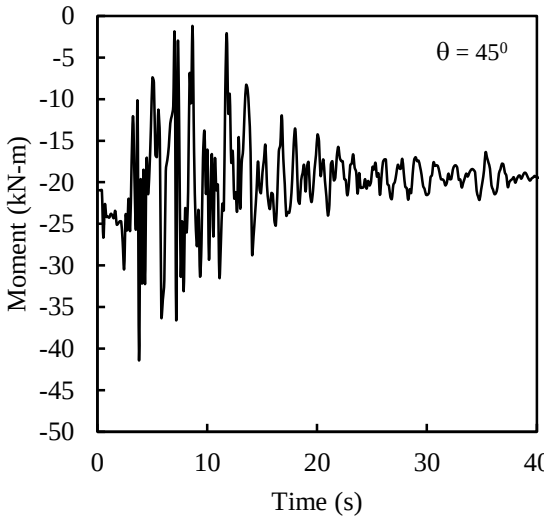
θ = 45⁰
Moment (kN-m)
Time (s)

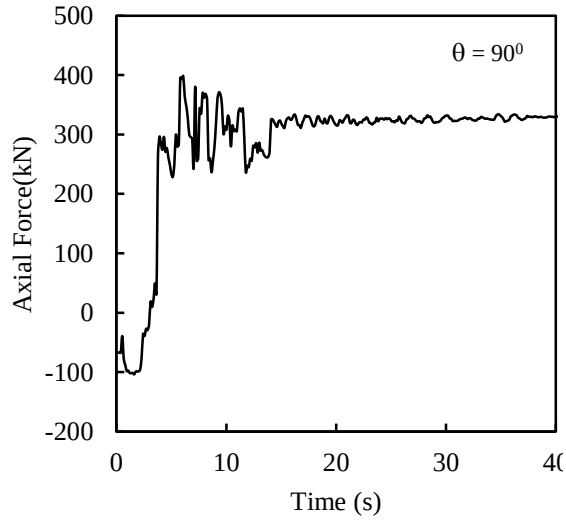
θ = 90⁰
Axial Force(kN)
Time (s)

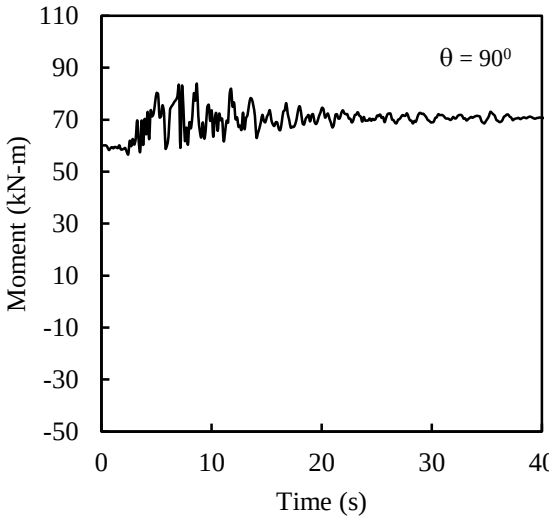
θ = 90⁰
Moment (kN-m)
Time (s)

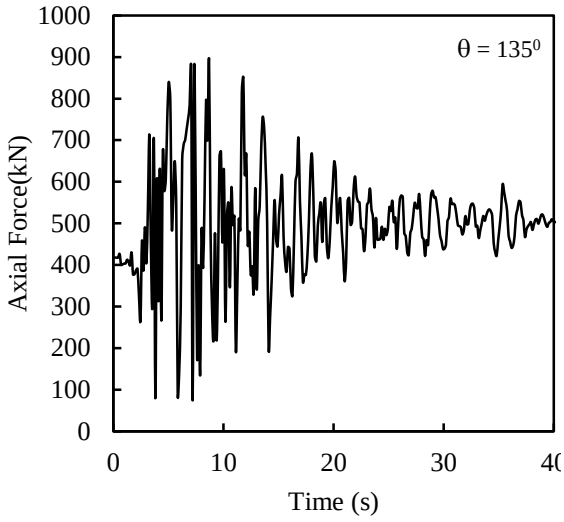
θ = 135⁰
Axial Force(kN)
Time (s)

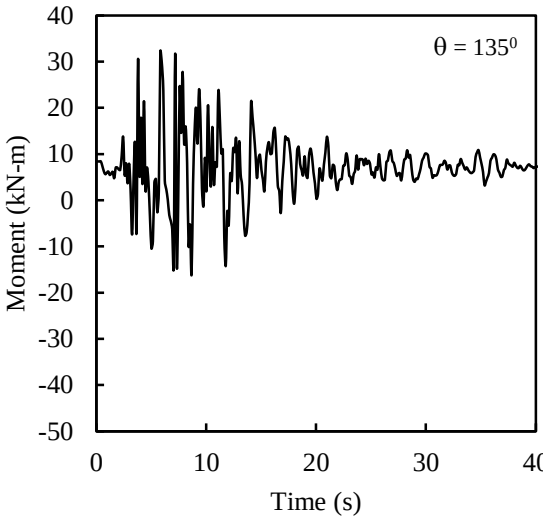
θ = 135⁰
Moment (kN-m)
Time (s)

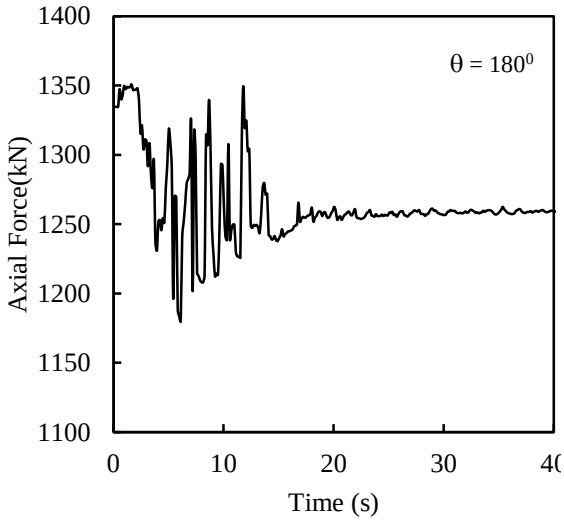
θ = 180⁰
Axial Force(kN)
Time (s)

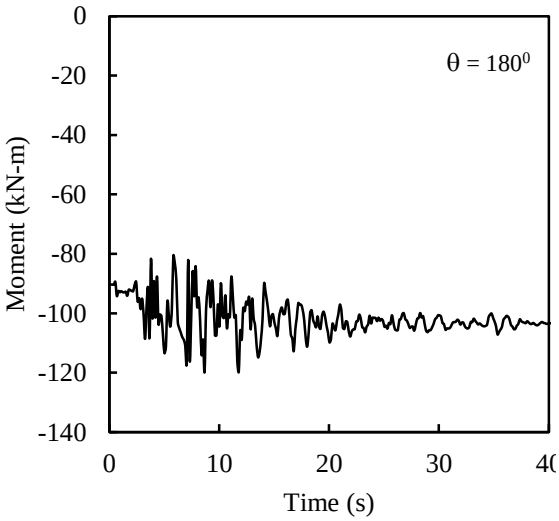
θ = 180⁰
Moment (kN-m)
Time (s)

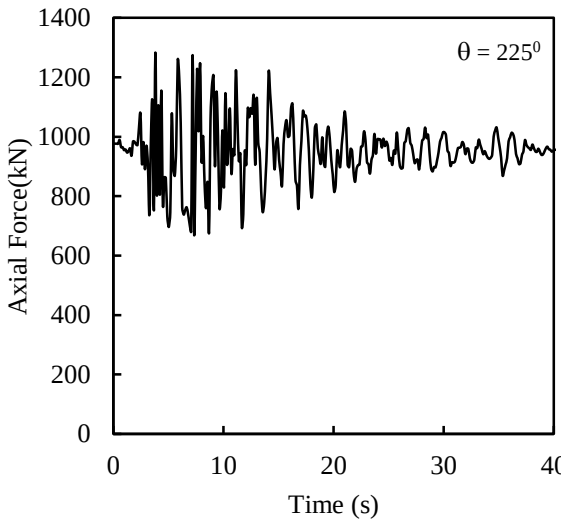
θ = 225⁰
Axial Force(kN)
Time (s)

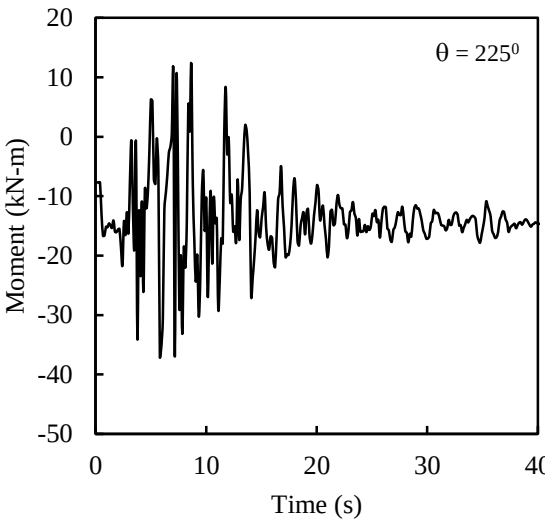
θ = 225⁰
Moment (kN-m)
Time (s)

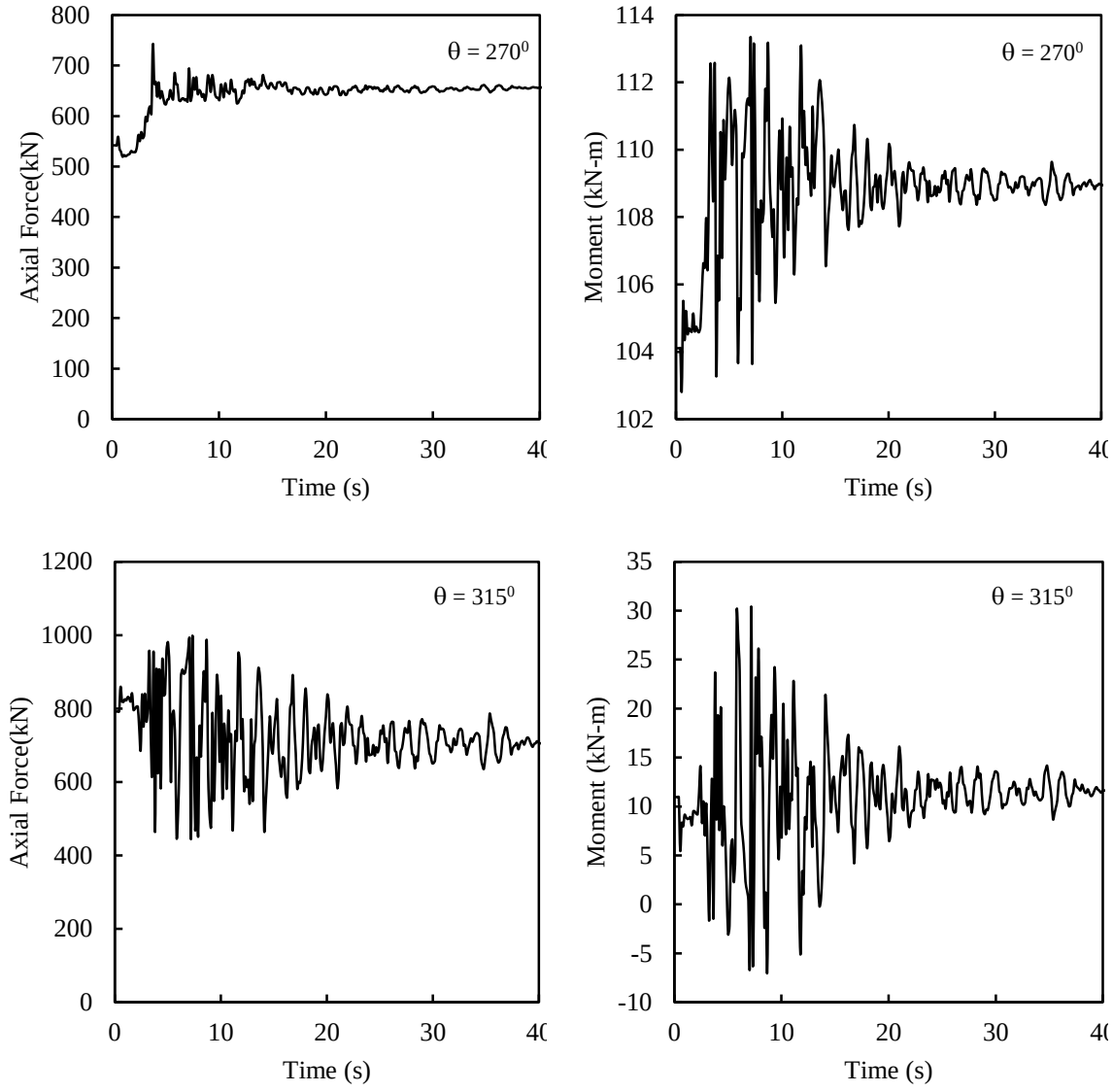

Fig. 7.5. Evolution of axial force and bending moment in the tunnel liner during the earthquake

7.3.2. Tunnel at 75m Depth with EPS Geofoam Isolation Layer

The distribution of maximum axial force and bending moment developed in the tunnel liner with an EPS Geofoam isolation layer is shown in Fig. 7.6 and Fig. 7.7 respectively. In comparison to the earlier case, a distinct drop in the maximum values of axial force and bending moment is noted. The maximum axial force and bending moment developed in the liner is 294kN and 87 kN-m respectively. However, the relative position of the maximum axial force and bending moment remains similar to the earlier case.

The evolution of the axial force and bending moment developed during the application of the acceleration time history is presented in Fig. 7.8. Unlike the earlier case where a distinct change in the axial force and bending moment was noticed at around 3.2 sec from the onset of the dynamic excitation, the change is observed at 5.4 sec. Thus, the EPS Geofoam acts as an effective wave barrier and absorbs the initial shock effectively. Moreover, the change in seismic demand on the liner in terms of the axial load is significantly reduced. The demand in terms of the peak bending moment is also reduced as compared to the earlier case. Also, the moments stabilize at comparatively similar or lower values at the end of the earthquake time history.

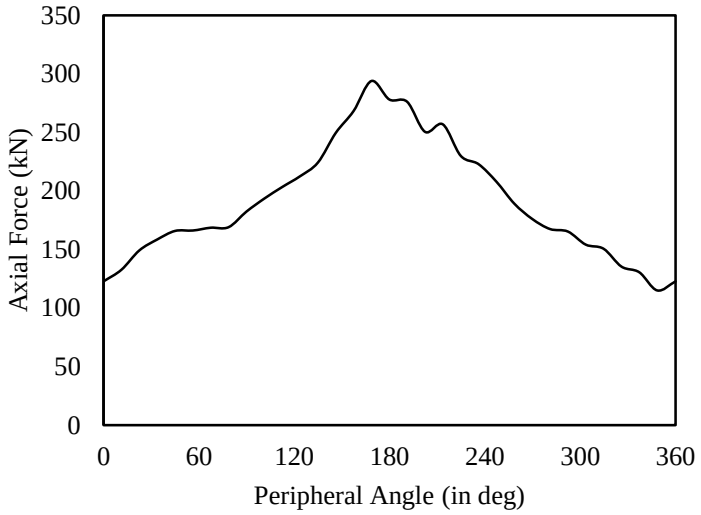

Fig. 7.6. Maximum axial force along liner

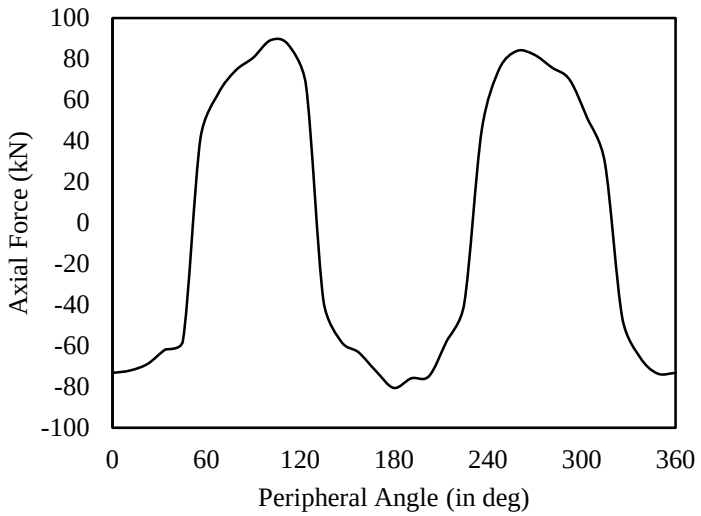

Fig. 7.7. Maximum bending moment along liner

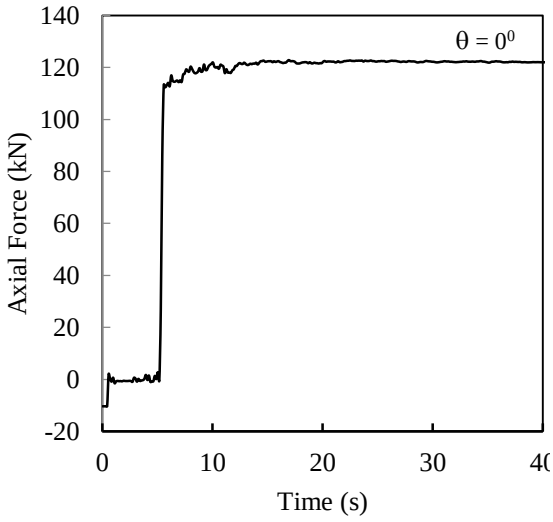
θ = 0⁰
Axial Force (kN)
Time (s)

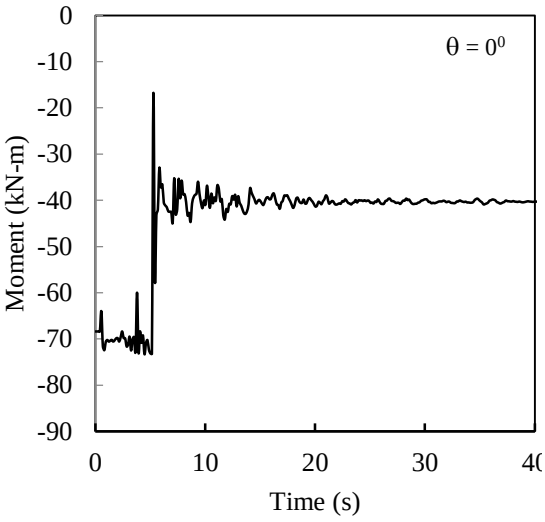
θ = 0⁰
Moment (kN-m)
Time (s)

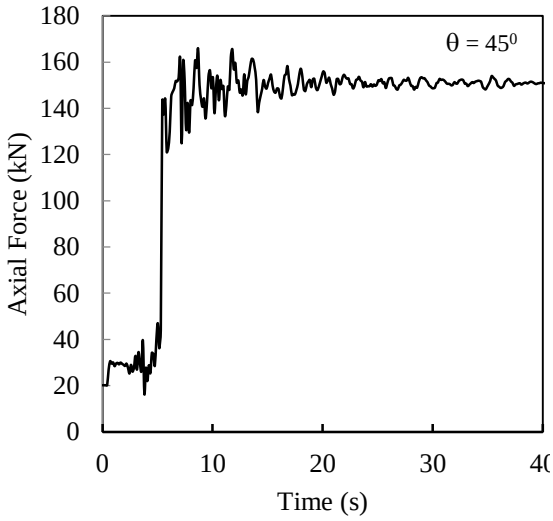
θ = 45⁰
Axial Force (kN)
Time (s)

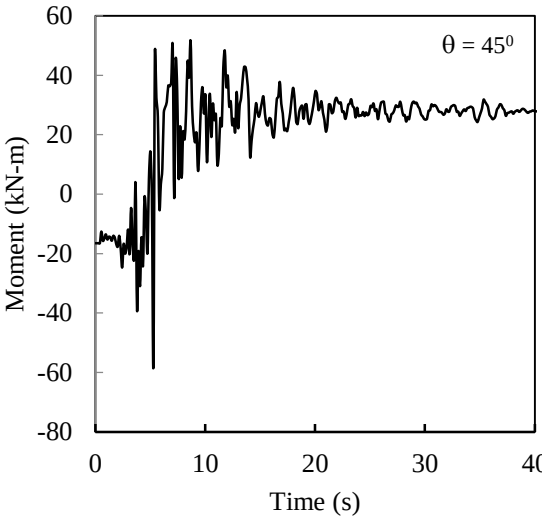
θ = 45⁰
Moment (kN-m)
Time (s)

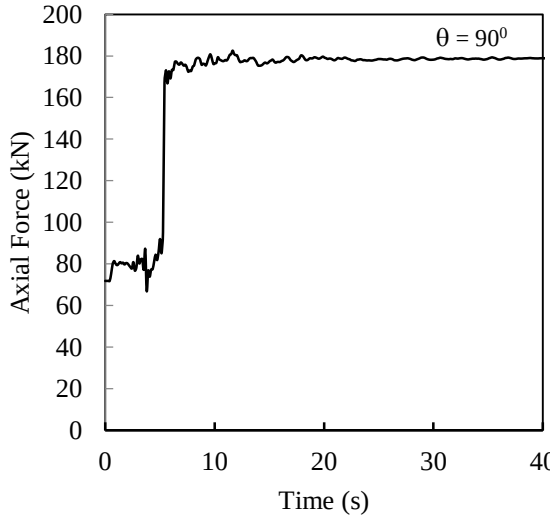
θ = 90⁰
Axial Force (kN)
Time (s)

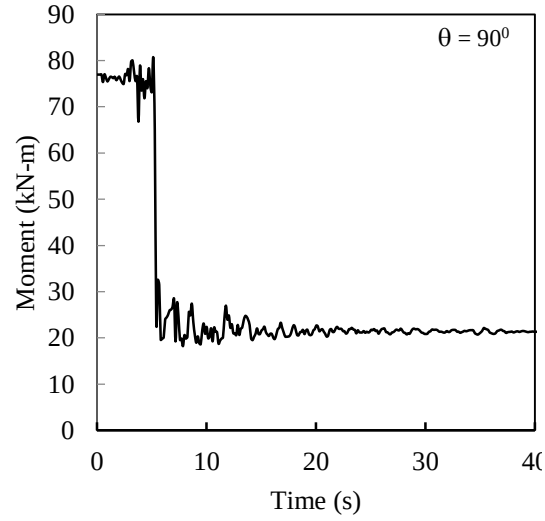
θ = 90⁰
Moment (kN-m)
Time (s)

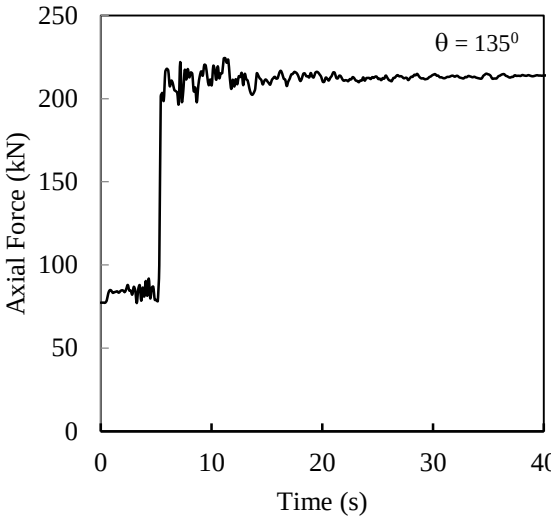
θ = 135⁰
Axial Force (kN)
Time (s)

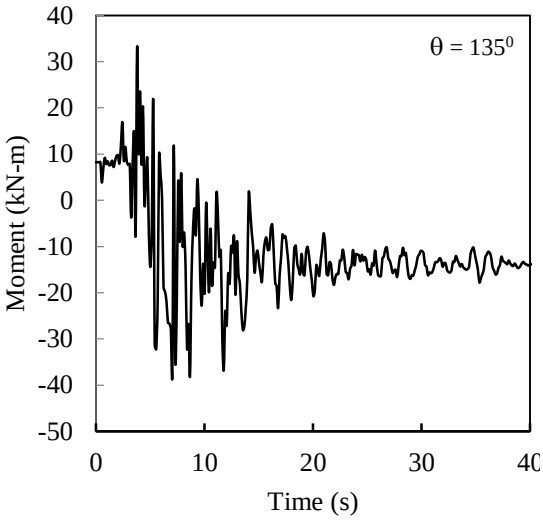
θ = 135⁰
Moment (kN-m)
Time (s)

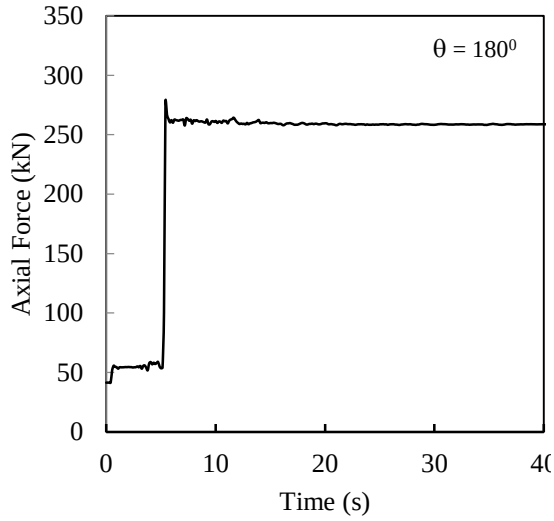
θ = 180⁰
Axial Force (kN)
Time (s)

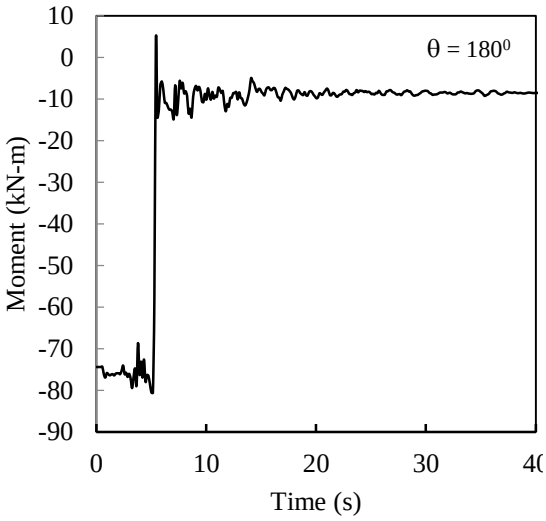
θ = 180⁰
Moment (kN-m)
Time (s)

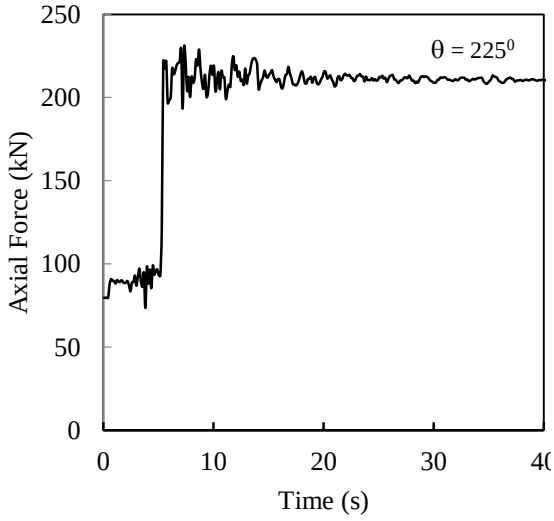
θ = 225⁰
Axial Force (kN)
Time (s)

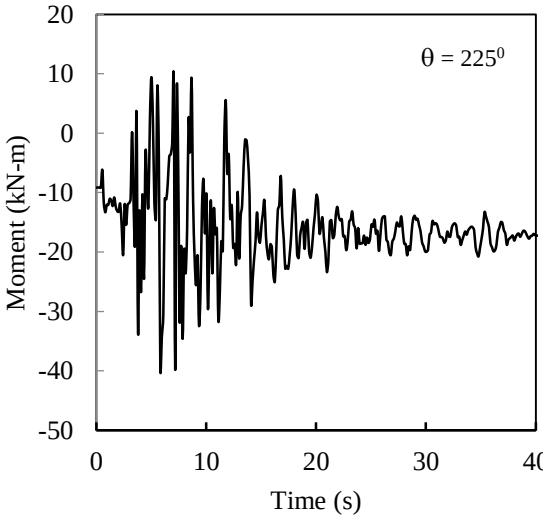
θ = 225⁰
Moment (kN-m)
Time (s)

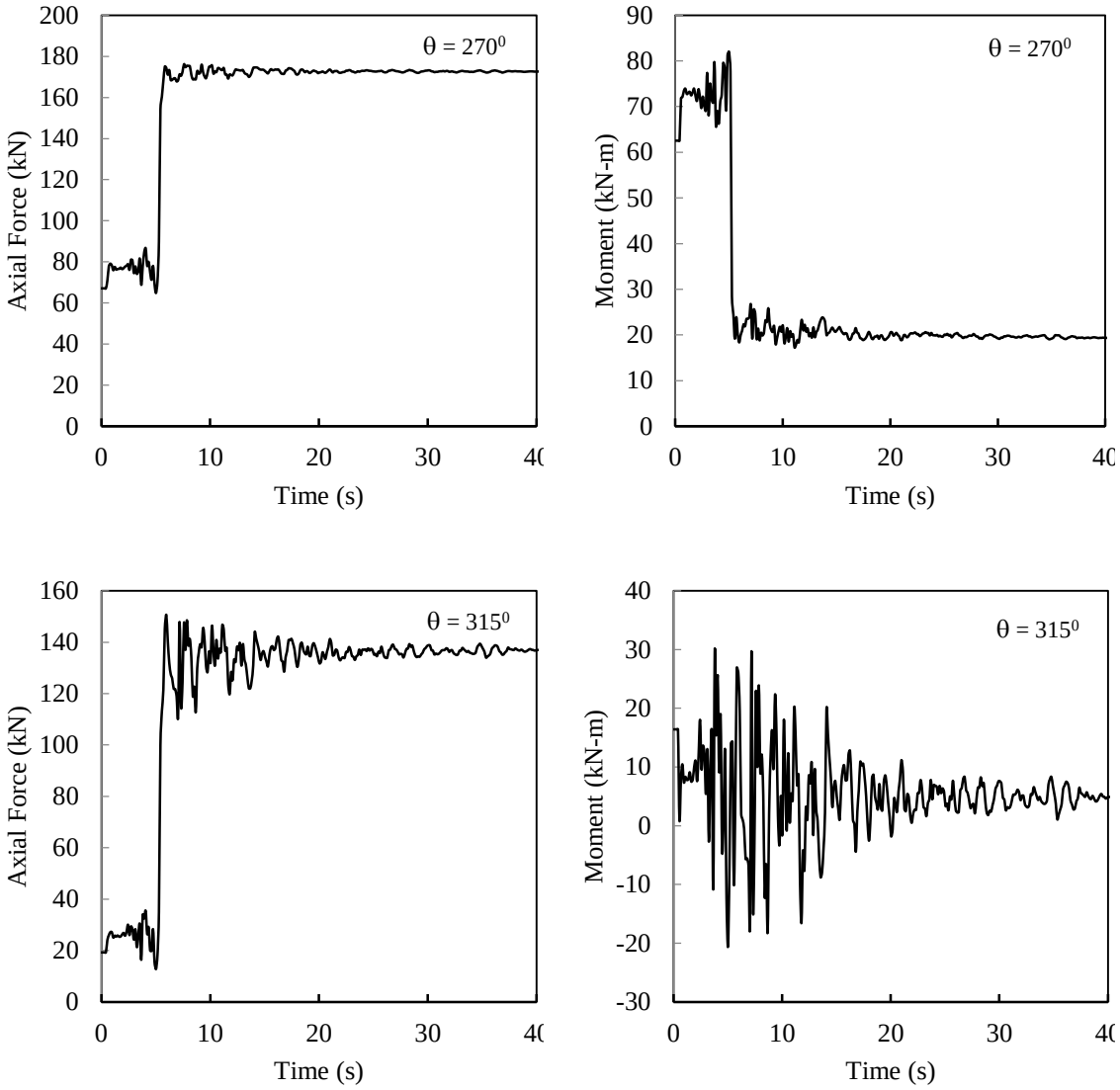

Fig. 7.8. Evolution of axial force and bending moment in the tunnel liner with EPS grofoam during the earthquake

7.3.3. Tunnel at 150m Depth without any Isolation Layer

The distribution of maximum axial force and bending moment developed in the tunnel liner is shown in Fig. 7.9 and Fig. 7.10 respectively. It may be noted that the value of the bending moment is largest at the floor. The maximum axial force is recorded between the right sidewall and the floor of the tunnel. The maximum axial force and bending moment is 3970 kN and 784 kN-m respectively. In comparison to the earlier case (tunnel depth of 75m), the forces and moments have become comparatively larger due to the increase in the tunnel depth.

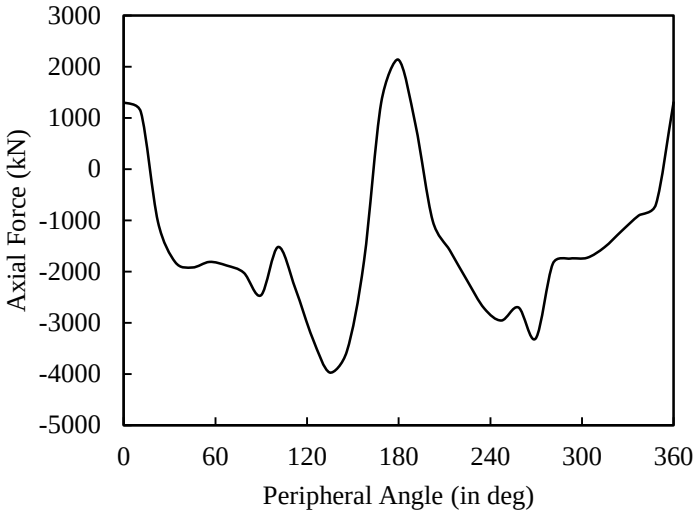

Fig. 7.9. Maximum axial force along liner

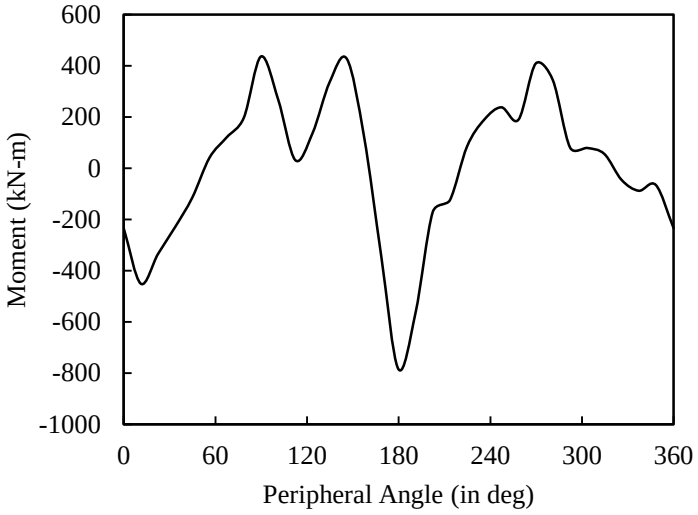

Fig. 7.10. Maximum bending moment along liner

The evolution of the axial force and bending moment during the application of the acceleration time history is presented in Fig. 7.11. The results are presented for various locations of the tunnel liner.

It is observed that the axial force and moments in the tunnel liner show transient response till 15sec of the earthquake following which they tend to stabilize towards a constant value. The effect of the dynamic action seems to be more pronounced at around 5sec for almost all the positions along the tunnel liner.

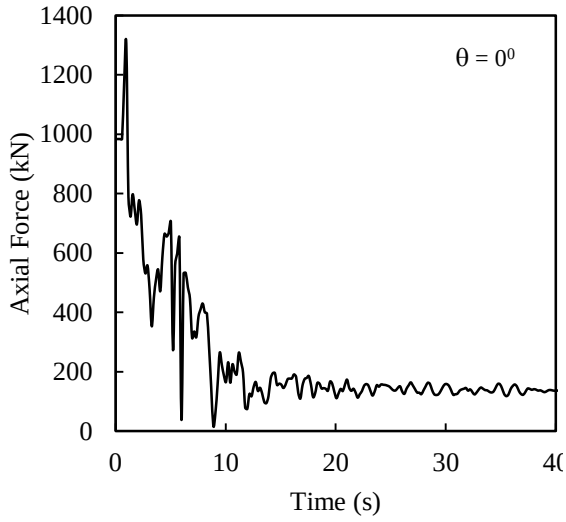
θ = 0⁰
Axial Force (kN)
Time (s)

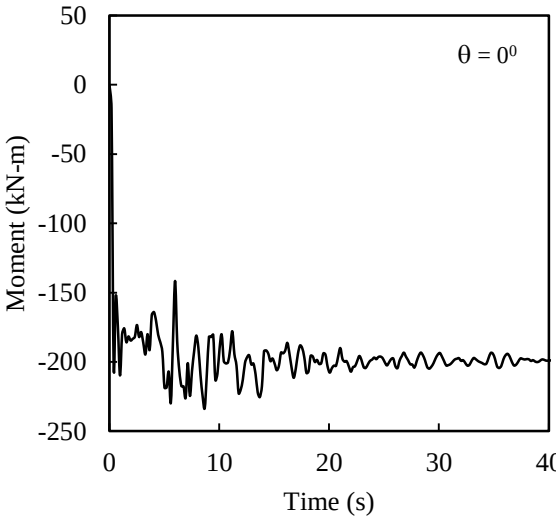
θ = 0⁰
Moment (kN-m)
Time (s)

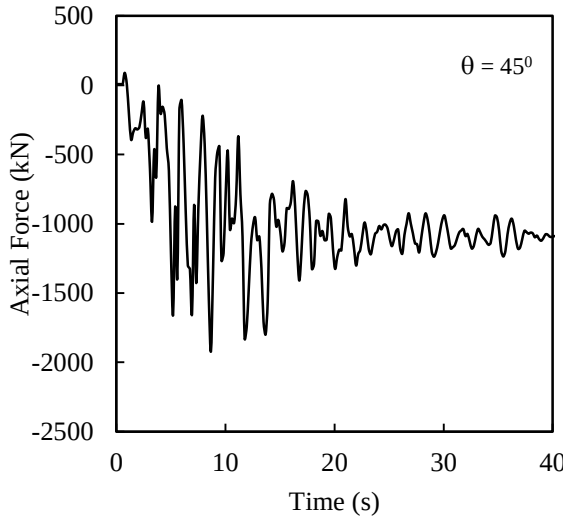
θ = 45⁰
Axial Force (kN)
Time (s)

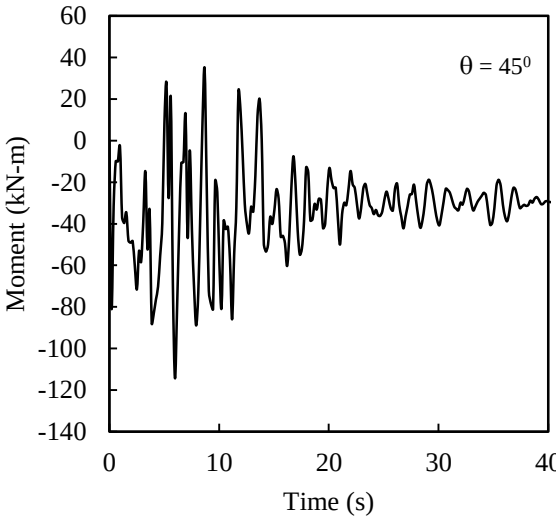
θ = 45⁰
Moment (kN-m)
Time (s)

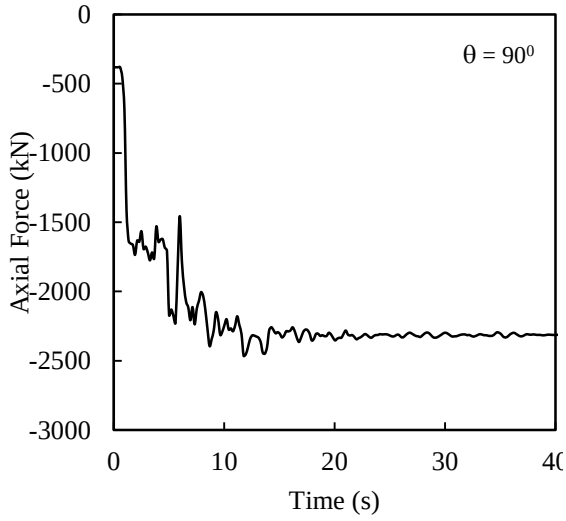
θ = 90⁰
Axial Force (kN)
Time (s)

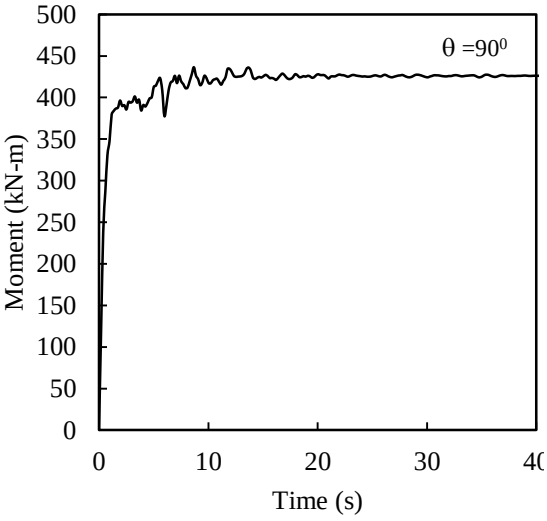
θ =90⁰
Moment (kN-m)
Time (s)

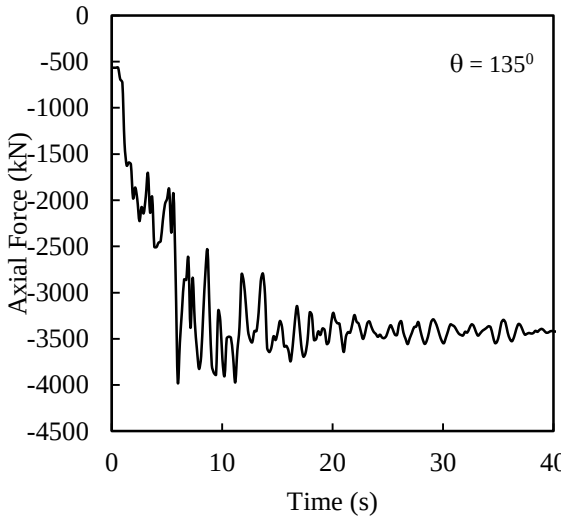
θ = 135⁰
Axial Force (kN)
Time (s)

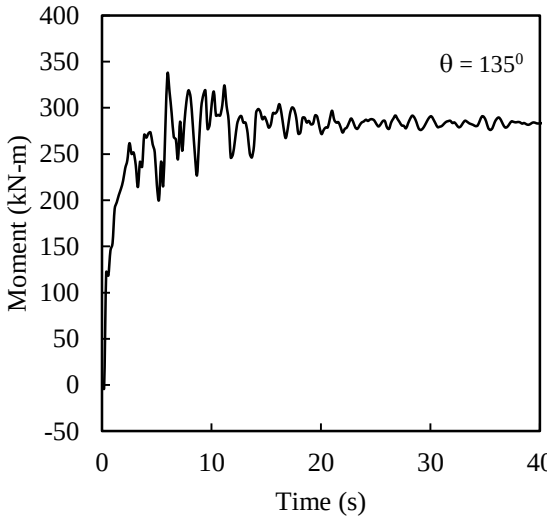
θ = 135⁰
Moment (kN-m)
Time (s)

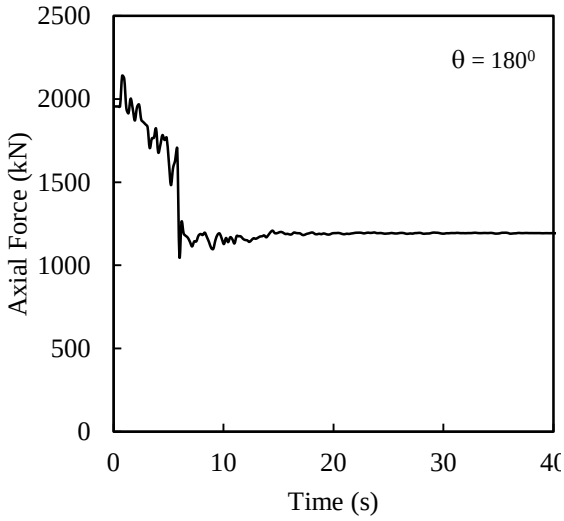
θ = 180⁰
Axial Force (kN)
Time (s)

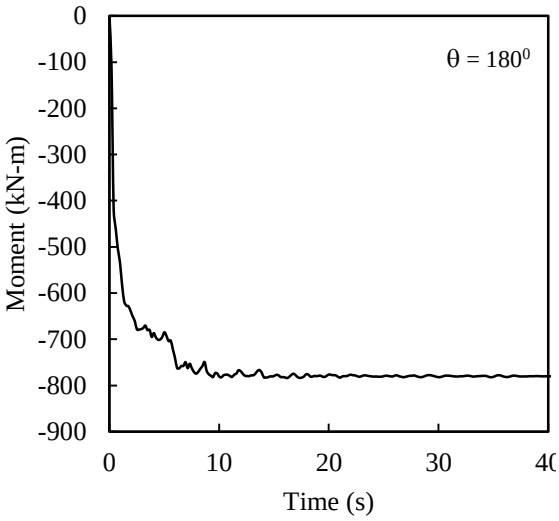
θ = 180⁰
Moment (kN-m)
Time (s)

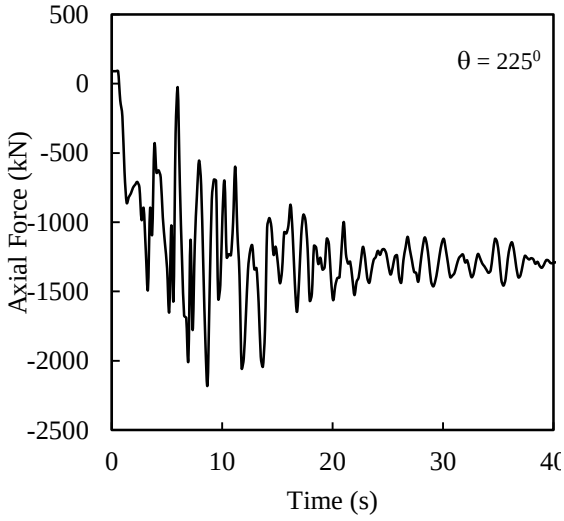
θ = 225⁰
Axial Force (kN)
Time (s)

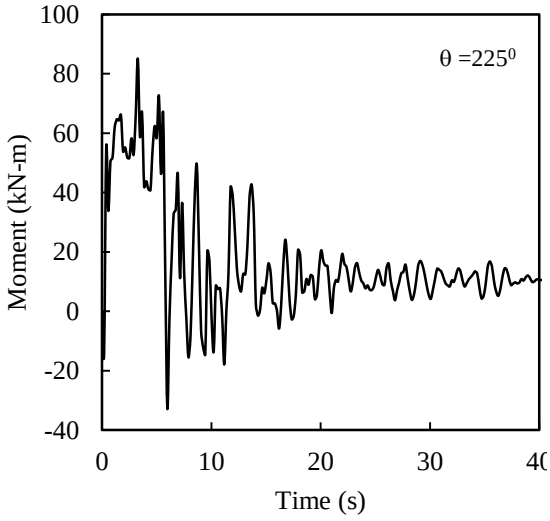
θ =225⁰
Moment (kN-m)
Time (s)

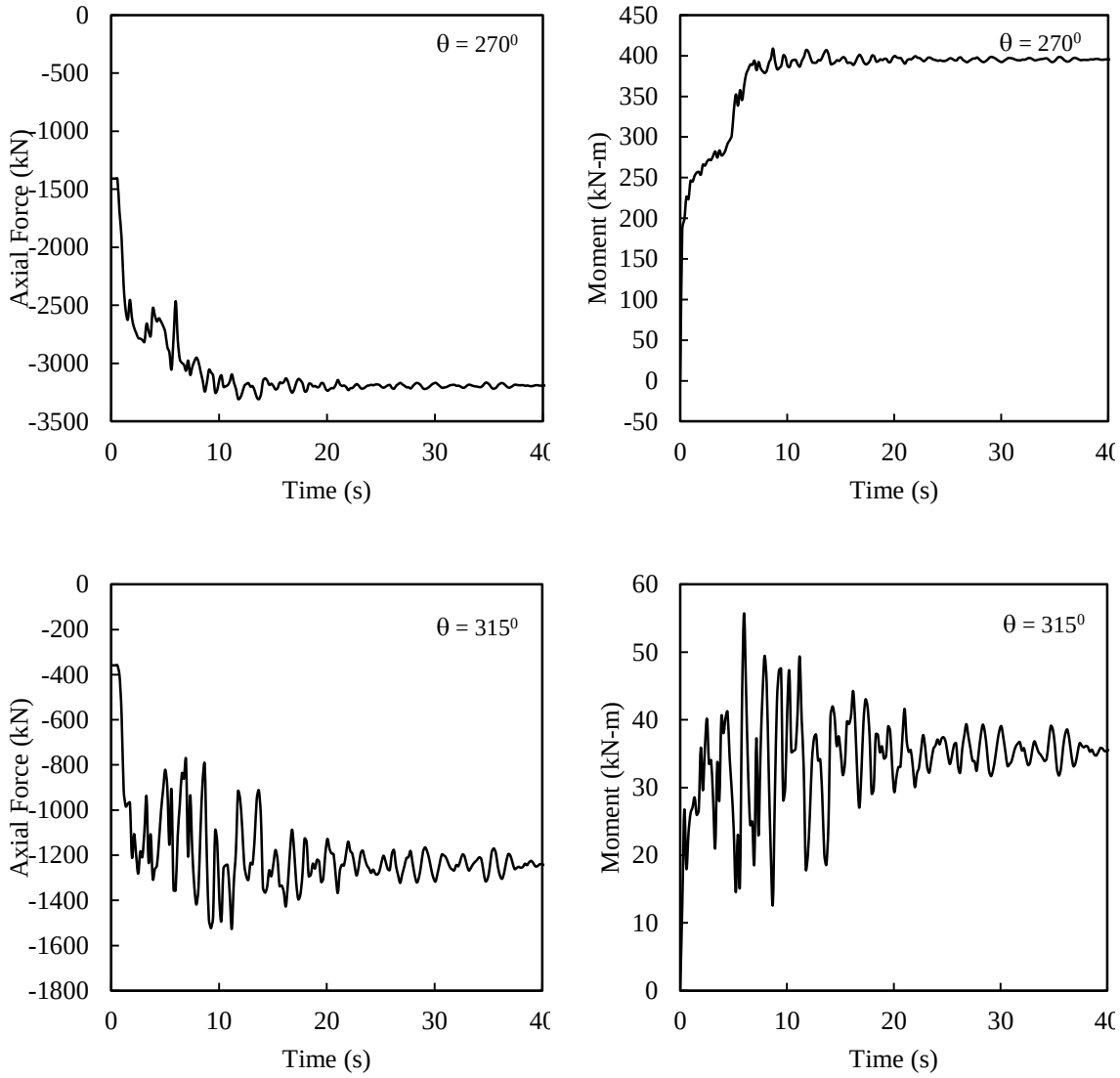

Fig. 7.11. Evolution of axial force and bending moment in the tunnel liner during the earthquake

7.3.4. Tunnel at 150m Depth with EPS Geofoam Isolation Layer

The distribution of maximum axial force and bending moment developed in the tunnel liner with an EPS Geofoam isolation layer is shown in Fig. 7.12 and Fig. 7.13 respectively. The evolution of the axial force and bending moment developed during the application of the acceleration time history is presented in Fig. 7.14. In comparison to the case without any isolation layer, a distinct drop in the maximum values of axial force is noted. The maximum axial force and bending moment developed in the liner is 620kN and 327 kN-m respectively. In addition, the axial force and moment stabilize at comparatively lower values at the end of the

earthquake time history. These results highlight the efficacy of EPS Geofoam as a promising measure to reduce the seismic demand on the tunnel liners.

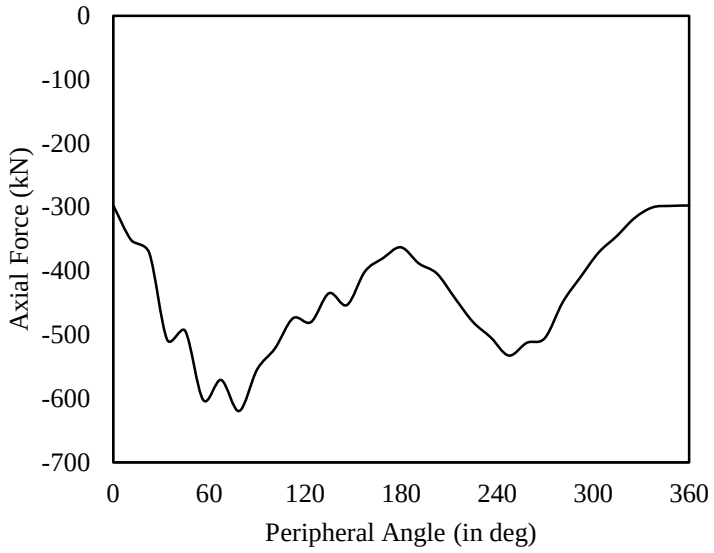

Fig. 7.12. Maximum axial force along liner

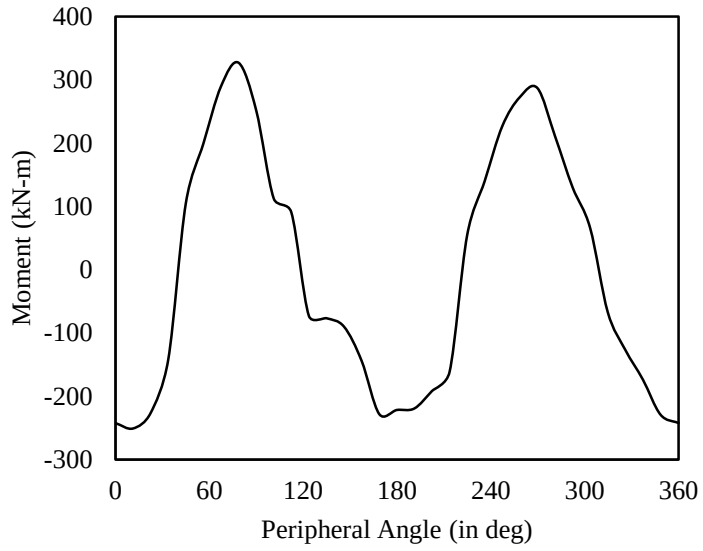

Fig. 7.13. Maximum bending moment along liner

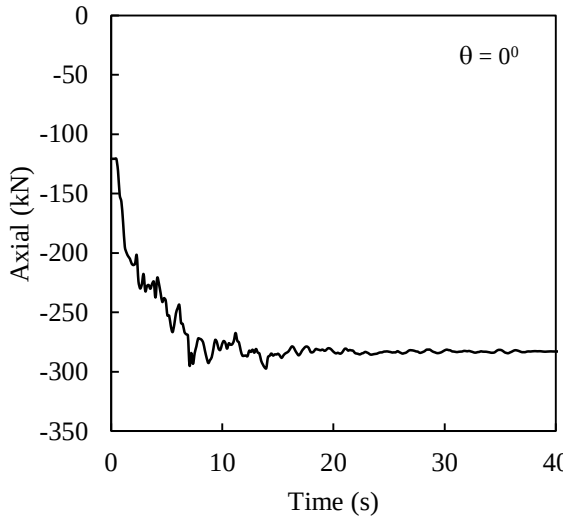
θ = 0⁰
Axial (kN)
0
-50
-100
-150
-200
-250
-300
-350
0
10
20
30
Time (s)

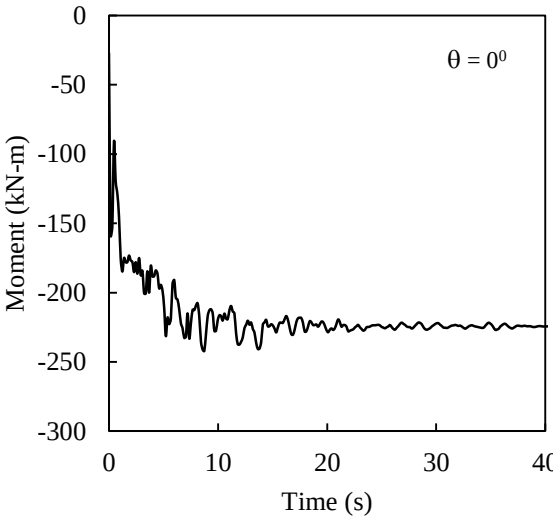
θ = 0⁰
Moment (kN-m)
0
-50
-100
-150
-200
-250
-300
0
10
20
30
Time (s)

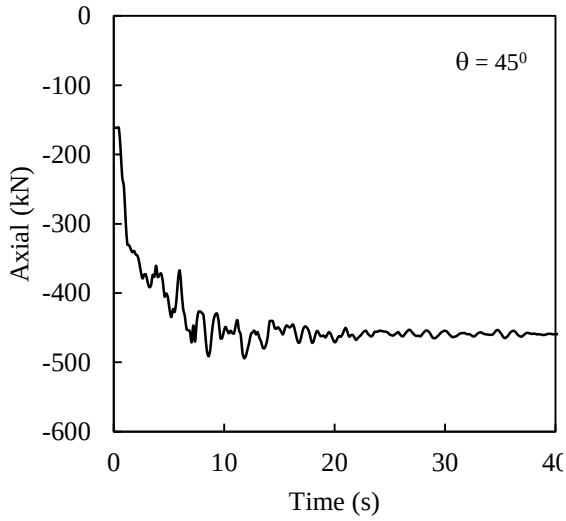
θ = 45⁰
Axial (kN)
0
-100
-200
-300
-400
-500
-600
0
10
20
30
Time (s)

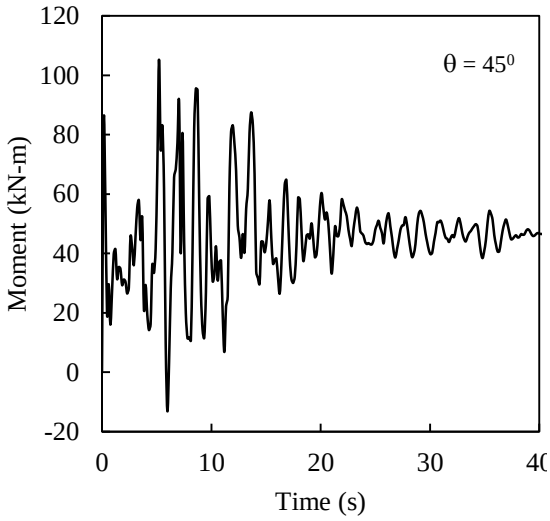
θ = 45⁰
Moment (kN-m)
120
100
80
60
40
20
0
-20
0
10
20
30
Time (s)

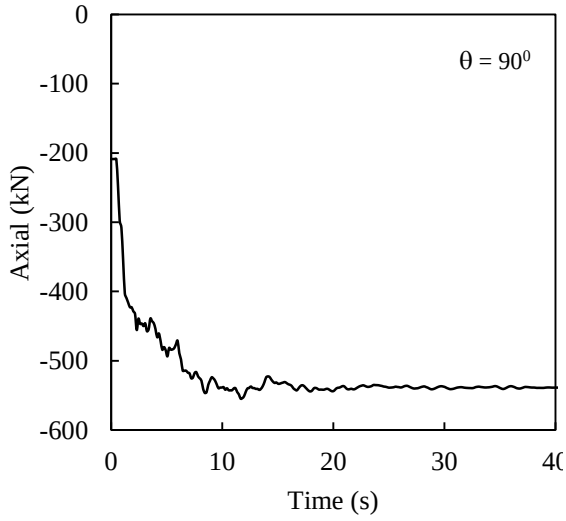
θ = 90⁰
Axial (kN)
0
-100
-200
-300
-400
-500
-600
0
10
20
30
Time (s)

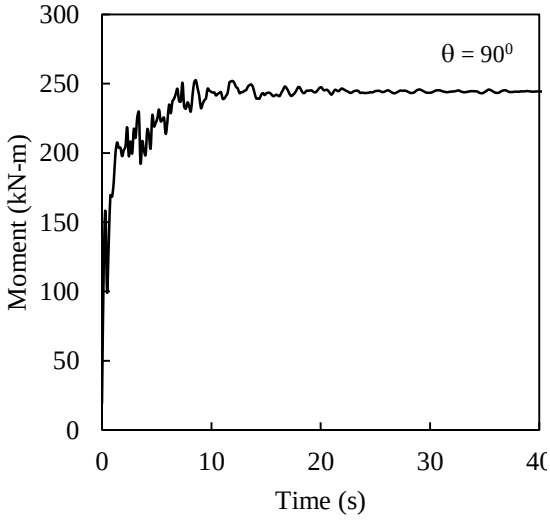
θ = 90⁰
Moment (kN-m)
300
250
200
150
100
50
0
0
10
20
30
Time (s)

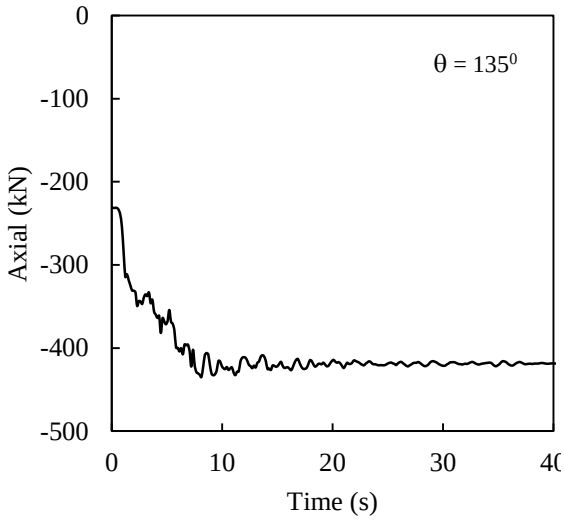
θ = 135⁰
Axial (kN)
Time (s)

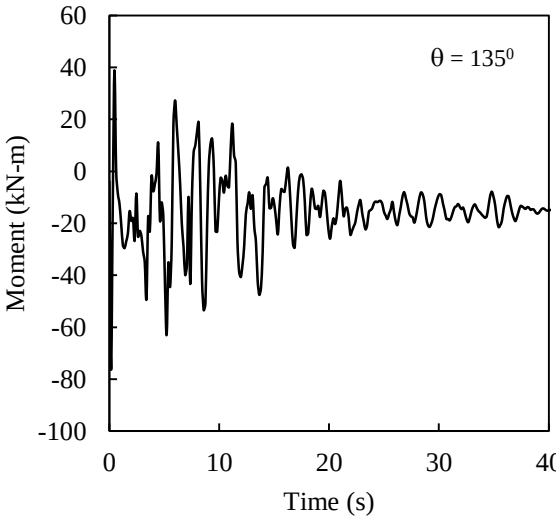
θ = 135⁰
Moment (kN-m)
Time (s)

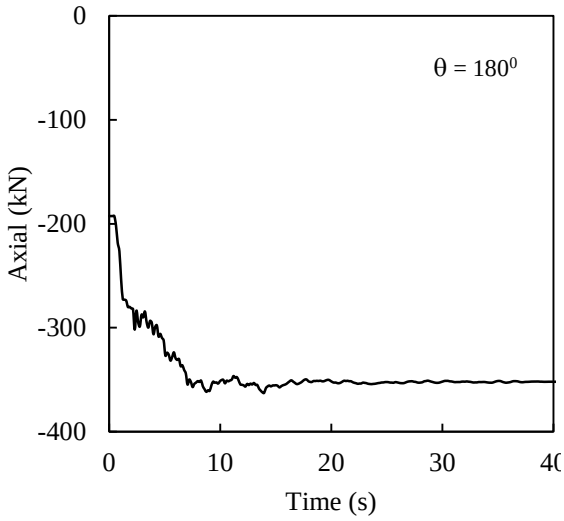
θ = 180⁰
Axial (kN)
Time (s)

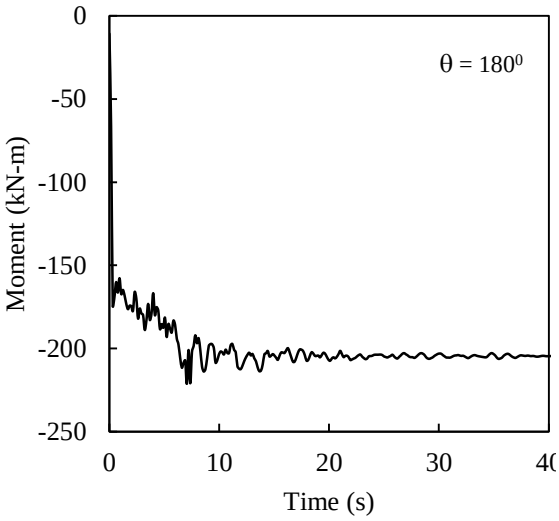
θ = 180⁰
Moment (kN-m)
Time (s)

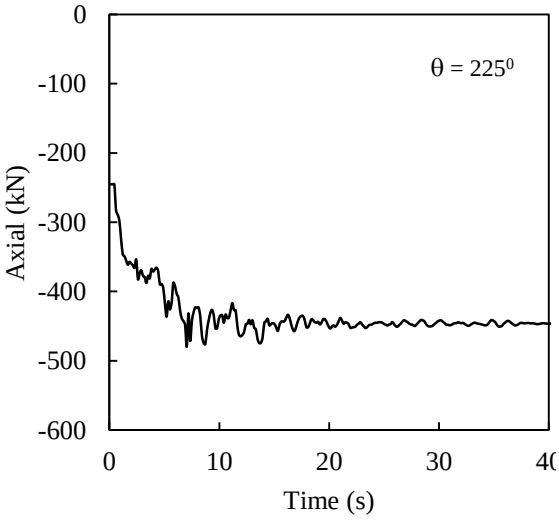
θ = 225⁰
Axial (kN)
Time (s)

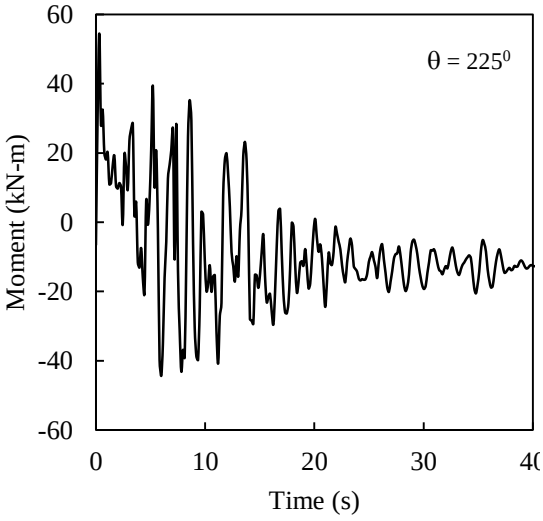
θ = 225⁰
Moment (kN-m)
Time (s)

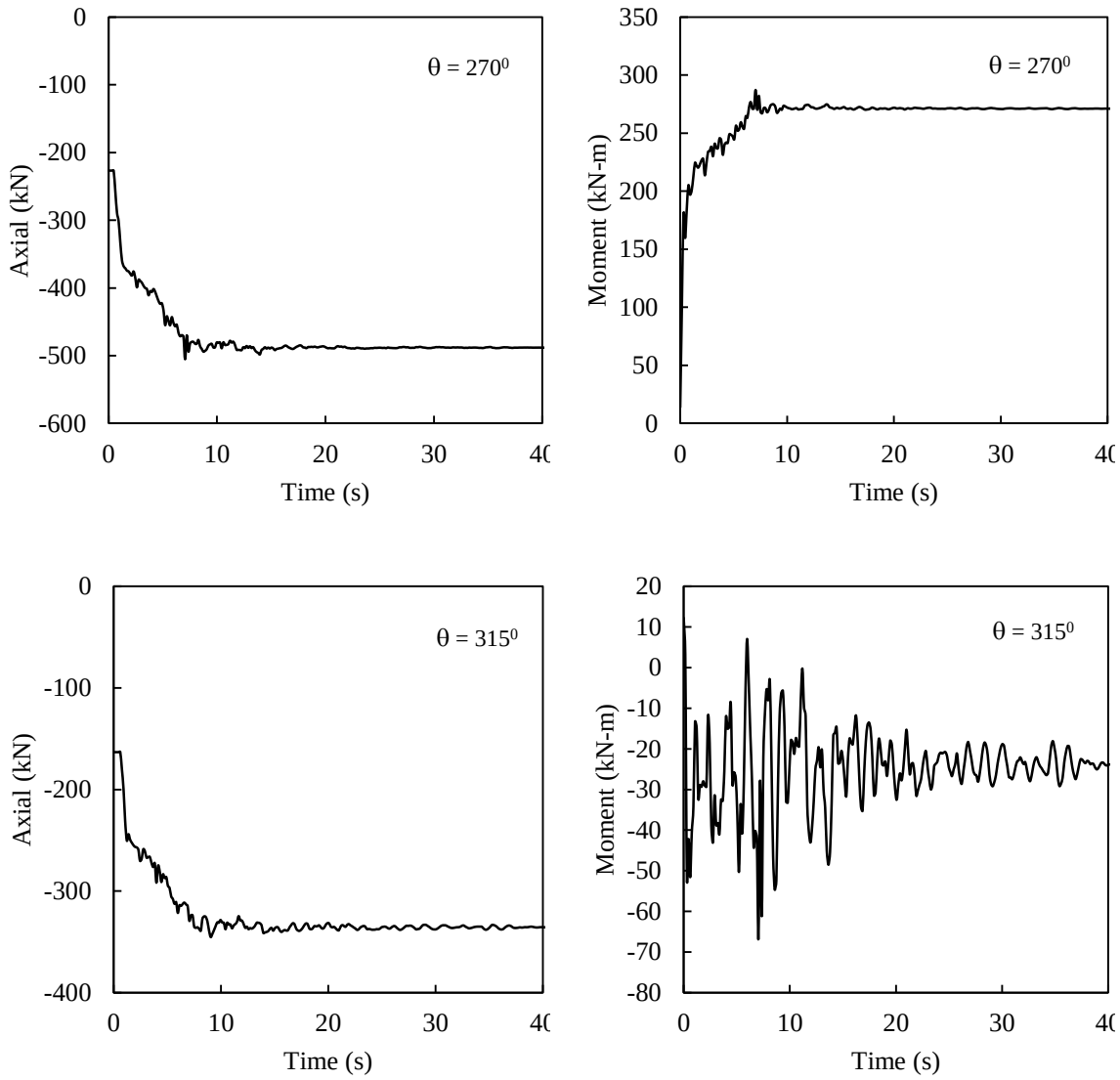

Fig. 7.14. Evolution of axial force and bending moment in the tunnel liner during the earthquake

Table 7.1. Absolute maximum axial force and bending moment developed in the tunnel liner

Tunnel depth (m)	Axial Force (in kN)			Moment (in kN-m) R_M		
	No Isolation	EPS Geofoam	Reduction (%)	No Isolation	EPS Geofoam	Reduction (%)
75	1350	294	78	3970	620	84
150	113	87	23	784	327	58

The reduction in the demand imposed on the tunnel liner for the two tunnel depths are highlighted in Table 7.1. The inclusion of EPS Geofoam is around the liner causes a reduction of axial force by 78% and bending moment by 23% for tunnel at 75m depth. For the case of tunnel at a depth of 150m, the reduction in the axial force and bending moment is 84% and 58% respectively.

7.4 SUMMARY

The present chapter discusses the feasibility of using the seismic isolation method for the reduction of the demand imposed on the liner. The suitability of Expanded Polystyrene (EPS) Geofoam as a seismic buffer material around the liners in numerically studied. Tunnels at depth of 75m and 150m are subjected to the acceleration time-history recorded in the Kobe (1995) earthquake.

The evolution of the axial force and bending moment along the tunnel liner is presented for tunnel with and without isolation layers. For no isolation case, it is observed that the maximum axial force and bending moment correspond well with the vulnerable sections reported in the literature following seismic events. A marked reduction the seismic demand is observed when EPS Geofoam is utilized as a coating material around the liner. EPS Geofoam is found to have excellent capabilities to attenuate the seismic load and reduce the seismic demand. Thus, EPS Geofoam offers promising capabilities as a protective material for underground tunnels.

…

Chapter 8

SUMMARY AND CONCLUSIONS

8.1. Introduction

Major instabilities during the excavation phase of tunnels in the jointed rock mass have been noted in the mountainous regions. Most of these cases are related to the large movement of well-defined rock blocks along joints. Although attempts have been made to assess the role of the joints on the deformation response, most of them are based on a simplified idealization of the discontinuities, i.e., parallel joint sets. Such idealization may not hold true for the cases where blocky rock mass is encountered. Also, the joints have a significant impact on the propagation of waves which influences the behavior of lined tunnels during earthquakes. However, the present understanding of the behavior of tunnels are primarily based on continuum based numerical investigations.

The work presented in this thesis made use of the distinct element method to evaluate the static and dynamic behavior of tunnels which pass through weathered and fractured rock mass conditions. First, the influence of the pattern of idealization of the joints on the deformation response of excavations has been studied. The role of the strength and deformation parameters of the joints and the in-situ stress ratio has been assessed. For the dynamic case, the influence of frequency of input motion, PGA, type of wave action, tunnel depth and in-situ stress ratio on the behavior of a circular lined tunnel has been investigated. Moreover, the promising capability of Expanded Polystyrene (EPS) Geofoam, as a seismic buffer material for lined tunnels, has been identified.

8.2 Summary of the Study

In the present study, the distinct element method has been used to assess the behavior of tunnels in the jointed rock mass. The features of the distinct element method to replicate the behavior of the discontinuous nature of the rock mass is

highlighted. The details of the numerical model and boundary conditions for investigating the static and dynamic behavior of tunnels in the jointed rock mass are explained.

Verification studies in UDEC dealing with the distribution of stresses around an excavation and propagation of waves across joints are presented. The applicability of Voronoi polygonal blocks to idealize the blocky rock mass is assessed by highlighting its capability in simulating the field-reported deformation behavior of an underground powerhouse cavern.

The influence of strength and deformation of the joints, and the in-situ stress ratio on the deformation response of a circular excavation is investigated for two different patterns of joint idealization – i. parallel joints sets and ii. joints idealized with Voronoi polygonal blocks. The mode of rock block movement is found to be significantly influenced by the pattern of idealization of the joints. The relative contribution of the parameters is also found to vary with the mode of deformation. Major implications of the findings with regard to the current state of practice for assessment of excavation stability is presented.

Dynamic numerical simulations are performed to assess the behavior of a lined circular tunnel in the blocky rock mass. The influence of the wave frequency, tunnel depth, type of wave action and the in-situ stress ratio on the demand imposed on the tunnel liner is investigated. The results of the dynamic simulations are utilized to corroborate the damage patterns reported in the literature. The feasibility of the seismic isolation approach for enhancing the performance of tunnels under earthquake loading is investigated. The promising capability of using Expanded Polystyrene (EPS) Geofoam for reducing the seismic demand imposed on the tunnel liner is highlighted.

8.3 Major Conclusions

The major conclusions of the present study are as follows:

- The pattern of idealization of joints has a significant influence on the deformation response of tunnel excavations.

- For the parallel joint sets, the deformation response is significantly influenced by the in-situ stress ratio (K_0) and the frictional angle of the joints (ϕj) for both the crown-floor and the sidewall section.
- The primary mode of rock block movement for parallel joint sets is the sliding of the rock blocks along the joints followed by subsequent rotation and detachment.
- The parallel joints provide potential pathways along which rock blocks can slide. In case of low shear resistance and minimal interlocking from the surrounding rock blocks, the movement may become large. This behavior is observed for the crown where sliding along joints eventually leads to rotation and subsequent detachment of the rock blocks.
- For excavation in the blocky rock mass (idealized with the Voronoi polygonal blocks), the interlocking effect is comparatively high. Also, the absence of well-defined straight line path minimizes the possibility of large movement of blocks. The chances of detachment and rotation are also minimized.
- The joint normal stiffness (k_{nb}) has the most significant effect on the deformation of excavation in the blocky rock mass.
- Detachment of rock blocks followed by their interlocking governs the entire deformation of the excavation in the blocky rock mass.
- The randomly oriented joints in the geological medium acts as low pass filter. Hence, the transmission of waves of high frequency is restricted through the blocky zone.
- The frequency filtering phenomenon has a direct consequence on the dynamically induced tunnel axial force and bending moment. The seismic demand on the tunnel liner are more for low frequency waves for both S and P-waves. The lined circular tunnel is more vulnerable under the influence of low frequency waves.
- Numerical simulations suggest maximum dynamically induced axial force and bending moment to develop at the sidewalls and the floor of the tunnel. This corresponds well with the damage sustained by tunnels under past seismic events.

- The vulnerability of the tunnel sections passing through weathered and fractured rock mass sections increases with an increase in the overburden depth.
- At lower in-situ stress ratio of K_0=1.0, the effect of P-waves is found to be more detrimental for the integrity of the tunnel. However, as the in-situ stress ratio increases, the adverse influence of S-waves increases. Tunnel at deeper depth is found to be more vulnerable for higher in-situ stress ratio.
- Peak Horizontal Acceleration (PHA) is a critical parameter governing tunnel damages. A higher PHA increases the demand imposed on the tunnel liner. The correlation of PHA with cases of tunnel damages sustained during 1999 Chi-Chi and 2008 Wenchuan earthquakes also confirms the same.
- The seismic demand imposed on the tunnel liner passing through the blocky rock mass can be reduced by using EPS Geofoam as a seismic buffer material around the tunnel liner.

8.4 Some Recommendations Based on Present Findings

- The accuracy and reliability of deformation predictions for excavations in the jointed rock mass is significantly influenced by the pattern of idealization of the joints. For more realistic representation of field joint patterns, the use of Discrete Fracture Networks (DFN) using joint set generators is suggested.
- The present study identifies the joint normal stiffness to significantly influence the deformation response of tunnel excavation in the blocky rock mass. Although well established guidelines i.e., ASTM: 5607-02 and ASTM: 4554-12, elaborately discusses the procedure to determine the strength and stiffness properties of the joints, large-scale field testing are rare. Hence, efforts must be made to evaluate the stiffness properties of the joints for major underground projects.
- For tunnels passing through highly weathered and fractured region, such as the blocky rock mass, seismic isolation techniques should be adopted to reduce the seismic demand imposed on the tunnel liners. In this regard, EPS

Geofoam provides a promising prospect as an effective seismic buffer material for application in underground construction.

8.5 Future Scope of Work

The future scope of work may be summarized as following:

- The Voronoi based numerical approach highlighted in the present work may be suitably substituted with more elaborate Discrete Fracture Networks (DFN) for any given site.
- More elaborate three-dimensional discontinuum based numerical modeling may be taken up to evaluate the behavior of tunnels along the longitudinal direction.
- Calibration of numerical model with field instrumented data may be taken up.
- The feasibility of various energy absorbing support system elements such as friction bolts, and D-bolts, may be investigated.

…

BIBLIOGRAPHY

1. Ahmadabadi, M., and Poisel, R. (2016). "Probabilistic analysis of rock sloes involving correlated non normal variables using point estimate methods." *Rock Mechanics and Rock Engineering*, 49(3), 909-925.
2. Alzo'ubi, A.M., Martin, C.D., and Cruden, D.M. (2007). "A discrete element damage model for rock slopes." *In: Rock Mechanics: Meeting Society's Challenges and Demands (1st Canada-US Rock Mechanics Symposium, Vancouver.*
3. Alzo'ubi, A.K., Martin, C.D., and Cruden, C.M. (2010). "Influence of tensile strength on toppling failure in centrifuge tests." *International Journal of Rock Mechanics and Mining Sciences*, 47(6), 974-982.
4. Asakura, T., and Sato, Y. (1996). "Damage to mountain tunnels in hazard area." *Soils Foundations*, Special Issue, 301-310.
5. Asakura, T., and Sato, Y. (1998). "Mountain tunnels in the 1995 Hyogoken-Nanbu earthquake." *Q. Rep. RTRI* 39 (1), 9-16.
6. ASTM D4554-12. (2012). "Standard Test Method for In Situ Determination of Direct Shear Strength of Rock Discontinuities." *ASTM International*, USA.
7. ASTM D5607-02. (2017). "Standard Test Method for Performing Laboratory Direct Shear Strength Tests of Rock Specimens Under Constant Normal Force." *ASTM International*, USA.
8. Athanasopoulos, G.A., Nikolopoulou, C.P., Xenaki, V.C., and Stathopoulou, V.D. (2007). "Reducing the Seismic Earth Pressure on Retaining Walls by EPS Geofoam Buffers - Numerical Parametric Study." *Proceedings of the Geosynthetics Conference*, Washington, DC, 16-19 January 2007, Industrial Fabrics Association International, St. Paul, Minn.
9. Baecher, G.B., and Christian, J.T. (2003). *Reliability and statistics in geotechnical engineering*, Wiley, Hoboken, NJ, USA.
10. Bathurst, R.J., Keshavarz, A., and Zarnani, S. (2007). "A simple displacement model for response analysis of EPS geofoam seismic buffers," *Soil Dyn. Earthquake Eng*., 4:344-353.

11. Bandis, S.C., Lumsden, A.C., and Barton, N.R. (1983). “Fundamentals of rock joint deformation.” *International Journal of Rock Mechanics and Mining Sciences*, 20(6):249–68.
12. Barton, N. (1974). "A review of shear strength of filled discontinuities in rock." *Norwegian Geotech Inst Publ No. 105*, Oslo.
13. Barton, N. (2013). "Shear strength criteria for rock, rock joints, rockfill and rock masses: Problems and some solutions." *Journal of Rock Mechanics and Geotechnical Engineering*, 5(4), 249-261.
14. Bhasin, R., and Hoeg, K. (1998). "Numerical modeling of block size effects and influence of joint properties in multiply jointed rock." *Tunnelling and Underground Space Technology*, 13(2), 181-188.
15. Bhasin, R., and Pabst, T. (2015). "Finite element and distinct element analysis of the stability of a large underground hydropower machine hall in the Himalayas." *KSCE Journal of Civil Engineering*, 19(3), 725-732.
16. Bidgoli, M.N., and Jing, L. (2014). "Anisotropy of strength and deformability of fractured rocks." *Journal of Rock Mechanics and Geotechnical Engineering*, 6(2), 156-164.
17. Bidgoli, M.N., Zhou, Z., and Jing, L. (2013). "Numerical evaluation of strength and deformability of fractured rocks." *Journal of Rock Mechanics and Geotechnical Engineering*, 5(6), 419-430.
18. Box, G.E.P., and Wilson, K.B. (1951). "On the experimental attainment of optimum conditions." *Royal Statistical Society*, 13(1),1-45.
19. Brown, I.R., Brekke, T.L., and Korbin, G.E. (1981). "Behavior of the Bay Area Rapid Transit Tunnels Through the Hayward Fault." *US Department of Transportation, Urban Mass Transportation Administration*. Report UMTA-CA-06-0120-81-1, Washington D.C.
20. BTS (British Tunnelling Society). (2004). "Tunnel lining design guide." *Institution of Civil Engineers (ICE),U.K.*, 92-95.
21. Cai, J.G., and Zhao, J. (2000). "Effects of Multiple Parallel Fractures on Apparent Attenuation of Stress Waves in Rock Masses." *International Journal of Rock Mechanics and Mining Sciences*, 37(4): 661-682.

22. Campbell, K.W. (1981). "Near source attenuation of peak horizontal acceleration." *Bulletin of the Seismological Society of America*, 71, 2039-2070.
23. Chen, Z., Shi, Z., Li, T., and Yuan, Y. (2012). "Damage characteristics and influence factors of mountain tunnels under strong earthquakes." *Natural Hazards* 61: 387-401. DOI: 10.1007/s11069-011-9924-3
24. Cundall, P.A. (1971). "A computer model for simulating progressive large scale movements in blocky rock systems." *In Proceedings of the Symposium of the International Society of Rock Mechanics. ISRM*, pp. 129-136.
25. Cundall, P.A., and Strack, O.D.L. (1979). "A discrete numerical model for granular assemblies." *Geotechnique*, 29, 47-65.
26. Curran, J.H., Hammah, R.E., Yacoub, T., and Corkum, B. (2008). "The practical modeling of discontinuous rock masses with finite element analysis." ARMA -08–180.
27. Dowding, C.H., and Rozen, A. (1978). "Damage to rock tunnel from earthquake shaking." *Journal of Geotechnical Engineering Division ASCE*, 104 (GT2) 175-191.
28. Duke, C.M., and Leeds, D.J. (1959). "Effects of earthquakes on tunnels." *In RAND Protective Construction Symposium.*
29. Gaskin, A.P. (2000) "An Investigation into the use of Expanded Polystyrene for Seismic Buffers." *MSc thesis, Queen's University, Kingston, Canada*.
30. Gischig, V., Preisig, G., and Eberhardt, E. (2016). "Numerical investigation of seismically induced rock mass fatigue as a mechanism contributing to the progressive failure of deep-seated landslides." *Rock Mechanics and Rock Engineering*, 49(6), 2457-2478.
31. Goodman, R.E., Taylor, R.L., and Brekke, T.L. (1968). " A model for the mechanics of jointed rock." *Journal of Soil Mech Found Div*, 637-659.
32. Hashash, Y.M.A., Hook, J.J., Schmidt, B., and Yao, J.I.C. (2001). "Seismic design and analysis of underground structures." *Tunnelling Underground Space Technology*, 16:247–293. DOI: 10.1016/S0886-7798(01)00051-7.

33. Hao, Y.H., and Azzam, R. (2005). "The plastic zones and displacements around underground openings in rock masses containing a fault." *Tunnelling and Underground Space Technology*, 20(1), 49-61.

34. Hazarika, H. (2001). "Mitigation of Seismic Hazard on Retaining Structures - A Numerical Experiment", *Proceedings of the 11th (2001) International Offshore and Polar Engineering Conference*, Stavanger, Norway, 17-22 June 2001, pp. 459-464.

35. Hazarika, H. and Okuzono, S. (2004), "Modeling the Behaviour of a Hybrid Interactive System Involving Soil, Structure and EPS Geofoam." *Soils and Foundations,* 44 (5): 149-162.

36. Hoek, E. (1998a). "Tunnel support in weak rock." *Keynote Address, Symposium of Sedimentary Rock Engineering*, Taipei, Taiwan, 2-13.

37. Hoek, E. (1998b). "Reliability of Hoek–Brown estimates of rock mass properties and their impact on design." *International Journal of Rock Mechanics and Mining Sciences*, 35(1), 63-68.

38. Hoek, E. (2001). "Big tunnels in bad rock." *Journal of Geotechnical and Geoenvironmental Engineering*, 127(9): 726-740.

39. Huang, R.Q., and Li, W.L. (2009). "Analysis of the geo-hazards triggered by the 12 May 2008 Wenchuan earthquake, China." *Bull Eng Geol Environ,* 68:363–371. DOI: 10.1007/s10064-009-0207-0

40. Infanti, N., and Kanji, M.A. (1978). "In situ shear strength, normal and shear stiffness determinations at Agua Vermelha Project." *Proc., 3rd International Congress IAEG*, 175–183.

41. Inglis, D., Macleod, G., Naesgaard, E., and Zergoun, M. (1996). "Basement wall with seismic earth pressures and novel expanded polystyrene foam buffer layer," *In: Proceedings of the Tenth Annual Symposium of the Vancouver Geotechnical Society*, Vancouver: Canada, 1996.

42. Itasca Consulting Group Inc. (2004) *Universal Distinct Element Code (UDEC) User's Manual*, Minneapolis.

43. Jia, P., and Tang, C.A. (2008). "Numerical study on failure mechanism of tunnel in jointed rock mass." *Tunnelling and Underground Space Technology*, 23(5), 500-507.

44. Jiang, Y., Wang, C., and Zhao, X. (2010). "Damage assessment of tunnels caused by the 2004 Mid Niigata Prefecture Earthquake using Hayashi's quantification theory type II." *Natural hazards*, 53,425-441. DOI: 10.1007/s11069-009-9441-9

45. Jiao, Y.Y., Fan, S.C., and Zhao, J. (2005). "Numerical Investigation of Joint Effect on Shock Wave Propagation in Jointed Rock Masses." *Journal of Testing and Evaluation*, 33(3), 197-203.

46. JTA (Japan Tunnelling Association). (1983). *Lecture book for tunnel engineering*, 63-71.

47. Kawakami, H. (1984). "Evaluation of deformation of tunnel structure due to Izu-oshima-kinkai earthquake of 1978." *Earthquake Engineering and Structural Dynamics,* 12, 369–383. DOI:10.1002/eqe.4290120306

48. Kazerani, T., and Zhao, J. (2010). "Micromechanical parameters in bonded particle method for modelling of brittle material failure." *International Journal of Numerical and Analytical Methods in Geomechanics,* 34(18), 1877-1895.

49. KEC (Korea Expressway Corporation). (2009). *Practical manual for the expressway-tunnel design*, 4.

50. KGA (Korea Geotechnical Association). (1996). *Geotechnical series 7 tunnel*, 149-150.

51. Kitagawa, Y., and Hiraishi, H. (2004). "Overview of the 1995 Hyogoken-Nanbu earthquake and proposals for earthquake mitigation measures." *Journal of Japan Association for Earthquake Engineering*, 4, 3(Special Issue).

52. Kohno, S., Ang, A. H-S., and Tang, W.H. (1992). "Reliability evaluation of idealized tunnel systems." *Structural Safety*, 11(2), 81-93.

53. Kawakami, H. (1984). "Evaluation of deformation of tunnel structure due to Izu-oshima-kinkai earthquake of 1978." *Earthquake Engineering and Structural Dynamics,* 12, 369–383. DOI:10.1002/eqe.4290120306

54. Konagai, K., Hohansson, J., Zafeirakos, A., Numada, M., and Sadr, A.A. (2005). "Damage to tunnels in the October 23, 2004 Chuetsu earthquake." *Proceedings of the JSCE Earthquake Engineering Symposium*, 28, 75. DOI: http://doi.org/10.11532/proee2005a.28.75

55. Konagai, K. (2005). "Data archives of seismic fault-induced damage." *Soil Dynamics and Earthquake Engineering*, 25, 559–570. DOI: 10.1016/j.soildyn.2004.11.009

56. Kontoe, S., Zdravkovic, L., Potts, D.M., and Menkiti, C.O. (2008). "Case study on seismic tunnel response." *Canadian Geotechnical Journal*, 45, 1743–1764. DOI: 10.1139/T08-087.

57. Kumari, S.D.A., and Sitharam, T.G. (2012). "Tunnels in weak ground: Discrete element simulations." *ISRM India Journal*, 1(1), 17-24.

58. Li, T. (2012). "Damage to mountain tunnels related to the Wenchuan earthquake and some suggestions for aseismic tunnel construction." *Bulletin of Engineering Geology and the Environment*, 71, 297-308. DOI: 10.1007/s10064-011-0367-6.

59. Li, B., Jiang, Y., Tanabashi, Y., and Yamashita, Y. (2010). "Behaviour of large scale underground cavern located in jointed rock masses evaluated by using distinct element method." *Soils and Foundations*, 50(5), 609-621.

60. Li, H.Z., and Low, B.K. (2010). "Reliability analysis of circular tunnel under hydrostatic stress field." *Computers and Geotechnics*, 37(1), 50-58.

61. Lorig, L.J., and Cundall, P.A. (1989). "Modeling of reinforced concrete using the distinct element method." *Proc., Fracture of concrete and rock : SEM-RILEM International Conference*, Houston, Texas, USA, 276-287.

62. Lorig, L.J., Watson, A.D., Martin, C.D., and Moore, D.P. (2009). "Rockslide run-out prediction from distinct element analysis." *Geomechanics and Geoengineering*, 4(1), 17-25.

63. Low, B.K., and Einstein, H.H. (2013). "Reliability analysis of roof wedges and rock bolt forces in tunnels." *Tunnelling and Underground Space Technology*, 38, 1-10.

64. Low, B.K., and Tang, W.H. (2007). "Efficient spreadsheet algorithm for first-order reliability method." *Journal of Engineering Mechanics*, 133(12), 1378–1387.

65. Lu, A., Zhang, N., Wang, S., and Zhang, X. (2017). "Analytical solution for a lined tunnel with arbitrary cross sections excavated in orthogonal anisotropic rock mass." *International Journal of Geomechanics*, 17(9), DOI: 10.1061/(ASCE)GM.1943-5622.0000912.

66. Lu, Q., Chan, C.L., and Low, B.K. (2013). "System reliability assessment for a rock tunnel with multiple failure modes." *Rock Mechanics and Rock Engineering*, 46(4), 821-833.

67. Lu, Q., and Low, B.K. (2011). "Probabilistic analysis of underground rock excavations using response surface method and SORM." *Computers and Geotechnics*, 38(8), 1008-1021.

68. Lu, Q., Sun, H.Y., and Low, B.K. (2011). "Reliability analysis of ground-support interaction in circular tunnels using the response surface method." *International Journal of Rock Mechanics and Mining Sciences,* 48(8), 1329-1343.

69. Lunardi, P. (2008). *Design and construction of tunnels: analysis of controlled deformation in rocks and soils*, Springer, Berlin.

70. Lysmer, J., and Kuhlemeyer, R. (1989). "Finite dynamic model for infinite media." *Journal of Engineering Mechanics, (ASCE)*, 95:EM4, 859-877.

71. Miyabayashi, H., Tosaka, T., Isogai, A., Kojima, Y., Yashiro, K., Saito, J., and Asakura, T. (2008). "Basic studies on earthquake damage to shallow mountain tunnels." *Proceedings of the World Tunnel Congress 2008 – Underground Facilities for Better Environment and Safety – India.*

72. Manfredini, G., Martinetti, S., and Ribacchi, R. (1975). "Inadequacy of limiting equilibrium methods for rock slopes design." In: 16th Symposium on Rock Mechanics, Minneapolis, USA, p. 35–43.

73. Mollon, G., Dias, D., and Soubra, A.H. (2009a). "Probabilistic analysis of circular tunnels in homogeneous soil using response surface methodology." *Journal of Geotechnical and Geoenvironmental Engineering*,135(9), 1314–1325.

74. Mollon, G., Dias, D., and Soubra, A.H. (2009b). "Probabilistic analysis and 744 design of circular tunnels against face stability." *International Journal of Geomechanics*, 9(6), 237-249.

75. Montgomery, D. (2013). *Design and analysis of experiments*, John Wiley and Sons, New York.

76. Mostyn, G.R., and Li, K.S. (1993). "Probabilistic slope analysis- state of play." *Proc., Conference on Probabilistic Methods in Geotechnical Engineering*, A.A. Balkema, Canberra, Australia, 89-109.

77. Murano, T., and Takewaki, N. (1984). "On earthquake resistance of rock caverns." *A report prepared for the NEA Coordinating Group on Geological Disposal OECD/NEA.*

78. Myer, L.R., Pyrak-Nolte, L.J., and Cook, N.G.W. (1990). "Effects of Single Fracture on Seismic Wave Propagation." *In Rock Joints*, N. Barton and O. Stephansson, Eds., Balkema, Rotterdam, 467–473.

79. Myers, R.H., Montgomery, D.C., and Anderson-Cook, C.M. (2009). *Response surface methodology: Process and product optimization using designed experiments*, Wiley, New York.

80. Myers, R.H., Montgomery, D.C., Vining, G.G., Borror, C.M., and Kowalski, S.M. (2004). "Response Surface Methodology: a retrospective and literature survey." *Journal of Quality Technology*, 36(1), 53-78.

81. Nilsen, B. (2000). "New trend in rock slope stability analysis." *Bulletin of Engineering Geology and Environment*, 58(3), 173–178.

82. Oreste, P.P. (2005). "A probabilistic design approach for tunnel supports." *Computers and Geotechnics*,32(7), 520–534.

83. O'Rourke, T.D., Goh, S.H., Menkiti, C.O., and Mair, R.J. (2001). "Highway tunnel performance during the 1999 Duzce earthquake." *In Proceedings of the 15th international conference on soil mechanics and foundation engineering*, 2. Balkema, Rotterdam, pp 1365–1368

84. Otsuka, H., Mashimo, H., Hoshikuma, J., Takamiya, S., and Ikeguti, M. (1997). "Damage to underground structures (1995 Hyogoken Nanbu earthquake)." *Journal of Research,* 33, 481–509.

85. Owen, G.N., and Scholl, R.E. (1980). "Earthquake engineering of large underground structures." *NASA STI/Recon Technical Report*, 82, 16291.

86. Park, S., and Park, S. (2014). "Case studies for tunnel stability based on the critical strains in the ground." *KSCE Journal of Civil Engineering*, 18(3), 765-771.

87. Park, S.H., and Shin, Y.S. (2007). "A study on the safety assessment technique of a tunnel using critical strain concept." *Journal of Korean Geotechnical Association*, 23(5), 29-41.

88. Pathak, S., and Nilsen, B. (2004). "Probabilistic rock slope stability analysis for Himalayan condition." *Bulletin of Engineering Geology and Environment,* 63(1), 25–32.

89. Pelekis, P.C., Xenaki, V.C., and Athanasopoulos, G.A. (2000). "Use of EPS Geofoam for Seismic Isolation of Earth Retaining Structures: Results of an FEM Study", *Proceedings of the Second European Geosynthetics Conference, Bologna, Italy*, pp. 843-846

90. Penzien, J. (2000). "Seismically induced racking of tunnel linings." *International Journal of Earthquake Engineering and Structural Dynamics,* 29(5),683–691.

91. Phase2. (2010). *User's manual*, Version 7.0, Rocscience Inc., Toronto, Canada.

92. Power, M.S., Rosidi, D., and Kaneshiro, J.Y. (1998). "Seismic Vulnerability of Tunnels and Underground Structures Revisited." *Proc of North American Tunnelling '98*. Newport Beach, CA: Balkema, Rotterdam, The Netherlands, p. 243–250.

93. Pyrak-Nolte, L.J., Myer, L.R., and Cook, N.G.W. (1990). "Transmission of seismic waves across single natural fractures." *Journal of Geophysical Research*, 95(B6):8617-8638.

94. Rosenblueth, E. (1975). "Point estimates for probability moments." In *Proceeding of National Academy of Sciences*, USA, 72(10), 3812–3814.

95. Roy, N., and Sarkar, R. (2015). "Effect of mechanical properties of discontinuity on the seismic stability of tunnels in jointed rock mass." *Proceeding of the 50th Indian Geotechnical Conference*, Pune.

96. Roy, N., and Sarkar, R. (2017). "A review of seismic damage of mountain tunnels and probable failure mechanisms." *Geotechnical and Geological Engineering*, 35(1), 1-28.

97. Sakurai, S. (1978). "Approximate time-dependent analysis of tunnel support structure considering progress of tunnel face." *International Journal of Numerical and Analytical Methods in Geomechanics*, 2(2), 159-175.

98. Sakurai, S. (1982). "An evaluation technique of displacement measurements in tunnels." *Proc., Japan Society of Civil Engineers*, 317, 93-100.

99. Sakurai, S. (1997a). "Lessons learned from field measurements in tunnelling." *Tunnelling and Underground Space Technology*, 12(4), 453-460.

100. Sakurai, S. (1997b). "Strength parameters of rocks determined from back analysis of measured displacements." In *Proceeding of First Asian Rock Mechanics Symposium., ISRM*, Seoul, 95-99.

101. Sakurai, S., and Takuechi, K. (1983). "Back analysis of measured displacements of tunnels." *Rock Mechanics and Rock Engineering*, 16(3), 173-180.

102. Sengupta, S., Subrahmanyam, D.S., Joseph, D., and Sinha, R.K. (2007). "The role of National Institute of Rock Mechanics in in-situ geotechnical investigations (1979 to 2002) at Tala hydroelectric project Bhutan." In *Proceeding of International Workshop on Experiences Gained in Design and Construction of Tala Hydroelectric Project*.

103. Sharma, S., and Judd, W.R. (1991). "Underground opening damage from earthquakes." *Engineering Geology*, 30, 263-276.

104. Shen, Y., Gao, B., Yang, X., and Shuangjiang, T. (2014). "Seismic damage mechanism and dynamic deformation characteristic analysis of mountain tunnel after Wenchuan earthquake." *Engineering Geology,* 180, 85-98. DOI: 10.1016/j.enggeo.2014.07.017.

105. Shimizu, M., Saito, T., Suzuki, S., and Asakura, T. (2007a). "Results of survey regarding damages of railroad tunnels caused by the Mid Niigata Prefecture Earthquake in 2004." *Tunnelling and Underground*, 38(4), 265–273.

106. Shimizu, M., Suzuki, T., Kato, S., Kojima, Y., Yashiro, K., and Asakura, T. (2007b). "Historical damages of tunnels in Japan and case studies of damaged railway tunnels in the Mid Niigata Prefecture Earthquakes." In *Underground Space – the 4th Dimension of Metropolis*.

107. Shimizu Corporation. (1998). *Tunnel construction manual*, 30-60.

108. Singh, B., and Goel, R.K. (2006). *Tunnelling in weak rocks*, Elsevier Sciences.

109. Singh, R., Chowdhry, A.K., Sharma, R.N., Goyal, D.P., and Khazanchi, R.N. (2002). 804 "Wall support system for powerhouse cavern of Tala Hydroelectric Project in Bhutan Himalayas." In *Proceeding of Indian Rock Conference*, New Delhi, 132-142.

110. Singh, R., and Goyal, D.P. (2005). "Compendium of published papers on 1020 MW Tala hydroelectric project." *Tala Hydroelectric Project Authority Gedu*, Bhutan.

111. Singh, R., and Sthapak, A.K. (2007). *Experiences gained in design and construction of Tala hydroelectric project Bhutan*, International Workshop, New Delhi.

112. Song, K.I., Cho, G.C., and Lee, S.W. (2011). "Effects of spatially variable weathered rock properties on tunnel behaviour." *Probabilistic Engineering Mechanics*, 26(3), 413-426.

113. Spagnoli, G., Oreste, P., and Bianco, L.L. (2017). "Estimation of shaft radial displacement beyond the excavation bottom before installation of permanent lining in nondilatant weak rocks with a novel formulation." *International Journal of Geomechanics*, 17(9), DOI: 10.1061/(ASCE)GM.1943-5622.0000949.

114. Su, Y.H., Li, X., and Xie, Z.Y. (2011). "Probabilistic evaluation for the implicit limit-state function of stability of a highway tunnel in China." *Tunnelling and Underground Space Technology*, 26(2), 422-434.

115. Swarup, A., Goel, R.K., and Prasad, V.V.R. (2000). "Observational approach for stability of tunnels." In *Proceeding of Tunneling Asia*, New Delhi, 38-44.

116. Tao, S., Gao, B., Wen, Y., and Zhou, X. (2011). "Investigation and analysis on the seismic damage of mountain tunnels subjected to Wenchuan earthquake." *Applied Mechanics and Materials,* 99-100, 273-281.

117. UDEC (Universal Distinct Element Code). (2004). *User's manual*, Version 4.0, Itasca Consulting Group. Inc., Minneapolis.

118. Venugopala Rao, R., Alagh, P.K., Chowdhry, A.K., Sharma, B.N., and Theraja, D.V. (2003a). "Evaluation of rock bolt failure mechanism in Tala HE project, Bhutan." In *Proceeding of International Conference on Accelerated Construction of Hydropower Projects*, Gedu, Bhutan, 2, 30-37.

119. Venugopala Rao, R., Gupta, R.N., Raju, G.D., Chowdhry, A.K., Chug, I.K., and Alagh, P.K. (2003b). "Performance of rigid support system in cross openings around major caverns." In *Proceeding of International Conference on Accelerated Construction of Hydropower Projects*, Gedu, Bhutan, 2, 38-46.

120. Wang, W.L., Wang, T.T., Su, J.J., Lin, C.H., Seng, C.R., and Huang, T.H. (2000). "The seismic hazards and rehabilitation of tunnels in central Taiwan after Chi-Chi earthquake." *Sino-Geotechnics,* 81, 85-96.

121. Wang, W.L., Wang, T.T., Su, J.J., Lin, C.H., Seng, C.R., and Huang, T.H. (2001). "Assessment of damage in mountain tunnels due to the Taiwan Chi-Chi earthquake." *Tunnelling and Underground Space Technology,* 16, 133-150. DOI: 10.1016/S0886-7798(01)00047-5

122. Wang, Z.Z., Gao, B., Jiang, Y.J., and Yuan, S. (2009). "Investigation and assessment on mountain tunnels and geotechnical damage after the Wenchuan earthquake." *Sci China Ser E-Tech Sci*, 52(2), 546–558.

123. Wang, Z.Z., and Zhang, Z. (2013). "Seismic damage classification and risk assessment of mountain tunnels with a validation for the 2008 Wenchuan earthquake." *Soil Dynamics and Earthquake Engineering,* 45, 45-55.DOI: 10.1016/j.soildyn.2012.11.002

124. Xu, H., Busetti, S., and Arson, C. (2017). "Fracture-induced anisotropy of the stress-strain response of shale at multiple scales." *International Journal of Geomechanics*, 17(8), DOI:10.1061/(ASCE)GM.1943-5622.0000897.

125. Xu, Q., Chen, J., Li, J., Zhao, C., and Yuan, C. (2015) Study on the Constitutive Model for Jointed Rock Mass. PLoS ONE 10(4): e0121850. doi:10.1371/journal.pone.0121850

126. Xu, Q., Fan, X.M., Huang, R.Q., and Westen, C.V. (2009). "Landslide dams triggered by the Wenchuan earthquake, Sichuan Province, south west China." *Bulletin of Engineering Geology and Environment*, 68, 373–386. DOI: 10.1007/s10064-009-0214-1

127. Yan, M. (2008). *Numerical modelling of brittle fracture and step-path failure: from laboratory to rock slope scale*. Ph.D. Thesis, Simon Fraser University.

128. Yashiro, K., and Kojima, Y. (2007). "Historical earthquake damage to tunnel in Japan and case studies of railway tunnels in the 2004 Niigataken-Chuetsu earthquake." *Quarterly Report RTRI*, 48(3), 136–141.

129. Yeung, M.R., and Leong, L.L. (1997). "Effects of joint attributes on tunnel stability." *International Journal of Rock Mechanics and Mining Science*, 34(3-4), Paper No. 348.

130. Yoshikawa, K. (1981). "Investigation about past earthquake disasters of railway tunnels." *Quarterly Report RTRI (Railway Technical Research Institute)*, 22(3), 103–111.

131. Yoshikawa, K., and Fukuchi, G. (1984). "Earthquake damage to railway tunnels in Japan." *In Adv. Tunnelling Technol. Subsurf. Use v 4 n 31984, Prot of Underground Struct Against Seism Eff Jt Open Sess ITA/SOCVENOS. Caracas, Venezuela,* 75–83.

132. Zarnani, S., and Bathurst, R.J. (2006). "Application of EPS Geofoam as a Seismic Buffer: Numerical Study using FLAC." *Proceedings of the 59th Canadian Geotechnical Conference, Vancouver, B.C., 1-4 October 2006, The Canadian Geotechnical Society, Richmond, B.C.*

133. Zhang, J.X. (2013). "Earthquake mechanics study with health check for a seismic-damaged tunnel suffered from the Wenchuan earthquake." *Applied Mechanics and Materials*, 387, 68-71. DOI: 10.4028/www.scientific.net/AMM.387.68

134. Zhang, W.G., and Goh, A.T.C. (2015). "Regression models for estimating ultimate and serviceability limit 7 states of underground rock caverns." *Engineering Geology*, 188, 68-76.

135. Zhao, J. (1996). "Construction and utilization of rock caverns in Singapore, part A: bedrock resource of the Bukit Timah granite." *Tunnelling and Underground Space Technology*, 11, 65-72.

136. Zhao, X., Li, T.B., Tao, L.J., Hou, S., Li, L.Y., and Qiu, W.G. (2013). "Failure mechanism of tunnel portal during strong earthquakes." *International Efforts in Lifeline Earthquake Engineering,* 314-320. DOI: 10.1016/9780784413234.041.

137. Zheng, S., Jiang, S., and Wang, X. (2012). "Research on the mechanism of earthquake damage of tunnels." *Advanced Materials Research,* 538-541, 705-708.

138. Zheng, W.Z., Bo, G., YuanJun, J., and Song, Y. (2009). "Investigation and assessment on mountain tunnels and geotechnical damage after the Wenchuan earthquake." *Science in China Series E: Technological Sciences*, 52(2), 546-558. DOI: 10.1007/s11431-009-0054-z.

139. Zhu, H., Chen, M., Zhao, Y., and Niu, F. (2017). Stability Assessment for Underground Excavations and Key Construction Techniques. Springer Tracts in Civil Engineering (STCE)

Publications

Journals

1. Roy N, Sarkar R (2017). A Review of Seismic Damage of Mountain Tunnels and Probable Failure Mechanisms. *Geotechnical and Geological Engineering*, *Springer*, 35(1):1-28.
2. Roy N, Sarkar R, Bharti SD (2017). Prediction Model for Performance Evaluation of Tunnel Excavation in Blocky Rock Mass. *International Journal of Geomechanics, ASCE*. doi:https://doi.org/10.1061/(ASCE)GM.1943-5622.0001023
3. Roy N, Sarkar R, Bharti SD (2018). Transverse Dynamic Response of Circular Tunnels in Blocky Rock Mass Using Distinct Element Method. *International Journal of Geomechanics, ASCE*.

Conferences

1. Roy N, Sarkar R (2016). Identification of Critical Parameters of Seismic Behavior of Tunnels in Discontinuous Medium. *Indian Geotechnical Conference, IIT Madras*.
2. Roy N, Sarkar R (2015). Effect of Mechanical Properties of Discontinuity on the Seismic Stability of Tunnel in Jointed Rock Mass. *Indian Geotechnical Conference, COEP Pune*.

BIO-DATA

The author is currently serving as Visiting Faculty at Birla Institute of Technology and Science, Pilani. He obtained his Bachelor's Degree in Civil Engineering from Manipal Institute of Technology, Karnataka in 2012. He completed his Master's Degree in Rock Mechanics and Underground Structures with dissertation on "Stability Analyses of Jointed Rock Slopes", from the Indian Institute of Technology Delhi in 2014. His area of specialization is "Rock Mechanics".